THE MICROCLIMATOLOGY OF ANTARCTIC SOILS

A thesis
submitted in partial fulfilment
of the requirements for the Degree
of
Master of Science in Earth Sciences
at the University of Waikato

by

Roger James Lee MacCulloch

University of Waikato
1996

Wright Valley, McMurdo Sound, Antarctica.

A typical Antarctic Dry Valley, Barwick Valley, McMurdo Sound.

Abstract

An understanding of the microclimatology of the ice free areas in Antarctica is needed to better quantify the impacts of human activities on this fragile environment and to help monitor global climate change processes. This research was undertaken to characterise the surface and sub surface factors influencing Antarctic soil microclimates and quantify the sub surface thermal processes resulting from these conditions.

A measurement programme was developed and implemented at three contrasting sites within the Dry Valleys of the McMurdo Sound Region, Antarctica during the 1994-95 summer season, and samples were collected for further analysis in New Zealand. Climatic variables measured included the surface radiation and energy balance, soil and air temperature, and windspeed and direction. Important soil physical and thermal properties such as moisture content, bulk density, particle density, grainsize distribution, salinity, specific heat and thermal conductivity were also measured.

The sites investigated were located at Scott Base on Ross Island in the coastal climate zone, at the foot of Mount Brooke in the Coombs Hills which has a high mountainous climate, and in the Northwind Valley (Greenville Valley) in the Convoy Range which is climatically midway between the two. Apart from being climatically different, the soils examined at each site were also different. Basalt derived soil was examined at Scott Base, dolerite derived soil was studied at the Coombs Hills, and a sandy soil derived from sandstone was examined in the Northwind Valley.

Similar amounts of shortwave radiation were recorded at each site under comparable conditions, although surface albedo varied significantly which determined the amount of radiation reflected. Consequently, the Scott Base site, which had the darkest surface and lowest albedo, had the greatest net radiation inputs, and the Northwind Valley site had the lowest due to its pale colour and high albedo.

Despite this, the Northwind Valley soil had the largest soil heat flux. The reason for this is not fully understood, but involves the soil temperature gradient which is the main determinant of the soil heat flux. The warmer climate at Scott Base resulted in generally warmer soil temperatures which produced an active layer greater than two times that seen at either of the other sites. Due to its relatively high moisture content, ice-cement was found at about 0.25 m which delineates the summer 0°C isotherm, and indicates the permafrost is at a similar depth.

At the other two sites which were a lot colder, there was no permanent ice cement found due to their dry nature. The active layer was approximately 0.10 m deep at the Coombs Hills site, and was only 0.08 m at the Northwind Valley site. The permafrost at these sites would also be at about these depths. Soil temperatures, which were strongly negative, fluctuated by up to 5°C at a depth of about 0.20 m at these two sites.

Under snow cover, the soil heat flux at both the Scott Base and Coombs Hills sites became negative which means energy was being lost from the profile, and the penetration depth of diurnal temperature variations was reduced.

The main factors influencing the soil thermal regime are incoming solar radiation, air temperature, windspeed, and surface albedo. Soil properties including moisture content, thermal conductivity and heat capacity are less important in determining the variations observed.

Acknowledgements

I would like to acknowledge with sincere thanks the many people who have supported and assisted this research:

My supervisor Dave Campbell, for your time, patience, guidance and approachability throughout the course of this research. Your computer programming and operating skills were essential for the successful operation of the automatic data logging system and for processing the data. It is your enthusiasm and humour which inspired me at times of difficulty. It has been a pleasure to have you as a supervisor.

Land and Soil Consultancy Services; Ian Campbell and Graham Claridge for the financial support given, as well as help in the field, describing profiles, passing on a wealth of knowledge and information about Antarctic soils, geology and climatic processes, and for allowing me to take part in their research programme.

New Zealand Antarctic Programme staff who helped make my trip to Antarctica as memorable as it was. I thank in particular Scotty the cook for preparing top quality meals, including hot breakfasts, and an awesome Christmas feast, and keeping us informed with the latest gossip. Warren Herrick and Rachel Brown my field training instructors who taught me to survive in the Antarctic environment, and the management staff who ensured reliable transport and excellent provisions in the field.

Special thanks to my friends and fellow students who have helped and encouraged me throughout the year in times of need. We have been through a lot together and can now look back on a memorable year.

Lastly I would like to thank my family for their encouragement, enthusiasm and never-ending support. It is your guidance and support which has got me where I am today. For this I am truly grateful.

Table of Contents

List of Figures

List of Tables

CHAPTER ONE

INTRODUCTION

The polar regions are an important part of the global climate system because it is here that energy absorbed by the atmosphere/ocean system in the tropics and transported through the mid latitudes is finally reradiated back to space. Climatic processes in the polar regions therefore both force and respond to changes in the global climate.

Within the Antarctic, the atmospheric, oceanic and cryospheric elements of the climate system are strongly coupled, leading to a climate regime that is very sensitive to changes in these forcing functions. This sensitivity can be seen in the high interannual variability seen in the Antarctic climate record (B.A.S, 1995)[1].

1.1 MICROCLIMATIC RESEARCH IN THE ANTARCTIC

The earth's surface is the principle site of climatic activity in the Earth atmosphere system. Radiant energy is absorbed, reflected and emitted, energy is transformed from radiant to thermal, sensible to latent, precipitation is intercepted, moisture is evaporated and wind speed is reduced by friction (Oke, 1987). In this Thesis, these processes are collectively referred to as the soil's microclimate.

Due to the importance of these processes in relation to global climate, numerous microclimate studies have been carried out during land use and crop production research throughout the world. There is however, a scarcity of high quality information from Arctic, Antarctic and alpine areas due to the lack of intensive human activity in these regions, logistical difficulties, theoretical problems and instrumental limitations associated with research in these extreme environments. Many research sites are inaccessible, especially during winter, and the working conditions are often difficult for researchers and hard on equipment (Saunders and Bailey, 1994).

---

[1] B.A.S - British Antarctic Survey WWW home page "http://www.nbs.ac.uk/public/dotacs.html."

With increased availability of portable computerised data-acquisition systems, remote location measurements are becoming more feasible and the number of studies in these areas are increasing. The information obtained from these systems is providing essential baseline data needed to monitor long term climate change on a regional and global scale.

There is still a lack of information on the microclimatology of the ice free areas in Antarctica. Traditional macroclimatic regional studies have been carried out in numerous areas in both the Arctic and Antarctic. Soil moisture and temperature data has been collected for projects involving the construction of roads, airfields, pipelines and foundation in the Arctic, but there have not been many studies quantifying these processes in the Antarctic.

A description of the microclimatology of Antarctic soils is therefore needed if the impacts of human activities on this fragile environment are to be understood and minimised, and global climate change processes quantified.

1.2 RESEARCH OBJECTIVES

The main objectives of this research are to characterise the surface and sub surface factors influencing Antarctic soil microclimates and quantify the sub surface thermal and hydrological processes resulting from these conditions.

To achieve these objectives the following hypothesis will be investigated:

"the microclimatology and thermal regime of Antarctic soils is a function of their geographic location, external influences, and the physical properties of the soil".

To test this hypothesis:

1) variables influencing the soil microclimate such as incoming and outgoing solar radiation, wind speed and direction, and general weather phenomena will be quantified;

2) the sub-surface processes resulting from these surface conditions such as the soil thermal regime will be investigated;

3) the soil physical properties influencing the above processes including soil moisture content, bulk density, particle density, grain size distribution, and salinity will be described.

Each of these steps are carried out for three different soils in different climatic zones of the McMurdo Sound region of Antarctica so the dominant factors influencing Antarctic soil microclimatology can be identified.

1.3 THESIS LAYOUT

Chapter 2 describes the soils found in Antarctica and examines the factors influencing their microclimate. Surface and sub surface processes operating in the near surface layer will then be discussed along with the soil's physical properties. Previous research in this field will be reviewed and related to the current study.

Chapter 3 describes the measurement methods used and explains why these techniques were most suitable. Methods of data collection and analysis will also be described along with the main sources of error needing consideration.

Chapter 4 describes the geography, geology and macroclimatology of the three field sites studied.

The results of the study are presented in Chapter 5 which is divided into six sections. The first and second sections present the soil physical and thermal property data collected in the field and laboratory and outlines the influence these factors could have on the soil microclimate. The third, fourth and fifth sections present the radiation balance, energy balance, and soil temperature data collected and relates it to the physical properties of the soil. The final section compares the sites and describes the main features of each sites microclimate.

The conclusions of this study are summarised in Chapter 6 along with a discussion of future research needs.

CHAPTER TWO

ANTARCTIC SOILS AND THEIR MICROCLIMATE

Soil is usually defined in terms of the five soil forming factors which are time, climate, parent material, topography and biology. In Antarctica, the biological component is restricted in most places to isolated patches of mosses, lichens, and small bacterial and invertebrate populations, due to the lack of moisture and low temperatures during the winter period. As a result of this, Tedrow and Ugolini (1966), Tedrow (1977) and other workers, have questioned the classification of these materials as soils (Campbell and Claridge, 1987).

Despite this low, or non-existent biological component, the effects of time, weathering, climate, and parent materials on these soils is very noticeable. In this study, the view of Campbell and Claridge (1987) is adopted which classifies the materials seen in the dry Valleys and other ice free areas as soils which have an extremely small if not negligible biological component.

This chapter is divided into three parts. The first describes the main properties of many Antarctic soils and outlines the most important factors controlling their development, the second discusses the components of the soil microclimate such as the surface radiation and energy balance. The last section examines the thermal properties influencing the soil microclimate, and discusses the thermal regime of high latitude soils.

2.1 ANTARCTIC SOILS

Soils on regolith and weathered bedrock can be found in most ice free areas of Antarctica from the coast to the edge of the polar plateau. These soils undergo freeze/thaw cycles on a seasonal basis down to a maximum depth of about 0.6 m in coastal regions and only about 0.10 m in some of the colder inland locations. These soils are typically very dry, un-cohesive, coarse textured, and can contain distinguishable salt horizons (Campbell unpublished data, 1996).

Weakly cohesive horizons are sometimes present in the upper layers due to increased moisture content which gives the soil a weak vesicular structure. Cohesion also occurs as the salt content rises because the salt forms small binding crystals between grains (Campbell, unpublished data, 1996). Particle sorting, cryoturbation processes, oxidation and colour change within the profile can also cause horizon differentiation (Tedrow, and Ugolini, 1966).

2.1.1 SOIL CLIMATE INTERACTIONS

Antarctic soils are strongly influenced by climatic variables such as aridity and temperature because it is these features that determine the type and rate of processes forming them. Several distinct climate zones have been identified which affect soil development in a number of different ways (see Figure 2.1).

A. Intra-continental high mountain zone

The intra-continental high mountain zone is situated on the central Antarctic plateau bounded by the 3000 to 3200 m contour level. The lowest air temperatures on earth characterise this zone (minimum recorded is -88.3°C at Vostok Station in 1960) and the mean annual temperature is between -50°C and -60°C. The mean temperature of the coldest month reaches -70°C to -72°C and the warmest does not exceed -30°C to -32°C (Rusin, 1964).

The area is usually free from clouds and there are only weak winds present. Precipitation in this zone is between about 40–50 mm $yr.^{-1}$ and a maximum of 80 mm $yr.^{-1}$ is sometimes reached (Solopov, 1969)[2]. This entire zone is covered in snow and ice which prohibits soil development.

B. Glacial slope zone

The glacial slope zone is northward of the interior zone and surrounds Antarctica with a 700 to 800 km belt, reaching down to about the 300 m above sea level contour. The climate of the glacial slope zone is characterised by severe frost, strong, persistent katabatic winds and frequent snow storms. The katabatic winds die out over summer in the northern part of this zone and precipitation can be between 60–120 mm $yr.^{-1}$ (Tedrow and Ugolini, 1966).

[2] Snowfall is usually measured in g cm^{-2} $yr.^{-1}$, but 1 g cm^{-2} $yr.^{-1}$ is equivalent to 10 mm of rainfall.

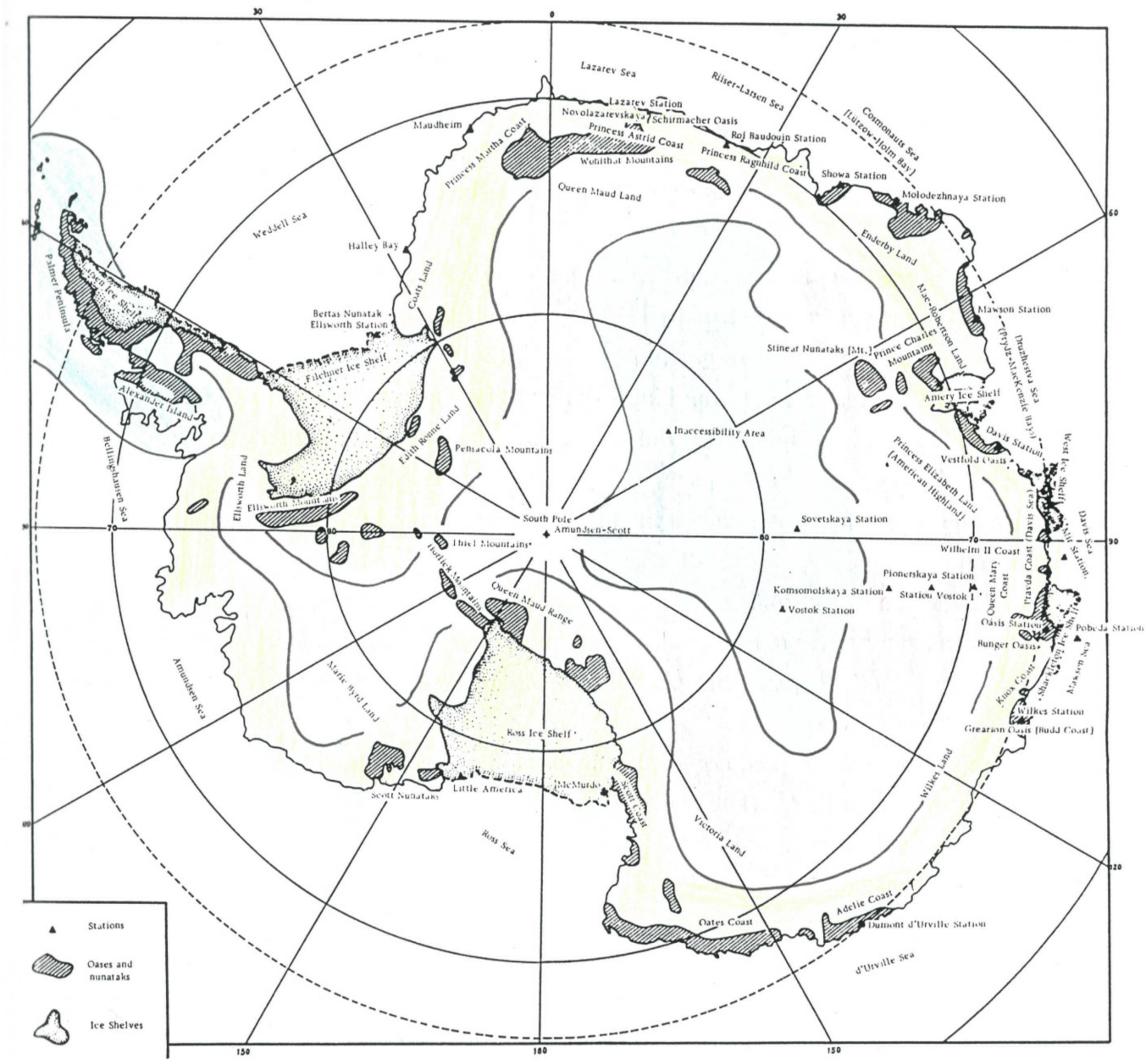

Key

Blue - Intra-continental high mountain zone
Red - Glacial slope zone
Yellow - Coastal Antarctic climate zone
Green - Maritime Antarctic climate zone

Figure 2.1 The main climate zones of Antarctica (adapted from Solopov, 1969).

The classification of the Glacial slope zone does not take into account the effect of the Transantarctic Mountains which contain several different climatic zones important for soil development.

Campbell and Claridge (1987) therefore introduced another zone called the Mountain zone which lies along the Transantarctic Mountains from Cape Adare across the continent to the Shackleton Mountains at the base of the Weddell Sea and the Ellsworth Mountain south of the Antarctic Peninsula. This zone contains three sub zones which are the inland mountain, central mountain, and coastal mountain subzones.

The *Inland Mountain subzone* is located on the inner edge of the Transantarctic Mountains and is usually above 2000 m at latitudes > 80°S. Extremely low precipitation (~100 mm $yr.^{-1}$) and temperatures (-5°C to -50°C) characterise this subzone and melting rarely occurs (Bull, 1966). Consequently there is little if any liquid moisture available for soil-forming processes which means soil development is very slow (Campbell and Claridge, 1987).

The *Central Mountain subzone* covers most of the ice free areas of the Transantarctic Mountains. Air and surface temperatures can reach 10°C and 30°C respectively during summer due to the positive radiation balance which allows limited melting of lakes and rivers to flow (Pickard, 1986). This combined with ~150 mm $yr.^{-1}$ precipitation allows movement of soluble materials within the profile (Schwerdtfeger, 1984).

Adiabatic heating in these areas often causes the air to become very dry and the resultant humidity regime is similar to that in a desert (Rusin, 1964). Soil development in this subzone is generally characterised by slow rates of chemical weathering due to the limited supply of moisture and low temperatures (+1°C to -40°C); predominance of physical weathering; and high concentration of soluble salts and calcium carbonate at the surface due to high evaporation rates (Campbell and Claridge, 1987).

The *Coastal Mountain subzone* lies along the edge of the Transantarctic Mountains where they border the Ross Sea or the Ross Ice Shelf (including areas around McMurdo Station and Scott Base. This zone is characterised by higher precipitation (170 mm $yr.^{-1}$) than the inland regions, warmer temperatures (+5°C to -30°C) and the ground surface usually remains unfrozen for longer periods. The soil also contains a lot more moisture to greater depths and remains moist for longer periods. As a result of these conditions, soils in this zone are usually significantly more developed than those in the zones further inland (Campbell and Claridge, 1987).

C. Coastal Antarctic climate zone

The Coastal Antarctic climate Zone lies along the outer fringes of the continent, not including the Ross and Weddell Sea embayments which are included in the coastal climate subzone, or the west coast of the Antarctic Peninsula north of 70°S which is included in

the Maritime Antarctic zone. This zone is characterised by greater cloudiness, more precipitation (400–600 mm $yr.^{-1}$) and generally higher mean temperatures (+10°C to -12°C) (Schwerdtfeger, 1984). The soils are moister than those in the Coastal Mountain subzone and remain unfrozen for long periods of time during the summer. These conditions allow more rapid soil formation due to enhanced chemical weathering (Campbell and Claridge, 1987).

D. Maritime Antarctic climate zone

The Maritime Antarctic climate zone covers the west coast of the Antarctic Peninsula, the southern Shetland and Sandwich Islands. These areas are the wettest parts of Antarctica and are dominated by circumpolar cyclonic storms which allow sleet and rain to fall in much higher quantities than anywhere else on the continent.

During summer the mean temperature is close to 0°C and the mean annual temperature never falls below -10°C due to the proximity of the ocean and the increased number of daylight hours (due to latitude). Strong chemical weathering has resulted in great profile development and the soil is warm and moist enough for plants to grow in sheltered spots (Campbell and Claridge, 1987).

2.1.2 SOIL PARENT MATERIAL AND AGE

The importance of parent material in the development of soils was first recognised in Antarctica by McCraw (1967) who used them to map and classify the soils of the Taylor Valley. Due to the slow weathering processes in this cold environment, the colour and texture of many soils closely resemble that of their parent material. Soil derived from dolerite for example is usually light brown and contains a large proportion of angular boulders due to dolerites brown colour and strongly jointed, coarse prismatic structure (Campbell and Claridge, 1987).

Soils comprising of a single parent material are however often difficult to find in Antarctica because most surface deposits contain materials derived from several different locations (Campbell and Claridge, 1987). Glacial advance is the main transport mechanism for redistributing surface materials, but alluvial and aolean processes are also significant.

The thermal and physical properties of the soil parent material also strongly influences the resultant soil microclimate. The colour, texture, structure and physical composition of the soil determines the amount of solar radiation absorbed into, or reflected away from the profile and the depth to which this energy flux travels.

The weathering processes which produce these properties are a function of a soil's age and can be quantified using the weathering stage classification developed by Campbell and Claridge (1975) (Table 2.1).

Table 2.1 Morphological development of soils with increasing weathering/age (Campbell and Claridge, 1987).

Weathering stage	Surface rock characteristics	Soil colour	Horizon development	Soil salts	Soil depth	Other
1	fresh, unstained, coarse and angular	pale olive to light grey (5Y 6/3–7/2)	nil	absent	very shallow, underlain by ice	moderate patterned ground development
2	light staining, slight rounding, some disintegration	pale brown to light brownish grey (10YR 6/3–2.5Y6/2)	weak	few flecks	shallow, underlain by ice	moderate patterned ground development
3	distinct polish, staining and rounding, some cavernous weathering, some ventifacts	light yellowish brown (10YR 5/3–2.5Y 6/4)	distinct	many salt flecks in upper party of profile and beneath stones	moderately deep	some disintegration of boulders in the soil, slight increase in fine fraction
4	boulders much reduced by rounding, crumbling and ventifaction, strongly developed cavernous weathering; staining and polish well developed; some desert varnish	yellowish brown (10YR 5/4) in upper horizons, paler in lower horizons	very distinct	in discontinuous or continuous horizon beneath surface	deep	(as for stage 3)
5	few boulders, many pebbles forming pavement, extensive crumbling, staining, rounding, pitting and polish	dark yellowish brown to yellowish red (10YR 4/4–5YR 5/8)	very distinct	in horizon 20–30 cm from surface and scattered throughout profile	deep	(as for stage 3)
6	weathered and crumbled bedrock, very strongly stained	strong brown to yellowish red and dark red (7.5YR 5/6–5YR 4/8 or 2.5YR 3/6)	very distinct	(as for stage 5)	shallow to deep	bedrock sometimes crumbled to 50 cm depth

Weathering stage one describes the least weathered soils which are characterised by a bouldery surface with unstained, angular rocks, and weakly consolidated material beneath the surface. The monochromatic profile is strongly influenced by the colour and texture of the parent material and shows no sign of salt accumulation on the underside of stones. These shallow soils are found on young glacial deposits, fans and other alluvial deposits, and on coastal benches.

With each weathering stage, the degree of staining, oxidation, rounding, polishing, exfoliation, pitting, ventifaction and cavernous weathering of surface rocks increases, and the profile becomes deeper, more strongly coloured, salty and contains more fine particles and different horizons. Weathering stage five soils therefore have a strongly developed polished desert pavement which consists of dark coloured, small rounded and pitted ventifacts, and deep, fine grained, dark coloured profiles as seen in the Asgard Range, Wright Valley. Examples of these features can be seen in Figures 4.4, 4.7, and 4.10.

Weathering stage six soils are the most weathered soils known in Antarctica and are unlike any of the soils in the other weathering stages due to their residual nature. Surrounding surface rocks are usually deeply etched and eroded due to the in situ weathering of local rocks. These soils characteristically contain minimal large rock fragments, are dark coloured and contain thick horizons of salt. Examples of this soil type can be found in the Asgard and Convoy Ranges (Campbell and Claridge, 1987).

2.1.3 SOIL DISTRIBUTION AND TOPOGRAPHY

The distribution of soil within most areas is highly variable due to the local distribution pattern of glacial deposits, weathered rock, and bare rock. Valleys containing patchy moraine deposits, weathered rock and fresh rock is quite common. Extensive till deposits usually occur on the lower valley surfaces in major glacial valleys due to ice retreat and well weathered bedrock derived soils are commonly found on the higher slopes which have been ice free for a long period of time (Campbell and Claridge, 1987).

In most places, varying elevation, slope, aspect and drainage greatly affects soil development, but in Antarctica's unique climate, many of these factors are unimportant. Weathered products are usually removed from steep slopes by gravitational and fluvial processes which accelerates soil development on the lower slopes. This relationship has not yet been established in Antarctica because there is a lack of water to move rock and soil particles on the till and scree covered slopes. Soils on the upper ridges are typically shallow weathered bedrock soils and soils on the lower slopes usually consist of erosional scree and moraine deposits.

There is however, evidence which suggests small differences in microtopography create significant differences within local soils. Campbell and Claridge (1967), for example, showed that soil moisture content varied in a small glacially scoured basin in response to changing slope and aspect.

Soil structure and composition also changes markedly across patterned ground polygons which are a common feature of many Antarctic soils caused by the seasonal freeze/thaw cycle (Martini and Chesworth, 1992). Berg and Black (1966) suggested polygon development over time can change a site's microtopography, drainage, soil moisture content, texture and mineralogical composition. This was also supported by Linkletter *et al.,* (1973) who showed how a soil profile varies from the centre of a polygon to its trough.

2.1.4 SOIL MOISTURE

The soil microclimate is strongly dependent on soil moisture content because it affects the soil thermal properties and influences energy movement and distribution throughout the profile (see Section 2.3.2). Moist soils, for example, show less temperature variations on a diurnal basis than dry soils, because a large proportion of energy is used to evaporate water instead of heating the profile. Moist surfaces also tend to stay warmer at night than dry soils due to the high specific heat of water (Koorevaar, 1983).

The main sources of moisture in this environment are from snowfall, drifting snow and possibly the thawing, or sublimation of the permafrost (Martini and Chesworth, 1992). In some coastal parts of Antarctica, particularly on the Antarctic peninsula, moisture from precipitation can be considerable, but in the ice free areas of McMurdo Sound, or in the Transantarctic Mountains, it has been noted that the sublimation of snow often occurs due to the low relative humidity. Only thin snowfalls during summer melt completely and increase soil moisture content.

2.1.5 SOIL SALTS

The composition and abundance of salts in Antarctic soils varies considerably due to geographic location, climate, parent material and age. Soils in coastal regions for example contain a high proportion of sodium, magnesium and calcium chlorides which reflect their marine, aerosolic origin, whereas soils in colder, more arid inland areas, contain nitrates and sulphates of atmospheric origin (Martini and Chesworth, 1992).

Salts are also more abundant in older soils because they have accumulated over a long period of time from atmospheric sources. Accumulations of salt ranges from less than 0.1 kg/m^2 in weathering stage one soils to 100 kg/m^2 in weathering stage six soils (Campbell and Claridge, 1987).

Soil salt content strongly influences the temperature water freezes at and consequently is important in determining its thermal regime. In a Beacon Valley soil containing ~30% soluble salts, 20% of the soil moisture remained unfrozen at -40°C. When the soluble constituents were removed by leaching, the unfrozen water content fell to less than 3% at the same temperature (Anderson *et al.*, 1989a).

The volumetric expansion of salt caused by temperature changes also influences the soil thermal regime because it changes the physical properties of the soil. For sodium

chloride, for example, a 54°C temperature change would result in a 1% change in the salts volume (Selby, 1970). This has the potential to change the number of thermal contact points within the soil. This phenomena is probably insignificant in most Antarctic soils due to the smaller soil temperature ranges experienced.

2.2 SOIL MICROCLIMATE

The receipt, absorption and reflection of solar radiation at the Earth's surface and its re-emission as longwave radiation are the main surface processes driving sub-surface climates. These processes drive the surface energy balance, which in turn determines the soil heat flux and thermal regime. Heat transfer within the soil is dependent on the soil thermal properties, moisture content, physical composition and structure. This section reviews the soil microclimate and thermal regime processes.

2.2.1 THE SURFACE RADIATION BALANCE

Solar radiation is the main source of energy which drives the global climate. Quantifying radiation inputs and losses is therefore fundamental if an understanding of an area's climate is required. Short wave solar radiation which reaches the Earth's surface and is not reflected away is absorbed by the surface and then either passes into it in the form of heat energy or is emitted back into the atmosphere as long wave radiation. These processes are described by the radiation balance:

$$Q^* = K\downarrow + K\uparrow + L\downarrow + L\uparrow \qquad (2.1)$$

where Q^* is net all-wave radiation, $K\downarrow$ is incoming shortwave radiation, $K\uparrow$ is outgoing short wave radiation, $L\downarrow$ is incoming longwave radiation, and $L\uparrow$ is outgoing long wave radiation (Oke, 1987)[3].

2.2.1.1 Shortwave radiation

The amount of short wave radiation which reaches the Earth's surface is determined by:

* Solar output which is affected by cyclic sunspot activity;

[3] Radiative fluxes directed towards the surface are +ve, and those directed away from the surface are -ve.

* The distance between the Earth and Sun which changes regularly due to the Earth's eccentric orbit. The Earth receives maximum solar radiation when it is closest to the sun (perihelion) at the beginning of January and receives least radiation in early July when it is furtherest away (aphelion);

* The angle of the solar beam which changes on a daily, seasonal and latitudinal basis due to the tilt of the Earth's axis;

* Day length which varies with latitude and time of year. In high latitudes for example, maximum day length occurs during the summer solstice, minimum day length occurs during the winter solstice, and equal daylight and darkness is experienced during the transitional equinoxes;

* Atmospheric composition regulates incoming shortwave radiation through the processes of diffusion, absorption and reflection which occur as radiation interacts with clouds, water vapor, carbon dioxide, ozone, and suspended particles within the atmosphere;

* Surface slope, aspect, and altitude (which determines atmospheric thickness) (Barry and Chorley, 1990).

When graphed, the daily receipt of shortwave radiation for a clear sky day in the mid latitudes takes the form of a bell-shaped curve which shows that maximum radiation reaches the Earth's surface at about midday and none at night (Oke, 1987). A similar curve to this is also seen in polar latitudes with the exception that at 'night' during summer, there is still incoming shortwave radiation reaching the surface, unlike in winter when there is 24 hour darkness.

On an annual basis, shortwave radiation nomograms have been developed using empirical relations between radiation, cloud cover, and sunshine hours. Thompson and Macdonald (1962), for example, derived a curve for the Antarctic from data collected at Scott Base in 1958 and 1959 which shows maximum incoming shortwave radiation received in mid December and none from the end of April to mid to late August.

2.2.1.2 Albedo

An important parameter to quantify when describing the surface radiation balance is surface albedo or shortwave reflection coefficient. The albedo describes the ratio of

reflected to incoming shortwave radiation as shown in Equation 2.2 and is given as a fraction or percentage (Barry and Chorley, 1987).

$$\alpha = \frac{K\uparrow}{K\downarrow} \tag{2.2}$$

Net shortwave radiation may be calculated as:

$$K^* = K\downarrow + K\uparrow \tag{2.3}$$

and from this, albedo can be derived as:

$$K^* = (1-\alpha)K\downarrow \tag{2.4}$$

The albedo of a surface is fundamental in determining the amount of energy available for evaporation, convective heat transfers, conduction of heat into the soil and many other physical and biological processes in the near surface layers (Brown and Fitzharris, 1993). The main variables determining surface albedo are it's: roughness; colour; moisture content; and in the case of snow and ice, its transparency which is a function of its thickness and density (Oke, 1987).

Under clear sky conditions, the albedo of many natural surfaces show a diurnal trend in response to changing solar altitude. Due to surface reflectivity increasing at low solar angles, surface albedo decreases throughout the morning as solar altitude increases, and then increases during the afternoon as solar altitude decreases (Brown and Fitzharris, 1993).

This trend is not so obvious on overcast days due to decreased atmospheric transmissivity which minimises solar variations and decreases the dependence of surface albedo on solar altitude. Under these conditions, there is a smaller diurnal range in albedo experienced due to the reduced extremes in solar radiation. Graham and King (1961), showed that the albedo of maize was slightly smaller under overcast conditions, and Stanhill *et al.*, (1966), showed that the degree of cloud cover had no discernible influence on albedo over natural and agricultural vegetation (Nkemdirim, 1972).

Albedo also commonly exhibits diurnal asymmetry with afternoon albedo measurements being higher than morning values. This has been attributed to diurnal variations in surface properties and/or solar radiation fluxes (Arnfield, 1975). For example, leaf wilting usually occurs during the afternoon which increases surface albedo on vegetated

surfaces. It has also been suggested that moist bare surfaces dry out during the day which increases afternoon albedo (Nkemdirim, 1972).

Coulsen and Reynolds (1971) reject this theory because the soil would have to change from completely wet to completely dry to account for this observed difference. The spectral quality of radiation received during the afternoon is however substantially different from that received during the morning in that there is an increase in airborne particulate and gaseous matter, and water vapour. These substances might filter out those wavelengths most susceptible to ground absorption and consequently increase surface albedo during the afternoon (Nkemdirim, 1972).

2.2.1.3 Longwave Radiation

Shortwave energy absorbed by the surface can be re-radiated into the atmosphere as longwave radiation. This process is a function of the surface temperature. The longwave radiation is then either re-radiated back towards the surface from the atmosphere and clouds and is absorbed once more, or is lost to space. The amount of incoming longwave radiation ($L\downarrow$) usually fluctuates slowly throughout the day because it is determined by the atmosphere's temperature and emissivity which also fluctuate slowly.

In overcast conditions, a large proportion of the incoming radiation flux can be longwave radiation. On King Christian Island which has a polar semi-desert climate, for example, $L\downarrow$ contributed 68% of incoming radiation during the summer period 15 July to 14 August, 1973 (Addison and Bliss, 1980).

Outgoing long wave radiation ($L\uparrow$) is governed by surface temperature and emissivity. Surface temperature changes significantly throughout the day which causes $L\uparrow$ to be more variable and larger than $L\downarrow$.

Net long wave radiation ($L^* = L\downarrow + L\uparrow$) is usually negative and small because of this, but can be larger if the surface temperature is much higher than the air temperature (Oke, 1987).

2.2.1.4 Net Radiation

Net radiation is the most important parameter to measure when considering microclimate because it represents the total amount of energy available to drive surface and sub-surface processes. There is usually a net radiation surplus during the day and a deficit at night

which causes the surface to heat up during the day as it absorbs short wave radiation and cool down at night as it emits long wave radiation (Oke, 1987).

2.2.1.5 Radiation balance of the Dry Valleys, Antarctica

The main reason Antarctica is cold is because it receives only a small amount of solar radiation. This is caused by: the low average angle of incidence of the sun's rays at high latitudes; the high albedo of snow which reflects most solar radiation; and the extensive ice and cloud cover over the continent (Hill, 1983). Consequently, the total amount of solar radiation received annually in Antarctica is only about 15% of that received at the equator (Campbell and Claridge, 1987).

In the ice free areas, the net radiation flux during most of the summer months is positive during the middle of the day, and negative at night when the sun is low in the sky (Thompson and Mcdonald, 1962).

At Scott Base, for example, Balks *et al.* (1995) found $K\downarrow$ peaked on clear sky days at approximately 680 Wm^{-2} at solar noon in early January and was a minimum of approximately 160 Wm^{-2} at night. The amount of radiation lost by the surface is extremely variable because it is determined by the surface albedo, temperature and emissivity which are also spatially and temporally variable (Oke, 1987).

Typical values for albedo measured in the ice free areas of Antarctica range from 0.05 for dark coloured basalt at Scott Base, (Balks *et al.*, 1995), to about 0.2 in the Wright Valley which have lighter coloured granitic pavements (Bull, 1966). Fresh snow has an albedo of between 0.75 and 0.95 which means snowfall events can significantly change a site's radiation balance (Thompson and Mcdonald, 1962).

2.2.2 THE SURFACE ENERGY BALANCE

Net radiation at the surface is converted to thermal energy which heats the soil and overlying air, and may be used to evaporate water or melt ice if it is present. These conductive and convective processes can be quantified using the surface energy balance:

$$Q^* = Q_H + Q_E + Q_G \qquad (2.5)$$

Where Q_H is the sensible heat flux, Q_E is the latent heat flux, and Q_G is the soil heat flux. These fluxes are considered positive when they represent energy fluxes away from the surface (as occurs during the day), and negative when they are directed towards the surface (Oke, 1987). Net all-wave radiation on the other hand is considered positive when the surface gains energy and negative when it loses it.

The partitioning of energy between these fluxes is the most important factor determining the microclimate of a surface and is determined by the nature of the surface, and the relative abilities of the soil and atmosphere to transport heat (Oke, 1987).

2.2.2.1 Sensible and latent heat fluxes

The principle energy sinks for net radiation at the soil-atmosphere interface during the day are to the overlying air by convection (Q_H) and to evaporate surface moisture if it's present (Q_E). The partitioning of energy between these two convective sinks is largely determined by the surface moisture content and its availability for evaporation. If moisture is freely available, the latent heat flux will dominate, but if surface moisture content is low, the sensible heat flux will dominate. The Bowen ratio describes the partition of Q^* between these fluxes:

$$\beta = \frac{Q_H}{Q_E} \tag{2.6}$$

If $\beta > 1$, Q_H is greater than Q_E, which means a large proportion of net radiation is used to heat the air and the resultant climate would be warm and dry during the day with a low relative humidity, and cold at night. A desert, for example, can have a Bowen ratio of greater than 10 (Oke, 1987).

If $\beta < 1$, Q_E is greater than Q_H and the climate would be relatively cool and moist. This is because moisture is freely available for evaporation and the latent heat flux will be the dominant heat sink. Tropical jungles are a good example of this type of climate and have Bowen ratios of between 0.1 to 0.3 (Oke, 1987).

The direction of the sensible heat flux towards or away from the surface determines the thermal climate in the atmosphere near to the ground and is dependent on the direction of the air temperature gradient. The sensible heat flux will be positive if the air is cooler than the surface and heat will be lost into the atmosphere. Alternately, the soil surface will gain heat if the overlying air is warmer than the surface and the sensible heat flux will be

negative. As a result of these processes, there is usually a positive sensible heat flux during the day and a negative heat flux late in the day, at night and when advection is strong (Oke, 1987).

Apart from moisture availability, the latent heat flux is dependent on the supply of energy for vaporisation, vapour concentration gradient away from the surface, and atmospheric turbulence to transport vapour away from the surface. Therefore, the latent heat flux is usually greatest during the day when energy is readily available, and continues at night at a significantly reduced rate (Oke, 1987).

2.2.2.2 Soil heat flux

The amount of heat transferred into the soil is largely determined by the strength of the soil temperature gradient and the soil's thermal properties, which vary with moisture content, composition, and compaction (Monteith, 1990). Soil heat flux can be directly measured using soil heat flux plates or alternatively calculated using the flux gradient equation (see Section 3.3).

On an annual basis, the soil normally experiences a net energy storage gain during the summer which causes the profile to warm, and a net energy loss during the winter due to colder surface temperatures. A similar trend also occurs diurnally where heat passes into the soil during the day, and is lost into the atmosphere at night. This however involves a much shallower layer of soil (Oke, 1987).

2.2.2.3 Energy balance of the Dry Valleys, Antarctica

Thompson *et al.*, (1971a) measured continuous meteorological and soil heat flux in the Wright Valley, Antarctica from December 1968 to December 1969 and concluded that the soil heat flux at any time was usually small compared with the above-surface radiation fluxes. This combined with the observation that moisture is not readily available for evaporation, indicates that the direct exchange of sensible heat between the ground and the air was the major component of the site's energy balance.

2.3 SOIL THERMAL REGIME

Temperature is the fundamental factor controlling the rate and type of biological, chemical and physical processes occurring within the soil such as microbial activity, weathering, water movement and evaporation (Koorevaar *et al.*, 1983).

Soil temperature is determined and regulated by the exchange of heat between the soil surface and atmosphere and heat transport processes within the soil. Thermal exchange processes at the soil surface are primarily regulated by meteorological conditions, such as solar energy receipt, wind speed, and sub surface heat flow occurs mainly through the processes of conduction and vapour convection.

The rate and depth to which soil temperature is influenced by the surface energy flux is determined by the soil's thermal properties. The thermal properties most important in determining the soil thermal regime are: specific heat, heat capacity; thermal conductivity; diffusivity; and thermal admittance.

2.3.1 SPECIFIC HEAT (c_S) AND HEAT CAPACITY (C_S)

Soil temperature is dependent on the specific heat and heat capacity of the soil which describe the amount of energy necessary to raise a unit mass (specific heat), or volume (heat capacity) of the substance through a temperature change of 1 degree Kelvin (Oke, 1987). In other words, they describe the resultant temperature change caused by the absorption or release of a certain amount of energy to or from the soil.

The specific heat of a substance (J kg^{-1} K^{-1}) can be determined using the equation:

$$c_s = \frac{Q}{\Delta T} \tag{2.7}$$

where Q is the amount of heat absorbed or lost by the substance and ΔT is the change in temperature, $\Delta T = T_1 - T_0$ (Taylor and Jackson, 1986). The most useful term for science is heat capacity which can be determined by multiplying the substances specific heat by its bulk density (Rosenberg, 1974).

The heat capacity of soil can be calculated using an equation developed by De Vries in 1963 (Oke, 1987) which sums the weighted heat capacity of each soil component:

$$C_s = C_{min}x_{min} + C_{org}x_{org} + C_w x_w + C_a x_a \qquad (2.8)$$

where x_{min}, x_{org}, x_w *and* x_a are the volume fractions of the soil's mineral, organic matter, water and air constituents respectively. The last term can usually be ignored without causing great error, because the heat capacity of air is negligibly small compared to the other values (Oke, 1987).

Due to the relatively high specific heat of water (4.18×10^3 J $kg^{-1}K^{-1}$) compared to that of most solids (~1.0×10^3 J $kg^{-1}K^{-1}$), both the specific heat and heat capacity of a substance, especially soil, are strongly dependent on moisture content (Jumikis, 1977). A dry sandy soil with 40% pore space, for example, has a specific heat of 0.80×10^3 J $kg^{-1}K^{-1}$, and the same soil when saturated has a heat capacity of 1.48×10^3 J $kg^{-1}K^{-1}$ (Oke, 1987).

When water freezes, its specific heat falls to about 2.1×10^3J $kg^{-1}K^{-1}$ which can effect the soil thermal regime. Therefore when dealing with frozen soils, the specific heat of frozen water should be used in Equation 2.7 instead of the specific heat of liquid water (Jumikis, 1977).

2.3.2 THERMAL CONDUCTIVITY (K_S)

Thermal conductivity characterises the rate of heat flow by conduction within a substance. It is defined as the quantity of heat that flows through a unit cross-sectional area (m^2) of the substance per unit time (s), under a unit temperature gradient ($1°C/cm^{-1}$) and is given the units Wm^{-1} K^{-1} (Taylor and Jackson, 1986a).

Heat is conducted through solid particles, through pore water and thin films surrounding aggregates or as annuli at the points of contact between particles, and through air and ice within soil pores (Sepaskhah and Boersma, 1979). A soil's thermal conductivity is variable with depth and time because it is dependent on a number of fluctuating variables such moisture content, temperature, composition, salinity, bulk density, and grain size (Jumikis, 1977).

Gavril'ev (1989) for example demonstrated that soil thermal conductivity varied significantly in sand, sandy loam and loam soil's with varying moisture contents. This occurs as air, which is a poor conductor (k_s = 0.025 Wm^{-1} K^{-1}) is expelled and replaced by water which has a thermal conductivity over 20 times that of air (k_s = 0.57 Wm^{-1} K^{-1}).

At sub zero temperatures, soil moisture plays an even more important role in determining the soil's thermal conductivity. Barkovskaya *et al.*, (1983) made detailed observations of the thermal conductivity of freezing and thawing soils and developed a general type curve of thermal conductivity versus temperature during the freeze-thaw process (Figure 2.2).

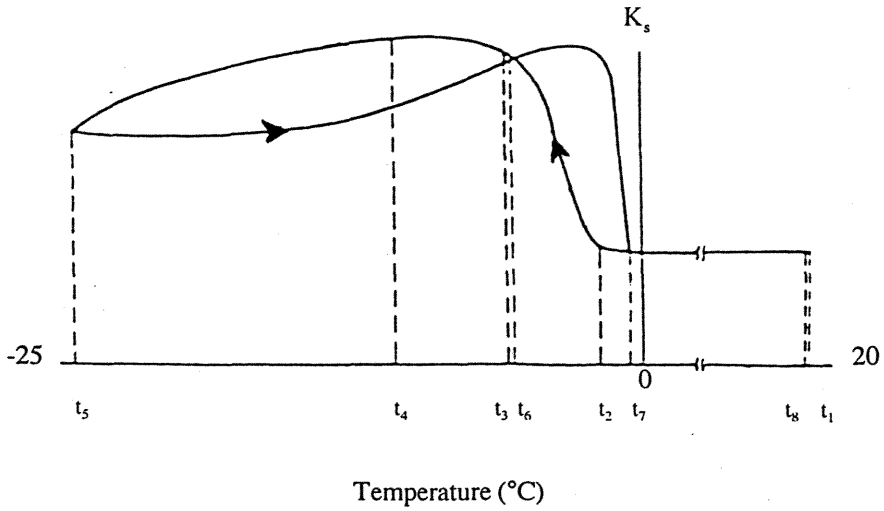

Figure 2.2 General type curve of soil thermal conductivity during the process of freezing and subsequent thawing (adapted from Barkovskaya *et al.*, 1983).

Soil thermal conductivity in the positive temperature range (t_1 - t_2) is fairly constant, but when freezing point is reached (t_2), the thermal conductivity increases rapidly (t_2 - t_3). This is caused by intense phase transformation of soil moisture into ice crystals which have a thermal conductivity four times that of water. The intensity of phase transition then decreases at t_3 and the soil's thermal conductivity begins to level off once the amount of moisture freezing decreases.

As temperature continues to decrease (t_4 - t_5), the soil thermal conductivity decreases due to microstructural changes in the frozen ground such as microcracks in ice and ice fragmentation. Thermal conductivity can decrease by 25-30% during this interval with least decrease found in sandy soils and most in peat.

During thawing, the soil thermal conductivity does not coincide with the values observed during freezing. This hysteresis can be attributed to the development of irreversible structural transformations and to the phase change of ice back to water. The hysteresis loop has been observed in practically all frozen ground studied and the area of the loop is dependent on the soil moisture content, structure and intensity of structural change.

During the phase transformation from ice to water (t_6 - t_7), the soil thermal conductivity can exceed that observed during the freezing process. T his is due to a difference in phase

content and structure at the same temperature. Throughout the entire freeze-thaw process, the maximum difference in thermal conductivity values observed was 30% (Barkovskaya *et al.*, 1983).

A decrease in temperature has also been found to slightly increase thermal conductivity in crystalline rocks and reduce it in amorphic rocks due to the different modes of heat transfer in each media (Barkovskaya *et al.*, 1983). This might be significant in Antarctic soil's because many are covered with pebble pavements which strongly influence the amount of heat entering the soil

The thermal conductivity of the individual components making up the soil is also important in determining its overall thermal conductivity. Pure quartz for example has a relatively high thermal conductivity as shown in Table 2.2. A quartz rich soil therefore has a relatively high thermal conductivity compared to other mineral soils. Organic matter has a very low thermal conductivity and has an insulating effect which minimises heat conduction (Richter, 1987).

Table 2.2 Thermal Conductivity of various substances
(Oke, 1987 and Koorevaar *et al.*, 1983).

Material	**Remarks**	**Density (ρ) (kg $m^{-3} \times 10^3$)**	**Thermal Conductivity (k_s) ($Wm^{-1} K^{-1}$)**
Sandy soil (40% pore space)	Dry	1.6	0.3
Sandy soil (40% pore space)	Saturated	2.0	2.2
Peat soil (80% pore space)	Dry	0.3	0.06
Peat soil (80% pore space)	Saturated	1.1	0.5
Quartz	Dry (10°C)	-	8.8
Snow	Fresh	0.1	0.08
Snow	Old	0.48	0.42
Ice	Pure (0°C)	0.92	2.24
Water	Still (4°C)	1.0	0.57
Air	Still (10°C)	0.0012	0.025

Soluble salts such as magnesium chloride, sodium chloride, sodium sulphide and calcium chloride to a lesser affect, have also been found to affect soil thermal conductivity. Noborio and McInnes (1993), found that a 1 mol kg^{-1} increase in salt concentration can reduce soil thermal conductivity by up to 20%. The reasons for this are not fully understood but could be due to microstructural and/or ionic changes occurring under highly saline conditions.

Barkovskaya *et al.,* (1983), also found that the thermal conductivity of salinised sandy soil stops decreasing at about -15°C and slowly begins to increase. This is because the number of thermal contacts within the soil increases as salt crystallises out of solution during the freezing process.

Soil bulk density and grain size also affects soil thermal conductivity due to the number of contact points and air spaces allowing or restricting conduction. Highly compacted soils, for example, contain few pores and have many particle contact points which is ideal for heat conduction (McLaren and Cameron, 1990).

2.3.3 THERMAL DIFFUSIVITY (κ_S)

The thermal diffusivity of a soil describes the rate at which a change in temperature travels through the soil (m^2/s^{-1}) and is a function of the soils thermal conductivity and heat capacity:

$$\kappa_s = \frac{k_s}{C_s} \tag{2.9}$$

Temperature change is therefore most rapid in materials with a high thermal conductivity and a low heat capacity such as dry sand (Jumikis, 1977). When water is added to a dry soil, the thermal diffusivity will initially increase because its thermal conductivity increases faster than the soil's heat capacity, but in a wet soil, the increase in thermal conductivity is slower than the increase in heat capacity and the thermal diffusivity consequently decreases (Monteith and Unsworth, 1990).

Thermal diffusivity also determines the depth of penetration and amplitude of the diurnal and annual temperature wave. For example, the daytime heat input will generate a temperature wave that travels rapidly and to considerable depth in a soil where conductivity is high, but if it takes large amounts of heat to warm intermediate layers because of high heat capacity it will be slowed and not penetrate as far (Oke, 1987).

2.3.4 THERMAL ADMITTANCE (μ_S)

Thermal admittance is a measure of the ability of a surface to accept or release heat and is determined by the soil heat capacity and thermal diffusivity, but can also be calculated using the soil thermal conductivity:

$$\mu_s = C_s \kappa_s = k_s \sqrt{C_s} \tag{2.10}$$

Surfaces with large thermal admittance will usually accept or release heat from storage fairly easily and consequently show relatively small surface temperature changes throughout the day (Oke, 1987).

2.3.4.1 Soil Heat Flow

The movement of heat within soil can be quantified using Fourier's law which is a one-dimensional *steady state heat flow* Equation.

$$Q_G = -k_s \left(\frac{\Delta T}{\Delta z}\right) \tag{2.11}$$

where $\Delta T/\Delta z$ is the temperature gradient defined as the rate of change in temperature (T) with depth (z). The negative sign indicates the heat flux is in the opposite direction to the temperature gradient which means heat flows from areas of high to low temperature (Oke, 1987). Consequently, under isothermal conditions, there is no heat flow which means the soil temperature is in equilibrium with its surroundings (Rosenberg, 1974).

For this heat flow model to work, the following assumptions have to be made: surface temperature remains constant; the soil is homogenous; and the soil thermal properties do not change with depth (Koorevaar *et al.*, 1983). This approach therefore allows a basic understanding of the processes involved in heat transport, but is not applicable to many real world situations.

The transient, or *non-steady heat flow* Equation (2.12) is however, more realistic because it considers temperature change (∂T) over time (t) and depth (∂z), and takes into account the soil thermal diffusivity $(\kappa_s = k_s/C_s)$.

$$\frac{\partial T}{\partial t} = \kappa_s \frac{\partial^2 T}{\partial z^2} \tag{2.12}$$

This equation can be solved numerically if the initial temperature and depth is known and gives results comparable to field conditions (Hanks and Ashcroft, 1980). Where moisture flow in the liquid and vapour phase is likely however, local heat sinks and sources created by these processes must also be considered.

A. Coupled Heat and Moisture Flow

The interaction of heat and liquid water flow in saturated and dry soils is negligible, but is very important in moist soils like those found in permafrost environments. The main forms of coupled heat and water flow can be explained in terms of thermally driven water flow, and water-potential-driven heat flow.

Thermally driven water flow can be explained using the classic example of the rapid migration of water and water vapour under a temperature gradient towards a freezing front (Hillel, 1980). Water flow is induced by spatially variable surface tension caused by the temperature gradient, and vapour moves in response to the resultant vapour pressure difference (Buchan, 1991).

A thermal gradient of $1°C/cm^{-1}$ for example, can causes a vapour flow of about 0.4 to 2.0 $mm\ day^{-1}$ due to this redistribution of kinetic energy (Rosenberg, 1974). As a result of these processes, large amounts of vapour can be transported within the soil which can form features such as ice lenses and frost heave.

Water-potential driven heat flow works on the principle that as water flows into soil, it also transports heat. Intense infiltration of water for example, can cause heat to be transported into the soil through the process of convection (Buchan, 1991).

B. Heat and water vapour flow

Heat and water vapour flow processes can also be strongly coupled causing the resultant conductive heat flux to be accompanied by a sizeable latent heat flux. This occurs because the vapour flux is partitioned into two components, the thermal vapour flux and the isothermal vapour flux. The thermal vapour flux transports latent heat via a thermal gradient from hotter (high vapour pressure) to cooler (lower vapour pressure) regions and the isothermal vapour flux operates on a water-potential-driven latent heat transfer (Buchan, 1991). These processes are important features of the soil thermal regime and could potentially influence the microclimate of Antarctic soil if a large amount of water vapour is present in the active layer.

2.3.5 PERMAFROST AND ACTIVE LAYER PROCESSES

As a result of the surface conditions and resultant soil heat flux which is dependant on the soil physical and thermal properties, many soils have a distinct thermal regime. On a daily basis, the soil surface layers usually undergo a period of warming during the morning and early afternoon when the soil surface is relatively warm, and cool during the late afternoon and evening when the surface temperature is colder than the underlying soil. A similar cycle also occurs on an annual basis which if felt at greater depths, where the soil warms during summer and cools during winter (Koorevaar *et al.*, 1983).

These cycles also occur in cold climates during the summer months, although soils in the mid latitudes are subject to seasonal freezing, and much of the regolith of those at high latitudes is permanently frozen (Hillel, 1980). If the soil or rock material remains below 0°C for more than two consecutive years, it is called permafrost (Clark, 1988). This is one of the most important features of Antarctic soils, they always rest on a layer of permanently frozen and frequently ice-cemented material (Campbell and Claridge, 1987).

Balks *et al.* (1995), found that soil temperatures at Marble Point in McMurdo Sound, Antarctica, remained below 0°C for 10 months of the year, fell as low as -35°C in winter, surface temperature rose to +14°C during summer, while temperature at 0.55 m which was close to the ice-cemented permafrost rose to 2°C.

In most cold desert environments, the permafrost is overlain by an active layer which is affected by freeze/thaw processes throughout the summer months as shown in Figure 2.3. In Antarctic soils, the frozen ground table rises to the surface about the end of January and remains there until December when it migrates down to the permafrost.

The thickness of this active layer is highly variable because it is determined by the soil thermal and physical properties which are spatially and temporally variable. During the summer months, the thickness of the unfrozen soil increases, starting at the surface and following the 0°C isotherm down until the maximum thawing depth is reached. In moist soil, this active layer can be identified by its unfrozen nature, and its lower boundary is delineated by frozen, ice-cemented soil (Campbell, unpublished, 1996).

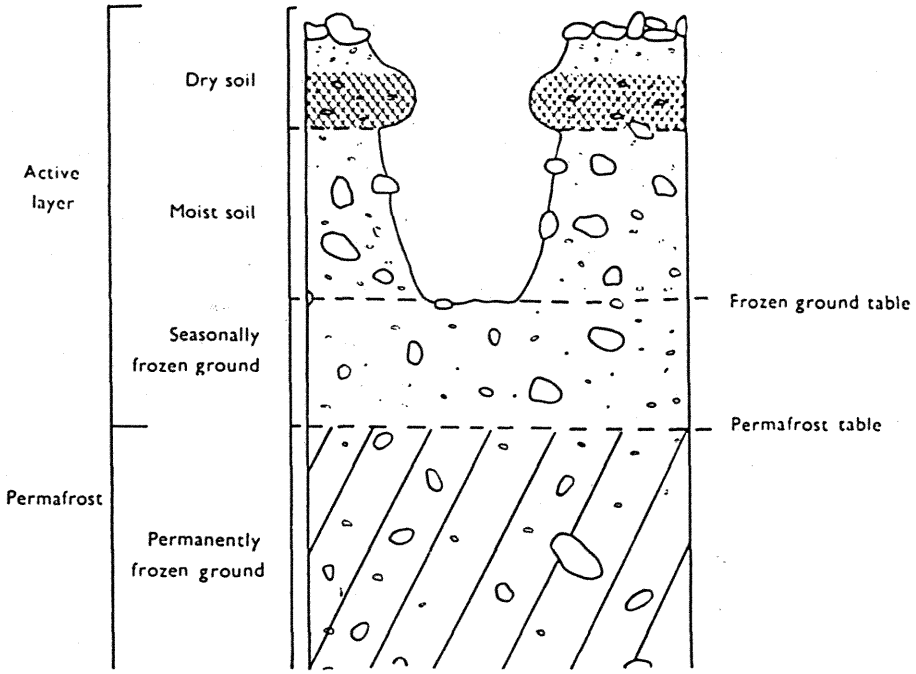

Figure 2.3 Idealised diagram of a typical soil profile found in the Antarctic Dry Valleys (adapted from McCraw, 1967).

CHAPTER THREE

METHODOLOGY

This chapter reviews the measurement methods available to characterise the soil microclimate and gives a detailed description of the techniques used, along with a discussion of the possible sources of error. There were however several challenges associated with this extreme environment which had to be overcome. Equipment able to work at sub zero temperatures had to be used, surface instruments had to be well secured to ensure they were not affected by strong winds, data-logging equipment and junction boxes had to be placed in a sealed box to prevent wind blown snow affecting the circuitry, and some instruments needed earthing to prevent static build-up within the system.

3.1 SURFACE AND NEAR-SURFACE MEASUREMENTS

Surface variables which need to be quantified are: incoming and outgoing solar radiation; net radiation; surface albedo; air temperature; and wind speed and direction.

3.1.1 SOLAR RADIATION AND ALBEDO

Standard techniques have been developed for measuring incoming, outgoing and net radiation using pyranometers and net radiometers, all of which are readily available and accurate if calibrated correctly. Q^* was measured using a REBS Q6 net radiometer mounted between 0.6-0.8 m above the ground and upward and downward facing Kipp and Zonen pyranometers were used to measure $K\downarrow$ and $K\uparrow$ respectively. The longwave components of the radiation balance are not so easily measured, so $L\uparrow$ was calculated using Equation 3.1 and $L\downarrow$ determined by rearranging and solving the radiation balance (Equation. 2.1).

$$L\uparrow = -\varepsilon\sigma T_0^4 \qquad (3.1)$$

Where ε is the surfaces emissivity, σ is the Stefan-Boltzmann constant (σ = 5.67×10^{-8} Wm^{-1} K^{-4}), and T_0 is the surface temperature in degrees Kelvin. An estimate of ε=0.95 was used because most soils have an emissivity of between 0.9 and 0.98, depending on their colour and moisture content (Oke, 1987).

Surface albedo was calculated as:

$$\alpha = -\frac{K\uparrow}{K\downarrow} \tag{3.2}$$

3.1.2 OTHER MEASUREMENTS

Air temperature was measured with a shielded probe ~0.8 m off the ground, and an anemometer and windvane (Vector Instruments Skye 2031, A101M; and W200P respectively) were mounted on top of a pole ~1.5 m tall to measure wind speed and direction. These instruments, along with the radiation equipment were connected to a CR10 data logger which recorded data at set intervals.

All instruments were bolted to an aluminium pipe secured to a surveying tripod as seen in Figure 3.1. A weighted bag was suspended from the tripod to anchor it securely and guy ropes were also needed for strong winds. A wooden box was used to house the data logger and a 12 volt battery which powered the system.

Figure 3.1 Instruments set up at the Scott Base field site. The pyranometers are the disk like instruments on each end of the attachment pipe and the shielded probe is the white instrument in the middle. The net radiometer is fixed to the arm perpendicular to the main pipe.

3.2 SUB-SURFACE MEASUREMENTS

Soil temperature and heat flux are the main sub-surface variables which need to be quantified to determine the soil's response to the surface conditions.

3.2.1 SOIL TEMPERATURE

The most suitable type of thermometer for this research are thermocouples because they are cheaply constructed, small in size, have a rapid response to temperature change, and are adaptable for automatic recording (Taylor and Jackson, 1986a).

Thermocouples operate on the principle that a circuit made of two dissimilar metals containing two thermoelectric junctions will produce a total electromotive force (emf)

proportional to the difference in temperature between the two junctions. Therefore, if the temperature at one junction is known (the 'reference' or 'cold' junction), the temperature at the other junction (the 'measuring' or 'hot' junction) will produce a proportional electromotive force which can be measured with a potentiometer, galvanometer, or millivolt meter which can then be converted into an equivalent temperature value (Taylor and Jackson, 1986a).

Type T (copper-constantan) thermocouples epoxied in 3 mm diameter, 50 mm long stainless steel tubes were used and a CR10 data logger recorded the data. The probes were calibrated in an ice bath before use and the data logger was insulated with foam rubber to ensure the junctions and the reference temperature sensor in the wiring panel stayed the same temperature.

Soil surface temperature was measured using a four junction thermocouple which gave an average measurement every half an hour (Figure 3.2 a). This was done to account for spatial variability of surface layer materials. Soil chips from each site were glued to the thermocouples to ensure the shiny probes behaved in a similar manner to the surface materials (Figure 3.2 b and c). The cables were also covered with a layer of surface material to prevent anomalous conduction of heat to the sensors.

Sub-surface measurements were made by inserting the thermocouples directly into the undisturbed face of the soil pit. The average of four measurements made at 0.01 m was also taken to take account of spatial variability in the near surface layers caused by surface stones.

The distribution of probes in each pit was site specific and depended on the soil texture, number of probes available, the depth to ice cement if present, and the feasibility of installation. The ideal distribution would be to have closely spaced probes in the active surface layers where soil temperature varies greatly, and less probes at depth where the temperature is less variable (Buchan, 1991). Fritschen and Gay (1979) suggest a reference board with pre determined thermocouple installation depths drilled through it could be used to ensure even sensor distribution.

Unfortunately this instillation method was not practical due to the loose, un-consolidated nature of Antarctic soils. The ideal distributions was also not always possible due to the large number of stones in the soil. It is very difficult to dig a pit with stable faces and it is even more difficult to insert temperature probes into them without the pit collapsing. Therefore, the probes had to be inserted where possible while trying to maintain a reasonable distribution as shown in Table 3.1.

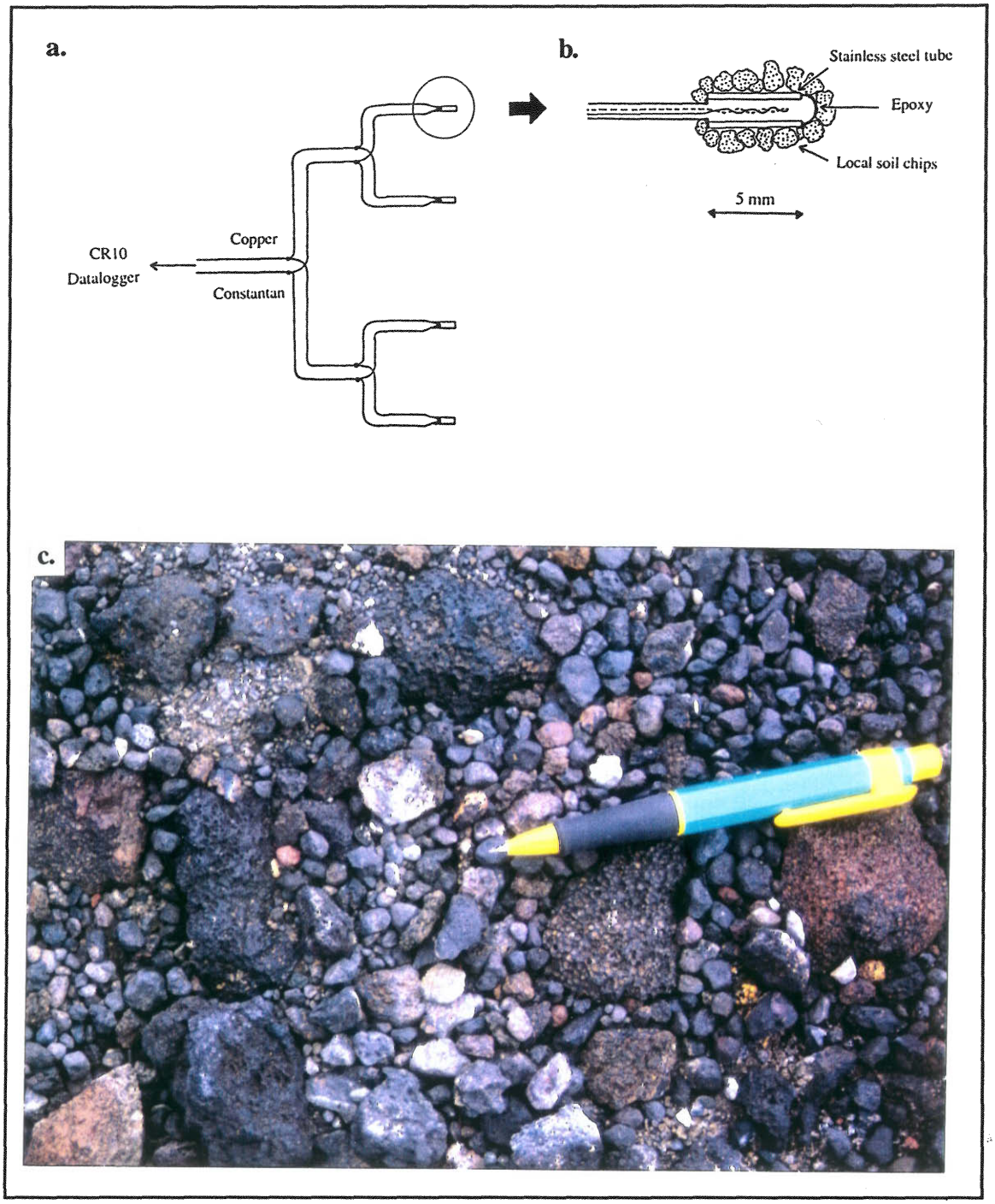

Figure 3.2 Soil surface thermocouple construction and instillation: a) thermocouple wiring configuration; b) measurement junction construction using local soil chips; c) measurement junction installed at the Scott Base site (sensor is at the tip of the pen).

Table 3.1 Thermocouple instillation depths at each field site.

Probe	Scott Base	Coombs Hills	Northwind Valley
TC 1	surface	surface	surface
TC 2	0.01	0.01	0.01
TC 3	0.02	0.02	0.02
TC 4	0.04	0.04	0.04
TC 5	0.06	0.06	0.07
TC 6	0.09	0.09	0.10
TC 7	0.12	0.12	0.13
TC 8	0.15	0.145	0.16
TC 9	0.18	0.17	0.19
TC 10	0.20	0.19	0.22
TC 11	0.24	0.23	0.24

To minimise disruption of the soil surface and temperature profile when installing the temperature probes, the following steps were taken:

I. an outline of the pit which was about 0.2 m^2 was marked on the soil surface and a ground sheet was placed around it to minimise surface disturbance;

II. surface stones were removed and placed in a bag so they could be used to restore the site once the probes were inserted and the pit refilled;

III. the next layer of surface material was then scraped away to a depth of about 1 cm and placed in a second bag;

IV. while trying to preserve a vertical, intact face on one side of the pit, the next layer of soil down to a depth of about 5 cm was removed, bagged, labelled and put into a chillybin to maintain the soils natural temperature;

V. step iv was repeated until ice cemented ground prevented further digging or consolidated material was reached.

VI. the depth of the pit was measured from a reference surface level and the probe insertion depths were determined. Probes were closely spaced (1-2 cm) near the

surface where temperature changes are most noticeable and further apart (4 cm) below 10 cm where the soil tends to be more isothermal.

VII. a small screwdriver was used to make a hole in the pit face for the deepest temperature probe to be inserted and the probe was gently pushed into the undisturbed soil. The soil taken from that depth was then replaced and compacted by hand to restore the soil bulk density;

VIII. step VII was then repeated for the remaining thermocouples;

IX. the soil surface was carefully restored to its original appearance (Figure 3.3).

Figure 3.3 Restored soil surface at the Coombs Hills site once the thermocouples had been installed.

It is assumed the soil thermal regime was not significantly altered during this process and the subsequent measurements are representative of an undisturbed profile because: the probes were inserted into undisturbed soil, the excavated soil was kept at its original temperature and returned to where it came from, and the depth of the pit did not exceed the soils diurnal temperature regime so it would have returned to normal within 24 hours.

3.2.2 SOIL HEAT FLUX

The main methods available for measuring soil heat flux are: the calorimetric method; the gradient method; and the soil heat flux plate method (Fuchs, 1986). The first two methods determine the heat flux of representative soil cores in the laboratory and consequently involve disturbing the soil structure. The heat flux plate method can be used in the field without significantly disturbing the soil. This method is therefore the most appropriate technique for this study because the actual amount of energy passing into the soil needs to be accurately quantified.

The soil heat flux plate method uses soil heat flux plates to measure the temperature gradient created by the flow of heat into the soil. The type used in this study were constructed from Peltier coolers (Melcor, model # 4CP 1.4-71-06L) which produce a voltage proportional to the temperature difference between its two surfaces (Weaver and Campbell, 1985). Three plates buried ~0.03 m below the surface were used to take account of spatial variability and a CR10 data logger was again used to record the data every half hour. This time was reduced to 10 minutes after a couple of days at the Coombs Hills to give more detailed data records.

Care was taken to ensure good thermal contact was made between the heat flux plates and the surrounding soil to prevent underestimation of the soil heat flux. The soil surface was also repaired carefully to maintain its natural characteristics, and the cables were buried to prevent heat conduction.

A depth of 0.03 m was chosen to ensure the plates were not exposed to direct radiation which can cause inaccurate measurements (Fritschen and Gay, 1979).

To determine the actual soil heat flux at the surface (Q_G), the rate of heat storage in the soil layers between the surface and the heat flux plates needs to be quantified:

$$\Delta Q_s = d(\frac{\Delta T_s}{t})\rho_s(C_s + wC_w) \qquad (3.3)$$

where ΔQ_S is the change in storage, d is the soil layer depth (0.03 m), ΔT_S is the change in temperature between measurement periods, t is the time interval (s), ρ_s is the soil dry bulk density (kg m^{-3}), C_S is the heat capacity of the dry soil and C_w is the heat capacity of water (4.18×10^3 Jm^{-3} K^{-1}), and w is the gravimetric soil moisture content of the layer (Balks *et al.*, 1995). If the surface is frozen, the heat capacity of ice (2.1×10^3 Jm^3 K^{-1}) should be used as a result of its changed thermal properties.

ΔT_s was measured at a depth of 0.01 m using the spatial average of four thermocouples as described for the surface measurements. The last five minutes of each measurement period was averaged and subtracted from the value for the previous period.

The surface soil heat flux was then determined using Equation 3.4 where Q_{Gp} is an average of the soil heat flux plate measurements.

$$Q_G = Q_{Gp} + \Delta Q_s \tag{3.4}$$

3.3 SOIL PHYSICAL CHARACTERISTICS

Physical soil characteristics which influence the soil microclimate and thermal regime include: heat capacity; thermal conductivity; moisture content; bulk density; particle density; grainsize distribution; and salt content.

3.3.1 HEAT CAPACITY (C_s)

The standard approach to measure the heat capacity of a unit volume of soil ($Jm^{-1} K^1$) is to determine its mineral *(m)*, water *(w)*, and organic *(o)* composition (x denotes the volume fraction), and sum the heat capacity of these components as shown in Equation 3.5 (Buchan, 1991).

$$C_s = x_m C_m + x_o C_o + x_w C_w \tag{3.5}$$

The main techniques used to physically measure specific heat involve using a calorimeter or a specific heat probe. The calorimetric method is laboratory based and involves placing a known mass of soil in a calorimeter either dry or as a dilute suspension, measuring the initial temperature of the sample, adding a known quantity of heat, and measuring the sample's final temperature. The heat capacity of the sample is then determined from the initial and final temperature difference, the amount of heat added, and the mass of the sample. Corrections do however have to be made for thermal leakage of the calorimeter and carrying out multiple measurements is very time consuming (Taylor and Jackson, 1986b).

Specific heat probes on the other hand can be used in the field and operate on the principle that if an instantaneous heat pulse is released into the soil by a line source, the maximum

temperature rise at a known distance from the source is directly related to the quantity of heat produced at the source, and inversely related to the heat capacity of the soil.

This method can give a variation coefficient of 1% on replicate samples if the probe is calibrated correctly, but any change in the distance between the heat source and the temperature sensor can significantly reduce its accuracy. A 2% uncertainty in the distance between the probes can result in a 4% error in the specific heat (Campbell *et al.,* 1991). Kluitenbenberg *et al.,* (1993) also concluded that a 1% error in the probe spacing resulted in a 2% error in soil heat capacity using the same technique.

The specific heat probe proved to be the only method available due to problems associated with setting up an accurate calorimeter. The specific heat probe was also most suitable because a large number of samples can be processed quickly and easily, and the size of the sample is not critical. It was not however available when work was done in the field, so measurements made in the laboratory on oven dry samples had to be corrected for field moisture content.

3.3.1.1 Measuring soil heat capacity using a specific heat probe

A specific heat probe (model SH2-20X) produced by Soiltronics Ltd, Seattle, USA, was used which consists of two parallel probes, one containing a heating wire and the other a thermocouple. The probe was connected to a CR10 data logger which was programmed to switch the heater probe on for 8 seconds and record the temperature change detected by the other probe for 98 seconds. ΔT_{max}, power and specific heat (MJ $m^{-3}s^{-1}$) are stored in the CR10 memory.

A portable PC was used to initiate an experiment and process the information to calculate the soil heat capacity using the Equation:

$$C_s = \frac{Q}{(e\pi r^2 \Delta T_{\max})} \tag{3.6}$$

Where C_s is the soils heat capacity, Q is the power used to heat the probe, e is the base of natural logs, r^2 is the distance between the probes and ΔT_{max} is the maximum temperature recorded by the thermocouple (Soiltronics Ltd, 1995).

As a result of the stony nature of Antarctic soil, the distance between the probes, which is critical in determining the soil heat capacity, changed with every insertion. To solve this

problem, a plastic divider was secured between the two probes to ensure they are kept a standard distance apart (6.1495 mm) (Figure 3.4).

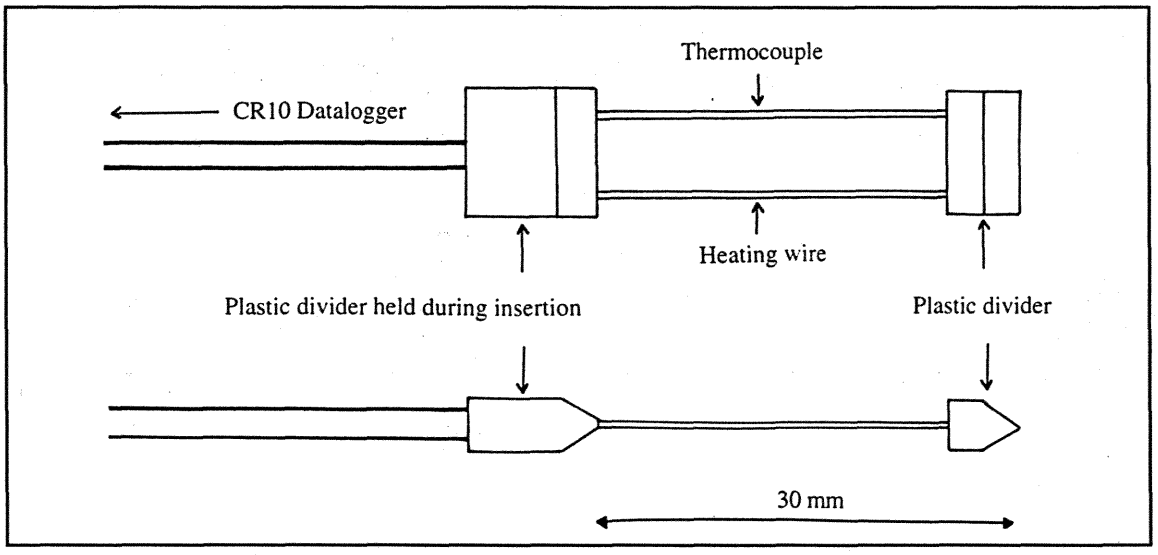

Figure 3.4 Specific heat probe construction and modification.

It is assumed that this does not alter the specific heat measurement significantly because a similar divider is at the other end of the probe which is held during insertion.

Calibration of the probe in agar immobilised water as recommended by Soiltronics Ltd (1995) was unsuccessful. The immobilised water around the probes became mobile as the heating probe warmed (≈60°C). Convection currents consequently formed around the probes and this caused considerable variation in heat capacity measurements of this standard.

Fine quartz sand was therefore used as an alternative standard to avoid these problems which has a heat capacity of ~2 MJ m^{-1} K^{-1} (Koorevaar *et al.*, 1983).

Five measurements were made on each sample to obtain an average value, and the sample was re-packed in between measurements to take account of natural variability within the sample and to minimise temperature changes around the probes which could affect subsequent measurements. To ensure the bulk density of each sample remained constant between measurements, the sample was packed to the same level each time.

Assumptions made when using this method which relies on the theory that an instantaneous line source of infinite length is used, are: (i) the heat source of finite length approximates an infinite source; (ii) the cylindrical source approximates a line source; and

(iii) the short-duration heat pulse approximates an instantaneous release of heat (Kluitenberg *et al.*, 1993).

Bristow *et al.*, (1994), found that measurements of volumetric heat capacity made for sand using this dual probe heat pulse method agreed well with independent estimates obtained using the de Vries method of summing the heat capacities of the soil constituents.

3.3.2 SOIL THERMAL CONDUCTIVITY (k_s)

The main methods used to measure soil thermal conductivity are : steady-state methods; transient-state methods; heat flux methods; and inverse methods (Buchan, 1991).

Steady-state methods involve establishing a steady, uniform temperature gradient $\Delta T/\Delta z$ in a containerised sample by supplying heat at a rate Q (Wm^{-2}) at one end. Conductivity is then calculated by rearranging Equation 2.11:

$$k_s = -\frac{Q}{(\frac{\Delta T}{\Delta z})} = -\frac{\Delta z Q}{\Delta T} \qquad (3.7)$$

However, a serious problem with this method is the moisture redistribution caused by the migration of water from warmer to colder zones, leading to non uniformity. Therefore this method should only be used for saturated or very dry soils (Jackson and Taylor, 1986).

Transient-state methods have been used extensively both in the laboratory and field. A cylindrical heat probe is inserted into the soil and the rate of temperature change is measured with a small, in-built sensor. A plot of T against log t can then be made and the soil thermal conductivity is a function of the lines slope (Jackson and Taylor, 1986).

An alternative to making this assumption is to develop a model of temperature change over time and adjust the thermal conductivity until the predicted probe temperature agrees with the measured values (Riha *et al.*, 1980).

This technique avoids major moisture redistribution and 'powerless probes' can be constructed which are durable, portable and do not need heater circuitry (Buchan, 1991).

Heat Flux methods involve measuring the soil heat flux (Q_G) and temperature gradient to solve Equation 3.7. This technique is simple but can give serious measurement errors if sub surface evaporation is high and freeze/thaw effects are not considered (Buchan, 1991).

Inverse methods involve measuring the soil's response to a known input (Eg solar radiation), and calculating its thermal conductivity from its response. A simple approach developed by Dr G. Buchan of the Soil Science Department at Lincoln University involves measuring soil temperature at several depths over time and determining the magnitude of the multi-day average diurnal variation. This is then plotted against depth to determine the damping depth (D), and soil thermal conductivity is calculated using the equation:

$$D = \sqrt{\frac{2\kappa_s}{w}} \tag{3.8}$$

where κ is the thermal diffusivity ($\kappa H_s = K_s/C_s$), and w is the diurnal angular frequency (7.27×10^{-5}).

Out of the four methods discussed, the best method to use is the transient-state method which can be used in the field and on samples in the laboratory.

3.3.2.1 Thermal Conductivity measurements in the field

For measurements in the field, an aluminium probe was constructed which contained a thermocouple that was connected to a CR10 data logger. The probe was then either heated to ~70°C in a hot thermos flask, or cooled to ~0°C, and quickly inserted into the face of the soil pit. Once the probe was fully inserted, the probe temperature change over time was recorded. The data logger was stopped after 3 minutes and the probe was removed and re-heated ready for the next measurement. This was done at regular intervals down the profile with care being taken to ensure the probe was dry before insertion and heating effects from each insertion were not affecting neighbouring measurements.

The recorded data was then fed into a thermal conductivity simulation programme based on a computer model in Campbell (1985) which compares a numerical solution for the probes temperature change, using an estimated thermal conductivity, with the actual

temperature change. The model's thermal conductivity is then adjusted until the numerical solution agrees with the recorded data.

A similar method was used by Riha *et al.,* (1980) who used a finite element model to solve the radial heat flow equation. They found that the calculated thermal conductivity of sand, silt loam, and forest litter were in good agreement with those obtained using a water bath method which is a steady-state method.

Riha *et al.,* (1980) noted that rapid insertion of the probe precisely at time zero was essential to minimise error, especially in highly conductive medium; a guide was useful to prevent an oversize hole in the soil which possibly causes contact resistance; that in highly conductive media, condensation around the cold probe may increase thermal conductivity.

3.3.2.2 Thermal Conductivity Measurements in the Laboratory

A powered probe acquired after the field work was complete was used in the laboratory to compare the powerless probe results. An outline of the measurement technique used is given.

The probe is produced by Soiltronics Ltd and consists of a heating element and thermocouple embedded in a stainless steel tube 0.9 mm diameter. The program TC20-CHR for a CR10 data logger is used to heat the probe for 90 seconds, record the temperature and power at logarithmically spaced time intervals. This information is then fed into the PC Basic programme TCV which is based on the Marquardt method to determine the samples thermal conductivity. It does this by using an algorithm for least-squares estimation of the non linear regression (Soiltronics Ltd, 1995).

Five measurements were made on each sample to obtain an average value and the sample was re-packed to the same level in the container each time to maintain its bulk density and to ensure subsequent runs were not affected by induced temperature gradients. The thermal conductivity of samples at various water contents was also investigated.

3.3.3 SOIL MOISTURE CONTENT

The amount of moisture in soil significantly affects its thermal regime and microclimate because of water's unique thermal properties.

The easiest and most common method for measuring soil moisture content is to take a soil sample, weigh, oven dry, re-weigh and calculate the moisture content as the difference between the two weights. This gives the soils gravimetric moisture content *(w,* kg/kg), which is not as useful as knowing the soils volumetric moisture content (θ_v m^3/m^3) which is given as a percentage. This can be obtained by dividing the gravimetric moisture content by the field moist volume of the sample or by multiplying it by the soil dry bulk density (McLaren and Cameron, 1990).

The procedures followed to measure soil moisture content in this study were:

I. soil samples were taken from the temperature probe pits at each site at 0.0–0.05, 0.05–0.10, 0.10–0.15, and 0.15–0.20 m depths when installing the temperature probes;
II. the samples were then sealed in separate, labelled plastic bags;
III. the samples were weighed to determine the wet weight *(Ww)* and dried in an oven at 105°C for 24 hours;
IV. after they had cooled, the samples were then re-weighed and their dry weights *(Dw)* determined.

Using these measurements, *w* was then calculated using the Equation:

$$w = \frac{(Ww - Dw)}{Dw} \tag{3.9}$$

The volumetric moisture content was calculated by dividing the gravimetric moisture content by the initial sample volume.

3.3.4 BULK DENSITY (ρ_b)

The main methods available for determining soil bulk density include the: clod method; core method; and excavation method (Blake and Hartage, 1986a). The only technique suitable for loose, dry, un-consolidated soils like those found in Antarctica is the excavation method.

This method involves excavating a quantity of soil, determining the volume of the excavation using a sand replacement technique, and drying and weighing the soil sample obtained (Burke *et al.*, 1986).

The steps followed when measuring the bulk density were:

I. in each of the soil profile pits dug at the three sites, a flat surface was made at 0.01, 0.05, 0.10 and 0.15 m depths;
II. a small hole (~ 7 cm wide by ~ 5 cm deep) was then dug at each level and the excavated soil was carefully bagged;
III. the volume of the hole *(v)* was then determined by filling it with a known quantity of fill. This would usually be sand, but due to the strict environmental standards in Antarctica, sand cannot be imported and the filler has to be removed once the holes volume is determined. Therefore, the hole was lined with glad-wrap and sago, the best available substitute for sand, was poured from a 100 cm^3 measuring cylinder. Sago was used because the small spheres consistently pack to a reproducible volume;
IV. the soil samples were then oven dried to obtain the soils dry weight (Dw) and the bulk density was then calculated using the equation:

$$\rho_b = \frac{Dw}{v} \tag{3.10}$$

3.3.5 GRAINSIZE DISTRIBUTION

The simplest and most common method for determining the range of grainsizes in sandy sediments such as Antarctic soil is dry sieving using different sized sieves to collect each sand fraction (Lewis and McConchie, 1993). This method was therefore used and an outline of the steps followed is given.

I. 100–200 g of oven dry soil *(Sw)* was placed on top of a sieve nest which consisted of the following sieve sizes: pebble size (> 4 mm); granule size (2 mm); very coarse sand (1 mm); coarse sand (0.5 mm); medium sand (0.25 mm); fine sand (0.125 mm); very fine sand (0.063 mm); and mud size (< 0.063 mm);
II. the sieve nest was then secured on a Frizken sieve shaker and shaken for ten minutes to ensure the sample was fully separated into its various fractions;
III. the sieve nest was then removed from the shaker and the contents of each sieve was weighed (*sw*);
IV. the abundance of grains (%) from each sieve was then calculated using the formula:

$$\text{Grainsize abundance} = \frac{sw}{Sw} \times 100 \tag{3.11}$$

and the cumulative weight percentages were calculated by adding the percentages of each size fraction incrementally (Lewis and McConchie, 1993).

3.3.6 PARTICLE DENSITY (ρ_b)

The most common method used to determine soil particle density (kg/m^2) is the pycnometer method which gives precise densities if volumes and weights are carefully measured (Blake and Hartge, 1986b). The main steps for determining soil particle density using this method are as follows:

I. weigh a clean, dry, 50 ml pycnometer (specific-gravity flask) including stopper;
II. place about 10 g of oven dry soil in the pycnometer and re-weigh;
III. 1/2 fill the pycnometer with distilled water and boiled gently for 3 minutes;
IV. after cooling to room temperature, add enough boiled distilled to fill the pycnometer and insert the stopper;
V. dry the pycnometer and re-weigh;
VI. empty, clean, and re-fill the pycnometer with distilled water at the same temperature as before and insert the stopper;
VII. after drying the outside of the pycnometer, re-weigh it once again an calculate ρ_b:

$$\rho_b = \frac{\rho_w(Ws - Wa)}{(Ws - Wa) - (Wsw - Ww)} \tag{3.12}$$

where: ρ_w = density of water;
Ws = pycnometer + soil weight (corrected to oven dry weight);
Wa = pycnometer weight;
Wsw = pycnometer + soil + distilled water weight;
Ww = pycnometer + distilled water weight.

3.3.7 SALT CONTENT

To determine the amount of soluble salt (%) in Antarctic soil, the following specific conductivity test was used (Blackmore *et al.*, 1987):

I. shake 20 g of soil with 100 ml water for 30 minutes at about 20°C and centrifuge.
II. place the extract in a soil conductivity meter (MC4 Soil Conductivity Meter made by Electronic Switchgear, London Ltd), and read off the solutions conductivity (K_{25}). Correct the reading for the cell constant (1 in this case), and temperature (see Appendix 4). Express the conductivity at 25°C as millimho/cm;
III. calculate the total soluble salt content of the sample (%) by multiplying K_{25} by 0.35.

3.4 MEASUREMENT ERRORS AND PROBLEMS

This section discusses the main sources and magnitudes of errors associated with the techniques used and identifies key authors who have investigated them in detail.

The main sources of error likely in this research are: improper instrument exposure and extreme environmental conditions; poor sensor calibration; data logging system resolution limitations; and uncertainties associated with newly developed measurement techniques.

The surface slope and height of the instruments is important when measuring radiation balance components and surface albedo because they determine the effective viewing range of the instruments. Balks *et al.,* (1995) for example, measured the radiation balance components at Scott Base on a slightly sloping surface. Albedo measurements obtained were approximately 0.05 during the middle part of the day which are slightly lower than the ~0.06 obtained at the flat site used in this study.

Site shading can also cause errors due to the reduced amount of incoming shortwave radiation. Albedo measurements, for example, are affected by low light levels, and results obtained under these conditions should therefore be examined (Balks *et al.,* 1995).

Rime on the pyranometers, net radiometer, and anemometer also makes some measurements unreliable. At Scott Base, riming often occurs due to the moist nature of the maritime air and the relatively mild air temperatures. Data for these periods is consequently not used.

Thermocouple measurements are also subject to errors associated with data-logger resolution limits and thermal gradients within the system. The major problem with thermocouples is that all connections represent additional junctions and are therefore potential sensors which may cause errors. Connection must therefore be kept at the same temperature. Temperature gradients within leads do not however cause these problems,

but it is suggested that all leads are insulated to eliminate connections to the ground (Buchan, 1991).

Kluitenberg *et al.,* (1993) analysed the errors associated with the heat pulse method and found the greatest source of error (~0.8%) comes from the assumption that the probe releases heat instantaneously because the measurements are conducted with short duration heating. This error decreases as the heating duration and thermal diffusivity decreases, and the probe spacing increases.

A 1% overestimation of the maximum probe temperature also results in a ~1% underestimation of heat capacity. Because temperature rise at the sensing probe is ≈1°C, 10% precision in heat capacity requires temperature measurements at the sensing probe with approximately 0.1°C precision which the data-logger has.

Probe spacing is also important because a 0.3 mm overestimation in probe spacing, for the case where the probe spacing is 6 mm, would result in a 10% underestimation of the heat capacity. This problem was eliminated with the plastic divider fitted between the probes, but could still be important if the probes get bent.

The precision of soil heat capacity measurements using the heat pulse method are therefore determined by the precision with which the maximum temperature, probe spacing, and the heat input can be measured (Kluitenberg *et al.,* 1993).

Riha *et al.,* (1980) reviewed the measurement of soil thermal conductivity using various probes and a finite element method to solve the heat flow equation. It was concluded that soil moisture variations were the main source of error. When a hot probe is used, thermally induced vapour flow can cause a thin layer of soil around the probe to dry which lowers the conductivity. When the cold probe is used, water vapour can condense on the probe which can increase conductivity as better soil/probe contact is made.

CHAPTER FOUR

SITE DESCRIPTIONS

The measurement programme described was carried out at three sites with contrasting soil types and climates within the McMurdo Sound Region of Antarctica (Figure 4.1). These were located near Scott Base on Ross Island, in the Coombs Hills on the edge of the polar plateau, and in the Greenville Valley which is also referred to as the Northwind Valley. This section describes each sites geographic location, climate, geology and soil type.

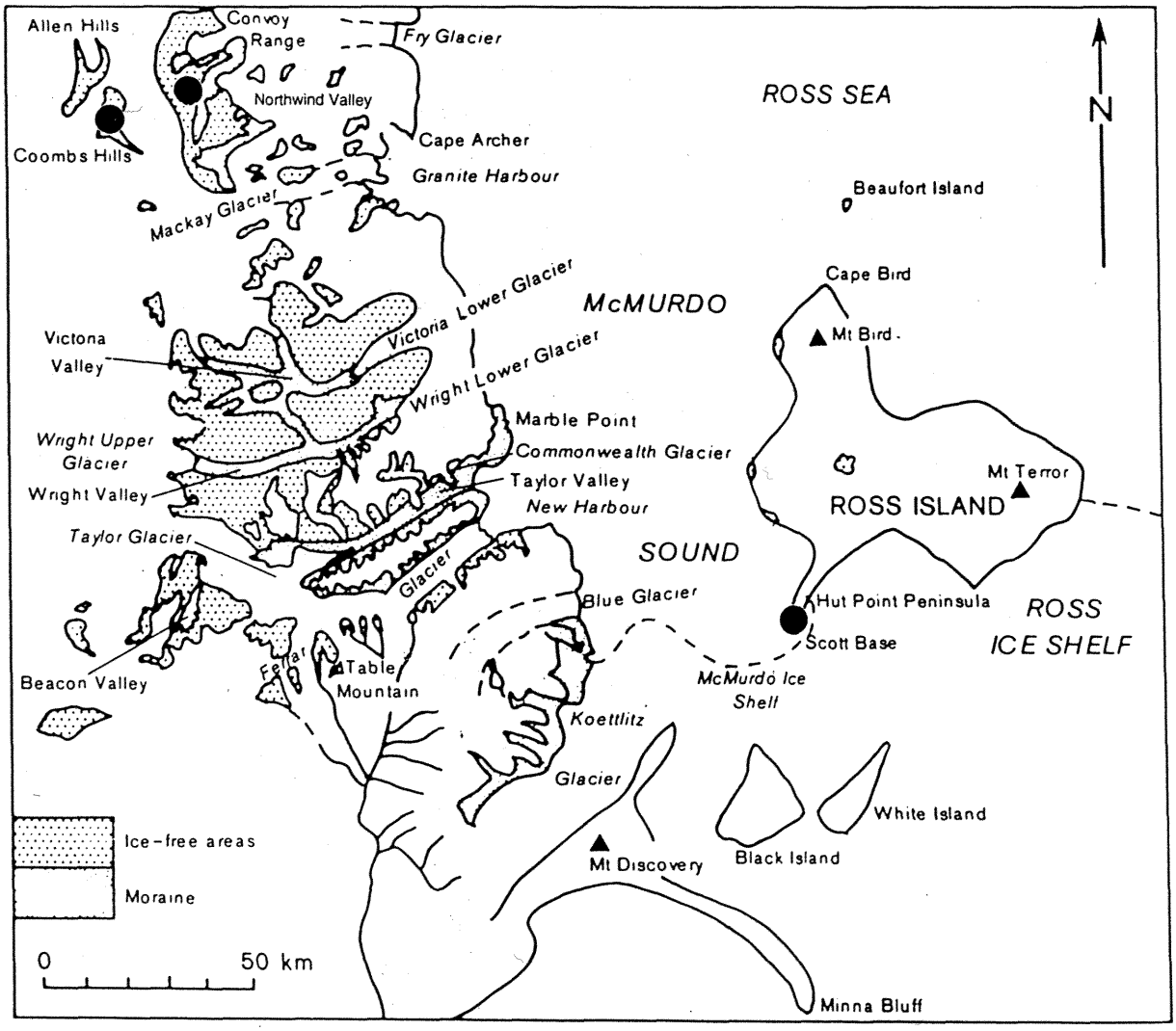

Figure 4.1 Study sites (●) within the McMurdo Sound, Antarctica (Campbell and Claridge, 1987).

4.1 SCOTT BASE

This site is in the coastal climate zone on Ross Island near Hut Point Peninsula (Figure 4.2). The geological history is well understood due to comprehensive studies in the area which began in 1901-1904 with Scott's Discovery Expedition and continues today at the American Base, McMurdo Station and New Zealand's Scott Base (Cole *et al.*, 1971).

Figure 4.2 Landscape around Scott Base field site, Pram Point, Ross Island. The arrow indicates the field sites location.

4.1.1 SCOTT BASE GEOLOGY

The dominant geological unit in the area is the Crater Hill sequence which consists of porphyritic olivine-clinopyroxene basaltic flows and pyroclastic rocks which originate from Crater Hill ~2 km west of Scott Base. These flows are thought to be about 1.6 million years old and are the oldest deposits on the island. Scott Base and the study site are located on a younger basaltic flow overlying the Crater Hill sequence which erupted from Crater Hill about 0.4 million years ago (Kyle, 1981).

The surface material at the site consists of basaltic pebbles, cobbles and boulders weathered from the lava flow, and a few small rounded pebbles of granite and sandstone which were probably transported from the mainland during the last Ross Sea Glacier expansion (Unpublished data, Campbell, 1994).

4.1.2 SITE GEOMORPHOLOGY AND LAYOUT

Although the study site showed little sign of human disturbance apart from a few overturned rocks, intensive human activity in the area over the past 50 years has resulted in virtually no undisturbed sites on Pram point. The study site is located on approximately 200 m north west of Scott Base on a flat step surrounded by hilly terrain at the foot of Crater Hill, and has the co-ordinates 75° 50's, 166° 45'E (Figure 4.3).

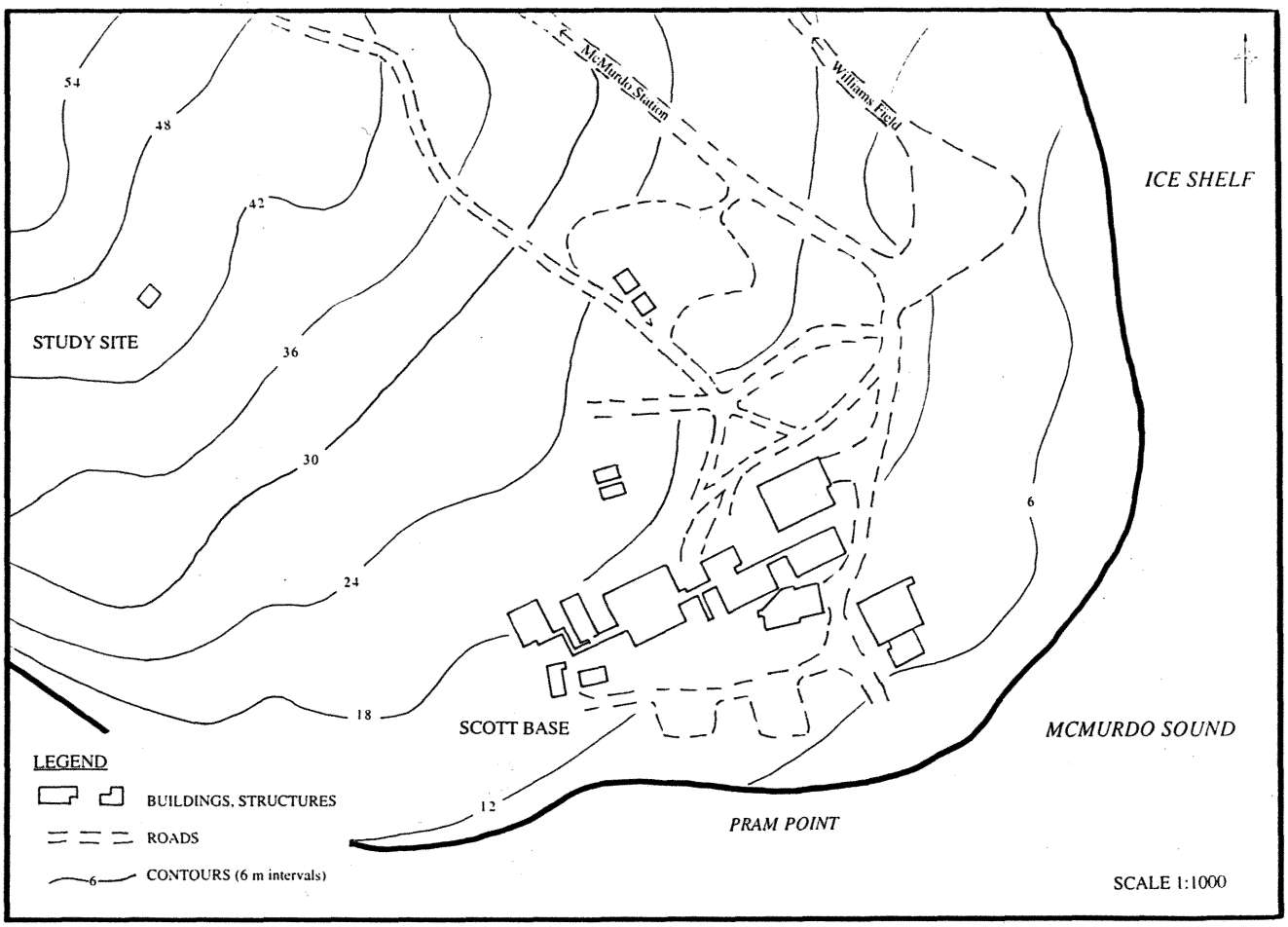

Figure 4.3 Location Map of Scott Base Field Site, Pram Point, Ross Island.

Weakly developed ground cracks around the site had to be avoided when setting up the instruments and the radiation balance equipment was sited on relatively flat ground to minimise measurement error.

4.1.3 SOIL DESCRIPTION

Basalt derived soils in Antarctica have been studied extensively by a number of researchers such as McCraw (1967) who examined the chemistry of a basalt soil near Scott Base, Campbell and Claridge (1987) who have described numerous basalt derived soils and investigated the effect of soil contamination, and Balks *et al.,* (1995) who studied soil disturbance near Scott Base.

Soils formed on basalt are typically dark coloured, coarse textured and contain few fine grains as shown in Figure 4.4.

Figure 4.4 Soil pit dug at the Scott Base site prior to temperature probe insertion.

These characteristics are clearly visible in the soil description which was made by Dr Iain Campbell on a pit 3 m away from the measurement site. Horizon depths altered slightly between the two sites, as did the composition of certain layers, but in general both profiles were essentially the same and indicate a reasonable degree of spatial homogeneity.

Soil description for Scott Base site

3 - 0 cm	surface pavement of black and reddish brown vesicular basalt pebbles, cobbles and boulders surrounded by small rounded pebbles of granite and sandstone; loose; sub-rounded to sub-angular clasts; un-weathered; pale carbonate coatings on underside of some larger clasts; small lichen and moss growing on surface stones,
0 - 4 cm	greyish olive (5Y 4/2) sandy granules; loose to weakly cohesive; rock particles subrounded to subangular and un-weathered; indistinct boundary,
4 - 8 cm	greyish olive (5Y 5/2) sandy granules; loose; rock particles subrounded to subangular and un-weathered; indistinct boundary,
8 - 15 cm	greyish olive (5Y 5/2) granule and pebble gravels; loose; rock particles mainly subangular; un-weathered; carbonate coatings on some granules; distinct boundary,
15 - 19 cm	greyish olive (5Y 5/2) sand with a few granules and small pebbles; loose; sub-rounded to sub-angular clasts; un-weathered overlying ice cemented ground.

4.2 COOMBS HILLS

The second site investigated was on the edge of the polar plateau in the Coombs Hills (Figure 4.5) which has an intra-continental high mountain zone climate. There has been little work done on the geology of this area due to its remote location and inhospitable climate. A lot of studies have however been carried out on the nearby Allen Hills, which is geologically similar to the Coombs Hills. Therefore, to understand the geology of this field site, information from the Allen Hills studies will be drawn on.

Figure 4.5 Landscape around the Coombs Hills site on the edge of the polar plateau. The arrow indicates the location of the field site used.

4.2.1 COOMBS HILLS GEOLOGY

The Coombs Hills consists of four main geological units which are the Lashly Formation; the Ferrar Dolerite; the Kirkpatrick Basalts; and the Mawson Formation. The Lashly Formation is part of the Beacon Supergroup which was deposited during the Triassic period (244-208 Ma) and consists of pale green siltstones and claystones, medium grained, tan, pale green and grey sandstones and arkoses. It was the most extensive rock type in the area prior to widespread volcanism during the Jurassic Period (208-144 Ma) which intruded the Ferrar Dolerite and deposited the Kirkpatrick Basalt and the Mawson Formation (Grapes *et al.*, 1972).

The Ferrar Dolerite is now the most widespread geological unit in the area and consists of tholeitic sills and dykes which intrude the Permian and Triassic Beacon sediments. The Kirkpatrick Basalt is found in greatest abundance on Mount Brooke and consists of tholeitic basaltic pillow lavas and lava flows, and hyaloclastic basalt breccia. The Mawson Formation covers an area of about 5 km^2 at the base of Mount Brook and is composed of quartz-lithic, volcanic and micaceous sandstones, explosion breccias, volcanic mudflows, basalt pods and flows, and clastic dykes and sills (Grapes *et al.*, 1972).

4.2.2 SITE GEOMORPHOLOGY AND LAYOUT

The field site is located approximately 2.3 km north-east of Mount Brooke on a flat terrace on the floor of an undulating 'U' shaped valley in the Coombs Hills at an altitude of about 2015 m (Figure 4.6). Approximately 50 m up valley of the site is a small ~ 5 m hill which shelters the site from the dominant south to south westerly wind and frequent snowdrift.

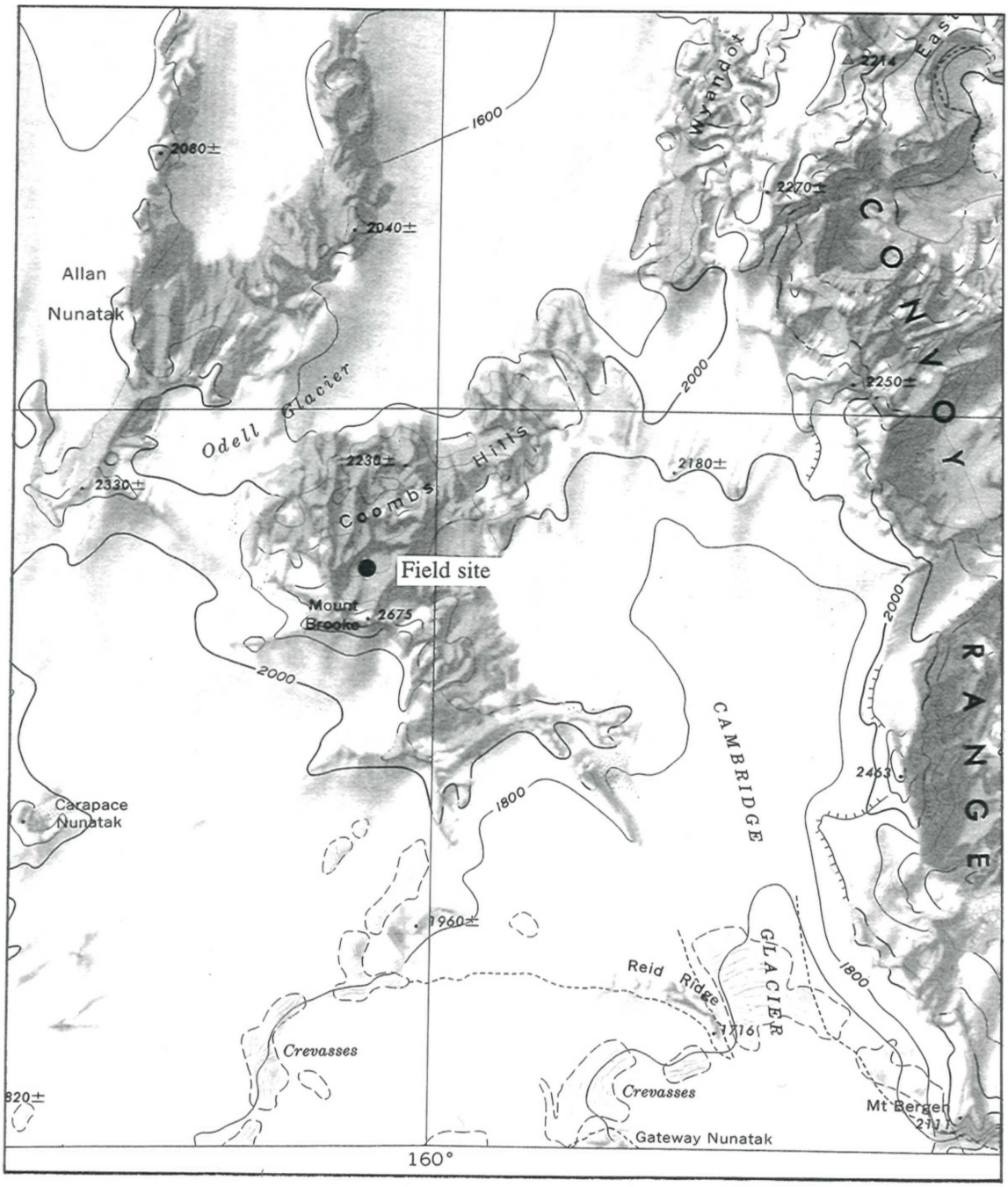

Figure 4.6 Location map of Coombs Hills field site, co-ordinates 76°48.3'S159°54.1'E (Antarctic 1:250,000 reconnaissance series - Convoy Range, 1962).

4.2.3 COOMBS HILLS SOIL DESCRIPTION

Soils formed from dolerite are typically coarse-grained, have a granular texture, and have an overall dark greyish brown to olive brown (2.5Y 4/2-4/4) colour when they are young. As they weather, the amount of fine material within the profile increases and the soil darkens to a brown or dark brown (10YR 4/3) colour. Based on this and the soil description made by Dr I Campbell, the soil at the site (Figure 4.7) is fairly old and strongly weathered (Campbell and Claridge, 1987).

Figure 4.7 Soil pit dug ~5 m from the Coombs Hills field site. Measurements were made in the surface layers only.

Soil description for the Coombs Hills site

3 - 0 cm dark brown surface cobbles, pebbles and granules ; subangular to subrounded and non to weakly stained,

0 -5 cm strong brown (7.5YR 5/6) gravelly to pebbly sand; loose; rock particles mainly subangular and unstained, distinct boundary,

5 - 12 cm strong brown (7.5YR 6/4) pebbly sand; moderately cohesive; many diffuse salts, rock particles subangular and unstained; distinct boundary,

12 - 20 cm yellowish brown to bright yellowish brown (10YR 5/6 - 6/6) sandy pebble and cobble gravel; firmly cohesive and salt cemented; abundant diffuse salts; rock particles subangular and unstained (Campbell, unpublished data, 1995).

4.3 NORTHWIND VALLEY

The third site was in the Northwind Valley (Figure 4.8) which is located on the Convoy Range, midway between the Coombs Hills and the coast in the glacial slope climate zone. Geological studies and mapping began in the area during G Taylor's expedition in 1913 and by 1960 a 1:250,000 geological map of the region had been published (Chinn *et al.*, 1994). Since then, several researchers have visited the area and consequently its topography and geological history is fairly well known and understood.

4.3.1 NORTHWIND VALLEY GEOLOGY

During the Jurassic period, the Convoy Range was a major intrusive centre for the Ferrar Dolerite which dominates the region's geology. Benches and terraces of dolerite are common in the area and represent structural and compositional variations between intrusion events. These features have been strongly weathered and now form a subdued, rolling relief. Sandstones from the Beacon Supergroup are also abundant beneath the dolerite and are commonly seen in outcrops and cliffs throughout the region.

Granite which originated from the Granite Harbour Intrusives is also present in small quantities in some areas. Extensive till and moraine deposits formed during the Pliocene

to Holocene ages are also present in the area and these are commonly patterned by ice-wedge polygons (Chinn *et al.*, 1994).

Figure 4.8 Landscape around the Northwind Valley site, Convoy Range. The arrow indicates the location of the field site.

4.3.2 SITE GEOMORPHOLOGY AND LAYOUT

The site was located 10.5 km south west of Larsen Crag at the head of the Northwind Valley, at about 1400 m altitude on a flat sandstone terrace about 100 m from the outcropping Weller Coal Measure Formation, which is part of the Beacon Supergroup (Figure 4.9).

A gently undulating dolerite bench extends to the north east which is the dominant surface type in the head of the valley. The sandstone bench was chosen because its quartz rich, light coloured soil was a good contrast to the other two sites.

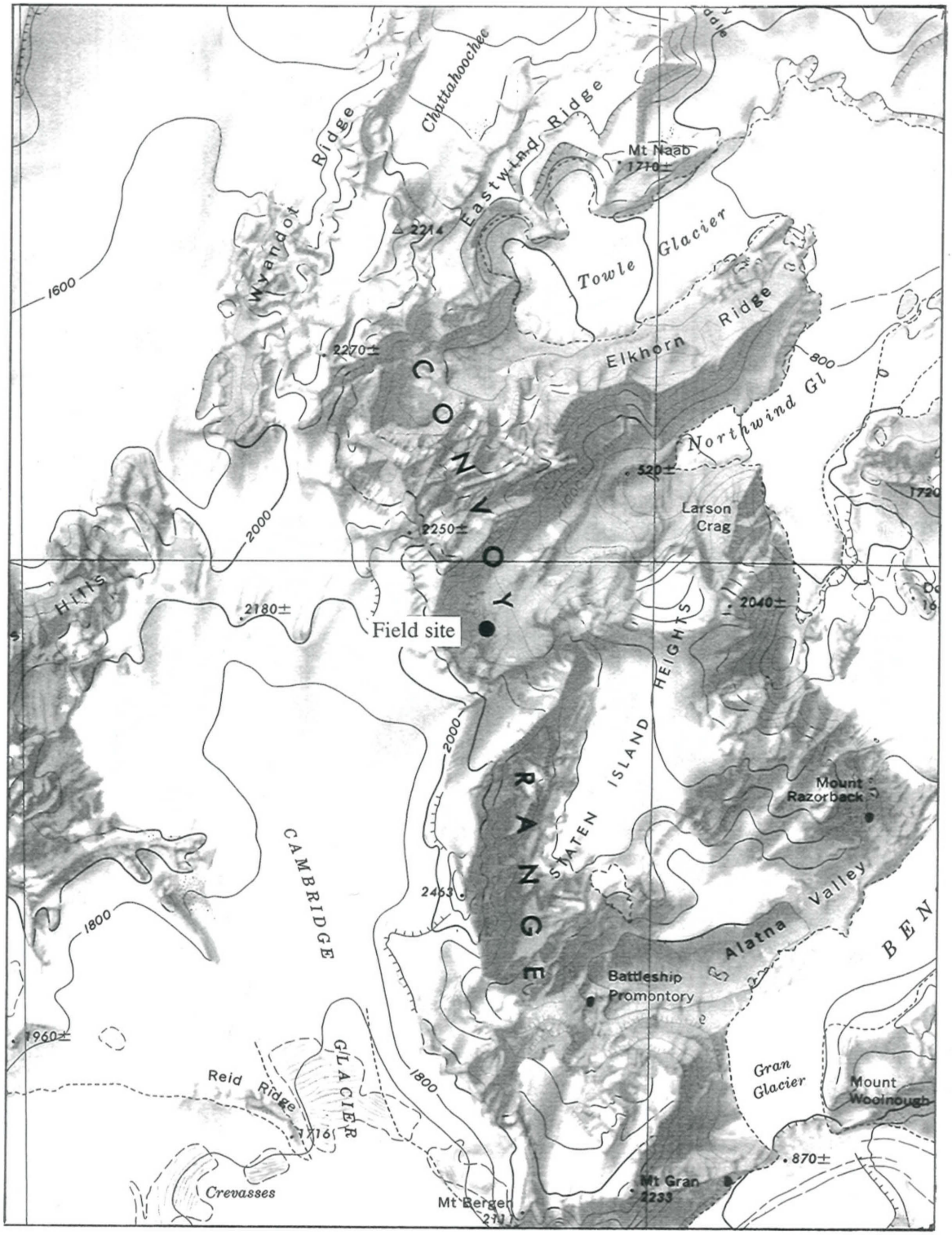

Figure 4.9 Location of the Northwind Valley Site, co-ordinates 76°46.3'S160°45.1'E (Antarctic 1:250,000 reconnaissance series - Convoy Range, 1962).

4.3.3 SOIL DESCRIPTION

Soils formed from sandstone in Antarctica (Figure 4.10) which are usually shallow due to the removal of individual grains by wind processes, have a sandy texture, and are mainly yellowish in colour as shown in the soil description made at the site by Dr I. Campbell (Campbell and Claridge, 1987).

Figure 4.10 Soil pit dug at the Northwind Valley site prior to temperature probe insertion.

Soil description for the Northwind Valley site

4 - 0 cm creamy white surface cobbles, pebbles, and small boulders made of sandstone; well developed pavement; clasts mainly subrounded to rounded, strongly stained and polished; some exfoliation; weakly ventiform, salts beneath many surface stones,

0 - 11 cm dull yellowish orange (10YR 7/3) coarse pebbly to granular sand; loose; patches of salt around and beneath stones; rock particles mainly subrounded, angular to rounded and non to moderately stained; some particles strongly altered; distinct boundary,

11 - 16 cm dull yellowish orange (10YR 7/4) pebbly to granular sand with a few boulders; weakly to moderately cohesive; few salt accretions; rock particles mainly angular to rounded and non to moderately stained; many smaller particles disaggregated; distinct boundary,

16 - 20 cm light yellowish orange (10YR 8/3) silty granular sand surrounding angular sandstone boulders; weakly to moderately cohesive; sand particles mainly subrounded to rounded and non to moderately stained; many smaller particles disaggregated and exfoliation of boulders (Campbell, unpublished data, 1995).

CHAPTER FIVE

RESULTS AND INTERPRETATION

This chapter presents the results of the measurement programme and discusses the main microclimatic features at each site studied. To begin with, a description of the soil's physical and thermal properties is given along with a discussion of their possible influence on the soil microclimate. This is followed by a description of the radiation balance, soil heat flux and temperature regime at each site under various conditions. A summary of the dominant microclimatic processes at each site is then given.

5.1 SOIL PHYSICAL PROPERTIES

Physical soil properties which influence a site's microclimate include the soil moisture content, bulk density, particle density, grain size distribution, and salinity. These properties were quantified in the temperature probe pit at each site and at six randomly chosen locations within the field sites to determine their spatial variability.

5.1.1 SOIL MOISTURE CONTENT

Soil moisture content at various depths for each site when the temperature probes were removed are shown in Table 5.1. When discussing these results, it is important to consider the climatic conditions prior to the samples being taken. Snowfall events and evaporation can significantly change the soil moisture status over a short period of time.

Fine weather was experienced for two days prior to sampling at the Scott Base site (December 31), but there was a lot of wind blown snow on the site on December 29 which melted quickly. Fine weather was also experienced at the Coombs Hills site leading up to probe removal (January 17), although snow deposited on January 14 was still present and had not melted.

Two days before probe removal (January 16) at the Northwind Valley site, the weather was cloudy and the snow covering the area on our arrival remained. Snow was swept off the site to allow comparisons to be made with the other two sites, and some melting occurred the day before probe removal due to relatively warm, cloudless weather.

Table 5.1 Volumetric soil moisture content (%) for the temperature probe pit at each field site on removal of the temperature probes.

Site	0.0–0.05 m	0.05–0.10 m	0.10–0.15 m	0.15–0.20 m	Average
Scott Base (31 Dec. 1994)	6.92	6.74	2.76	6.64	5.77
Coombs Hills (17 Jan. 1995)	3.08	6.89	3.49	3.32	4.20
Northwind Valley (22 Jan. 1995)	1.68	3.26	3.48	3.22	2.91

The Scott Base site was the overall wettest of the three sites due to its moist climate and the Northwind Valley site was the driest. At Scott Base, soil moisture content ranged between 6–7% at the 0.0–0.05, 0.05–0.10, and 0.15–0.20 m depth but was significantly lower (2.7%) at the 0.10–0.15 m depth. This is probably related to the coarse texture of the soil at this depth (see section 5.1.4).

Soil moisture content at the Coombs Hills site was between 3–3.5% at all depths except the 0.05–0.10 m depth which had nearly 7% moisture content. This is probably because soil particle distribution is fairly even at this depth and there is a relatively high percentage of fine particles compared to the other three depths. It is not due to an increase in salt content (see Section 5.1.5) which can increase moisture content through hygroscopic processes.

Soil below 0.10 m at the Northwind Valley site had a similar moisture content to that found at the Coombs Hills site, although the top 0.05 m was significantly drier with a moisture content of only 1.68%. This could be due to the slightly windy but sunny conditions experienced prior to sampling which is ideal for evaporation.

Similar soil moisture contents were reported by Cameron (1969) when he studied the soils of the Victoria and Wright Valleys where soil at a depth of 0.02–0.05 m had moisture contents of between 1–5%.

Independent soil moisture measurements carried out by Dr's Iain Campbell and Graeme Claridge in the same locations used in this study show that on average, non ice-cemented soil at the Coombs Hills and Northwind Valley had moisture contents of 2.55% and 3.17% respectively (Campbell *et* al., in prep., 1996). Scott Base measurements ranged from 5.7% at 0.15 m to 20% at the 0.25 m depth (Balks *et* al., 1995).

It was reported by Campbell *et al.*, in prep., (1996) that soil moisture content increases at the 0.05–0.15 m depth in some Coombs Hills and Northwind Valley soils due to the presence of salty horizons. This was also apparent in the soils studied (Table 5.8).

Soil moisture content showed noticeable spatial variability over distances less than ~10 m at both the Scott Base and Northwind Valley sites but was not great at the Coombs Hills site (see Table 5.2).

Table 5.2 Spatial variability of volumetric soil moisture content (%) at each field site. Samples were taken from the 0.0–0.05 m depth at the Scott Base and Northwind Valley sites, and 0.10–0.15 m at the Coombs Hills.

Site	loc. 1	loc. 2	loc. 3	loc. 4	loc. 5	loc. 6	Mean (s.dev.)
Scott Base	7.10	5.79	5.01	8.52	9.52	6.37	7.05
(29 Dec. 1994)							(1.55)
Coombs Hills	2.52	2.93	2.74	2.87	2.63	2.75	2.74
(11 Jan. 1995)							(0.14)
Northwind Valley	6.37	5.88	5.31	6.86	3.76	5.54	5.62
(21 Jan. 1995)							(0.98)

Greatest variation was seen at the Scott Base site where moisture content ranged between 5.01–9.52%. These differences, which were also present at the Northwind Valley site, are due to spatially variable surface conditions such as proximity to snow packs and ground cracks. Maximum soil moisture contents do not correspond to greatest salt content at either the Scott Base or Coombs Hills sites, but do at the Northwind Valley site.

At the Coombs Hills site, soil moisture content remained fairly constant with a standard deviation of only 0.14. Soil physical properties did not vary greatly within this site and there were no snow packs or ground cracks in the vicinity.

5.1.1.1 Soil moisture variations at Scott Base over time

To determine the significance of soil moisture variation with time, soil moisture content was measured in adjacent soil pits at the Scott Base site every second day. A flat plot was chosen which had uniform surface properties and was not noticeably influenced by ground cracks or snow melt. The soil pits dug within this plot were about 0.16 m^2 and samples were taken at 0.05 m intervals down to a depth of 0.2 m. The results of this experiment are shown in Table 3.

Table 5.3 Volumetric soil moisture content (%) and equivalent water depth (mm) for adjacent plots at the Scott Base site over a two week period in December 1994.

December, 1994	0.0–0.05 m	0.05–0.10 m	0.10–0.15 m	0.15–0.20 m	total water content (mm)	Notes
Dec. 17	**6.36**	**7.99**	**5.52**	**4.83**		Snowed Dec. 15
Equivalent depth (mm)	3.18	3.99	2.76	2.42	12.35	
Dec. 19	**2.50**	**2.42**	**2.36**	**2.10**		
Equivalent depth (mm)	1.25	1.21	1.18	1.05	4.69	
Dec. 21	**3.83**	**4.91**	**4.13**	**2.79**		
Equivalent depth (mm)	1.92	2.46	2.07	3.95	10.4	
Dec. 23	**3.87**	**6.17**	**3.58**	**2.60**		snowed Dec. 22
Equivalent depth (mm)	1.94	3.09	1.79	1.30	8.12	
Dec. 25	**3.42**	**2.75**	**2.49**	**2.08**		
Equivalent depth (mm)	1.71	1.38	1.25	1.04	5.38	
Dec. 27	**3.51**	**4.61**	**6.48**	**2.63**		
Equivalent depth (mm)	1.76	2.31	3.24	1.32	8.63	
Dec. 29	**8.66**	**5.57**	**7.18**	**7.03**		snowed Dec. 28
Equivalent depth (mm)	4.33	2.79	3.59	3.52	14.23	
Dec. 31	**4.05**	**2.70**	**1.73**	**4.16**		ice at 0.15 m
Equivalent depth (mm)	2.03	1.35	0.87	2.08	6.33	

Soil moisture content varies significantly between measurements days, and does not always show the expected pattern of increasing moisture content after precipitation and melting events, and decreasing moisture content thereafter until the next event. Total soil moisture content on December 21 for example was greater than it was on December 19 and there was no moisture additions during this period.

The same occurred between December 25 and December 27 and again there are no apparent moisture additions. Soil moisture content variations with depth also show no distinct trends over the measurement period. There are no consistently wet or dry layers for example.

It is therefore obvious that these results do not accurately represent soil moisture variations over time at a particular site. The small scale variations in volumetric moisture content are large which means they mask any temporal moisture content variations. For this experiment to be of any value, non-destructive soil moisture content measurements at one location need to be carried out.

5.1.2 SOIL BULK DENSITY

Soil bulk density for the temperature profile pit at each site was measured using the sand replacement technique when the probes were installed (Table 5.4).

Table 5.4 Soil bulk density (kg/m^3) for the temperature probe pit at each field site.

Site	0.0–0.05 m	0.05–0.10 m	0.10–0.15 m	0.15–0.20 m	Mean
Scott Base	1788	1807	1717	1800	1778
Coombs Hills	1475	1557	1719	1819	1643
Northwind Valley	1496	1605	1802	1650	1638

Scott Base has the overall highest soil bulk density which averaged 1778 kg/m^2. The 0.10–0.15 m soil layer at Scott Base does however have a relatively low bulk density of 1717 kg/m^2 and this is due to the relatively coarse texture of this layer.

Soil bulk density increases with depth at the Coombs Hills site from 1475 kg/m^2 at the surface to 1819 kg/m^2 at a depth of 0.15–0.20 m. This is caused by an increase in large soil particles with depth (Figure 5.2). Campbell *et al.*, in prep. (1996) have suggested that increased salt content can cause the soil bulk density to decrease. This does not occur at this site because salt content increases with depth.

The Northwind Valley site has the overall lowest soil bulk density due to its coarse, sandy texture (Section 5.1.4), and also has the lowest recorded value which was 1496 kg/m^3. This measurement was made at a depth of 0.10–0.15 m and is ~100 kg/m^3 lower than soil bulk density at the 0.05–0.10 and 0.15–0.20 m depths and ~200 kg/m^3 lower than the soil at the 0.10–0.15 m depth. This anomaly is caused by the relatively coarse particles at the 0.10–0.15 m depth. Campbell *et al.*, in prep., (1996) reported that soil bulk density commonly increases with depth due to a general increase in the coarse particle fraction.

Overall, these results are in good agreement with measurements made independently by Dr's Iain Campbell and Graeme Claridge at similar sites (Claridge, unpublished data, 1996). They are however higher than the bulk density of soils from more temperate regions. Sandy loam soils in the Conroy soil series in New Zealand, for example, has a bulk density of about 1200 kg/m^3 (McLaren and Cameron, 1990) The Northwind Valley soil, which is the most fine grained soil examined (Figure 5.3), has the closest bulk density to this, which suggests the bulk density of Antarctic soils is relatively high due to their coarse nature.

The spatial variability of soil bulk density in Antarctic soil is quantified in Table 5.5. These results show that soil bulk density is most variable at the Scott Base site and least variable at the Coombs Hills site. Scott Base had the highest overall bulk density once again and the Northwind Valley site had the lowest. The probe pit site at the Coombs Hills had a bulk density of 1475 kg/m^3 at the 0.0–0.05 m depth which is a lot lower than the mean spatial variability value for the same depth.

Table 5.5 Spatial variability of soil bulk density (kg/m^3) at each field site. Measurements were made using the sand replacement technique.

Site	loc. 1	loc. 2	loc. 3	loc. 4	loc. 5	loc. 6	Mean (s.dev.)
Scott Base (0.0–0.05 m)	1705	1665	1800	1283	2285	2293	1839 (357)
Coombs Hills (0.10–0.15 m)	1855	1605	1803	1650	1581	1763	1710 (103)
Northwind valley (0.0–0.05 m)	1856	1739	1599	1588	1789	1443	1669 (140)

This indicates soil bulk density is highly variable over short distances. According to Blake and Hartge (1986), this is typical for most soils due variations in soil composition and structure.

5.1.3 SOIL PARTICLE DENSITY

The density of soil particles is important in determining soil thermal properties. Soil particle density was therefore measured in the temperature probe pit at each field site and the results are presented in Table 5.6.

Table 5.6 - Soil particle density (kg/m^3) for the temperature probe pit at each field site.

Site	0.0–0.05 m	0.05–0.10 m	0.10–0.15 m	0.15–0.20 m	Mean (s.dev.)
Scott Base	2850	2787	2899	2926	2866 (53)
Coombs Hills	2767	2845	2447	2793	2713 (156)
Northwind Valley	2647	2629	2587	2624	2622 (21)

Scott Base has the highest mean soil particle density and the Northwind Valley has the lowest which is in keeping with the soil bulk density measurements previously discussed. Particle density at the 0.05–0.10 m depth at the Scott Base site was however slightly lower than the other three depths probably due to compositional differences. Increased salt content was not observed at that depth which could otherwise have explained it.

Soil at the 0.10–0.15 m depth at the Coombs Hills site has a significantly lower particle density than the other three depths at that site. This could be because soil at this depth has a higher salt content (see Section 5.1.5). This is highly likely because it was the overall lowest value recorded and that layer contained the overall highest salt content measured.

Soil particle density at the Northwind Valley site varied least with depth overall and was ~100-200 kg/m^3 lower than soil particle density at the other two sites.

For most mineral soils, particle density is usually assumed to be a standard value of about 2650 kg/m^3 due to the large proportion of quartz, feldspar and silicate minerals present (McLaren and Cameron, 1990). This is similar to the mean value obtained for the Northwind Valley soil, but the other two soils have a slightly higher particle density. This is because of their volcanic origin which means their mineralogy is different to most soils.

Particle density at each site does not vary significantly over the short distances examined in this study as shown in Table 5.7. Soil at location 3 at the Coombs Hills site does however have a significantly lower particle density than the other 5 locations at that site. This is probably due to mineralogical differences.

Table 5.7 Spatial variability of soil particle density (kg/m^3) at each field site. Samples were taken from a depth of 0.0–0.05 m at Scott Base and the Northwind Valley, and 0.10–0.15 m at the Coombs Hills site.

Site	loc. 1	loc. 2	loc. 3	loc. 4	loc. 5	loc. 6	Mean (s.dev.)
Scott Base (0.0–0.05 m)	2890	2864	2887	2910	2857	2848	2876 (21)
Coombs Hills (0.10–0.15 m)	2766	2771	2421	2771	2786	2766	2714 (131)
Northwind valley (0.0–0.05 m)	2768	2637	2619	2757	2658	2737	2696 (60)

Once again, the highest particle density was recorded at the Scott Base site and the lowest at the Northwind Valley site which supports the previous results.

5.1.4 SOIL PARTICLE SIZE DISTRIBUTION

The size of soil particles vary significantly with depth in Antarctic soils and could have a strong influence on the soil thermal regime. Soil grainsize distribution for the temperature probe pit at each site was therefore determined and the results are presented in Figures 5.1 to 5.3. The spatial variability of particle sizes are also shown in Figures 5.4 to 5.6.

5.1.4.1 Scott Base temperature probe pit

The most noticeable feature at the Scott Base site is over 80% by mass of the soil particles at a depth of 0.10–0.15 m are greater than or equal to 4 mm. This layer consists of gravel like particles which are non-cohesive and contains very few fines (<5%).

Moisture retention would therefore be poor as indicated by the low moisture content at this depth in Table 5.1, and the numerous air gaps would slow heat conduction into the profile. There is also a high percentage (~44%) of these gravel sized particles at the 0.15–0.20 m depth, but ~20% are smaller than 2 mm which allow soil cohesion when moisture is present.

The overall trend at the Scott Base site is that particle size generally increases with depth and fines decrease with depth. The majority of soil particles at each depth are greater than or equal to 4 mm and there are very few particles as small as 0.063 mm. Everett (1971), Campbell and Claridge (1987), and several other researchers have confirmed that the proportion of fine particles in Antarctic soils increases with age. Therefore, these results are in-keeping with the relatively young age of this soil.

5.1.4.2 Coombs Hills temperature probe pit

The grain size distribution at the Coombs Hills site is characterised by a high percent (>50%) of particles greater than or equal to 4 mm at the 0.10–0.15 and 0.15–0.20 m depths. Soil at the 0.05–0.10 m depth has similar amounts of all particle sizes although there are slightly more 0.5–1.0 mm sized grains. Overall, this site has more fine particles than the other two sites. This is due to the fine textured, easily eroded Mawson Formation which provides a constant supply of wind-transported fines to the site. In general, there is an increase in coarse particles with depth and a decrease of fine particle with depth as seen at the Scott Base site.

5.1.4.3 Northwind Valley temperature probe pit

At the Northwind Valley site, the most noticeable feature is that the grainsize distribution is centred around the 0.5–1.0 mm range. The majority of soil particles are however greater than 0.25 mm. The particle size distribution is different to that seen at the other two sites and reflects the soil's sandstone origin which results in a very even pattern of grainsize distribution with depth. This would account for the lack of fine particles and large grains.

Overall, these results agree with the findings of Campbell *et al.*, in prep., (1996) who found that <2 mm soil particles are often relatively low in surface horizons due to surface winnowing. The greatest abundance of fines can usually be found immediately below the surface layers and there is a general decrease in the <2 mm fraction with increasing depth.

The spatial variability of soil grainsize distribution was determined using soil from a depth of 0–0.05 m at the Scott Base and Northwind Valley site, and 0.1–0.15 m at the Coombs Hills site. These depths were chosen because they were representative of the soil profile and were ideal to measure soil bulk density.

5.1.4.4 Scott Base spatial variability

As shown in Figure 5.4, there is a high degree of spatial variability of large (>4 mm) soil particles at the Scott Base site but this trend is not apparent with the smaller grain sizes. Apart from location 5, all grain size distributions follow a similar pattern of greater abundance of larger (>4 mm) particles and less smaller ones, which again reflects the young age of the soil.

5.1.4.5 Coombs Hills spatial variability

Figure 5.5 shows that five out of the six locations at the Coombs Hills site have similar grainsize distributions, but at location 4, there is an unusually high percentage of >4 mm particles and a comparatively low percentage of most other grain sizes. This is because this location is situated on a weakly developed ground crack which causes coarser materials to accumulate near the surface (Campbell and Claridge, 1987). Fine particles tend to accumulate at the bottom of ground cracks and are therefore not present in abundance at this sampling depth (Tedrow, 1977).

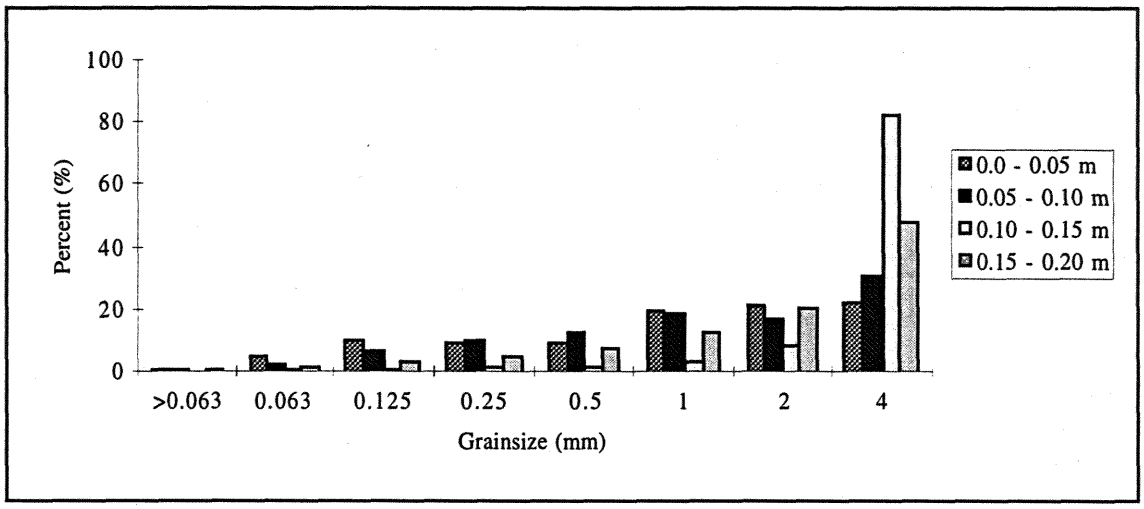

Figure 5.1 Soil grainsize distribution in the Scott Base temperature probe pit.

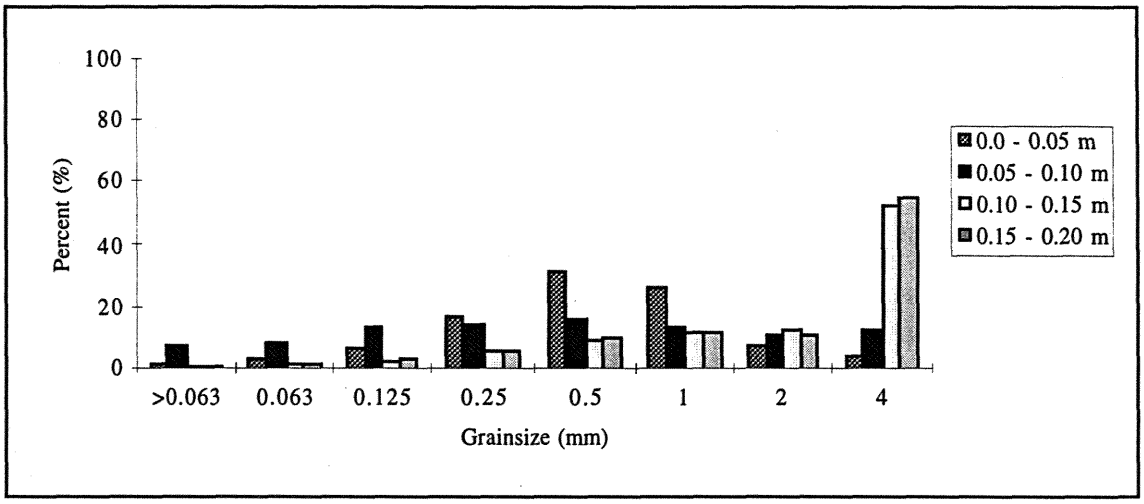

Figure 5.2 Soil grainsize distribution in the Coombs Hills temperature probe pit.

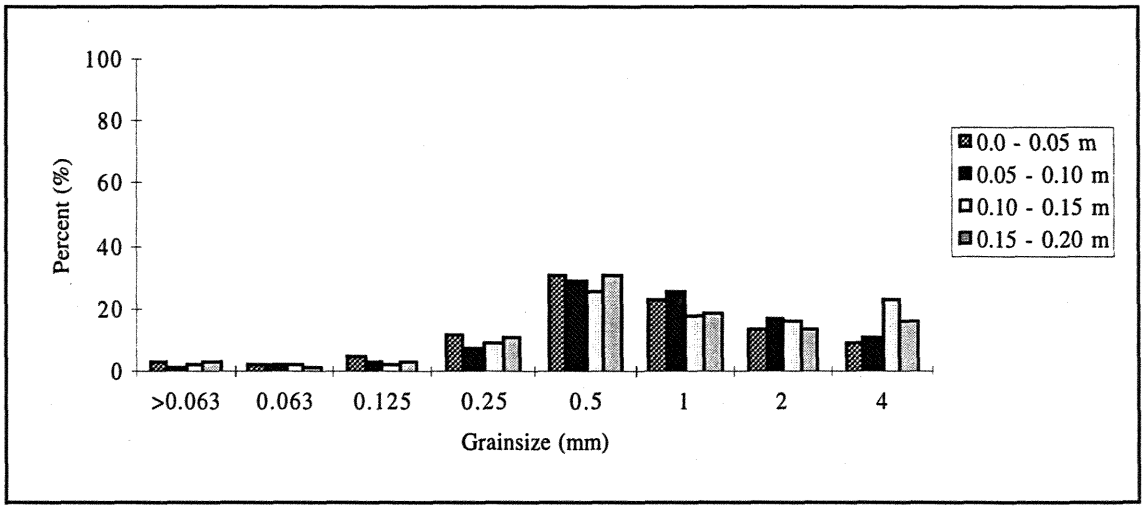

Figure 5.3 Soil grainsize distribution in the Northwind Valley temperature probe pit.

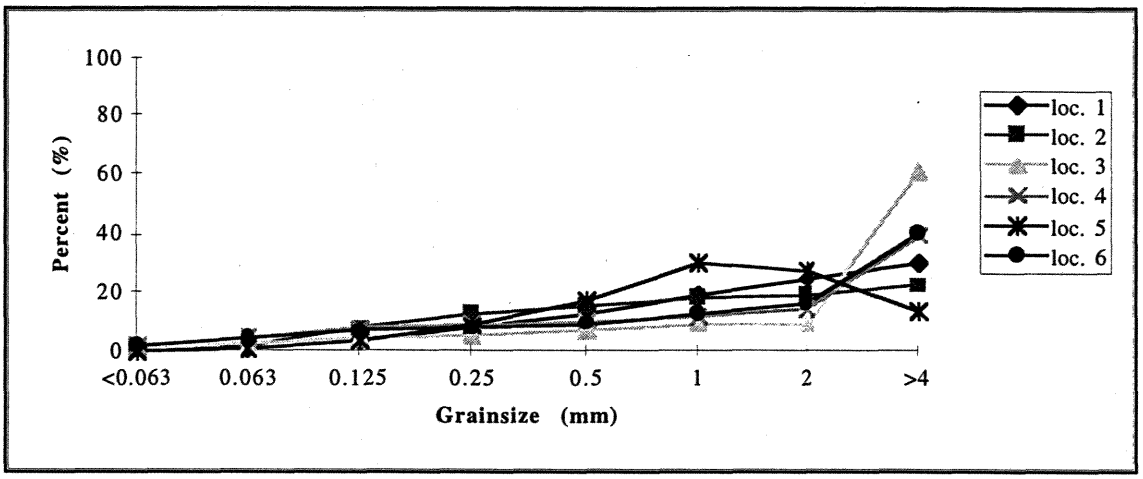

Figure 5.4 Spatial variability of soil grainsizes at the Scott Base site, samples taken from a depth of 0.0–0.05 m.

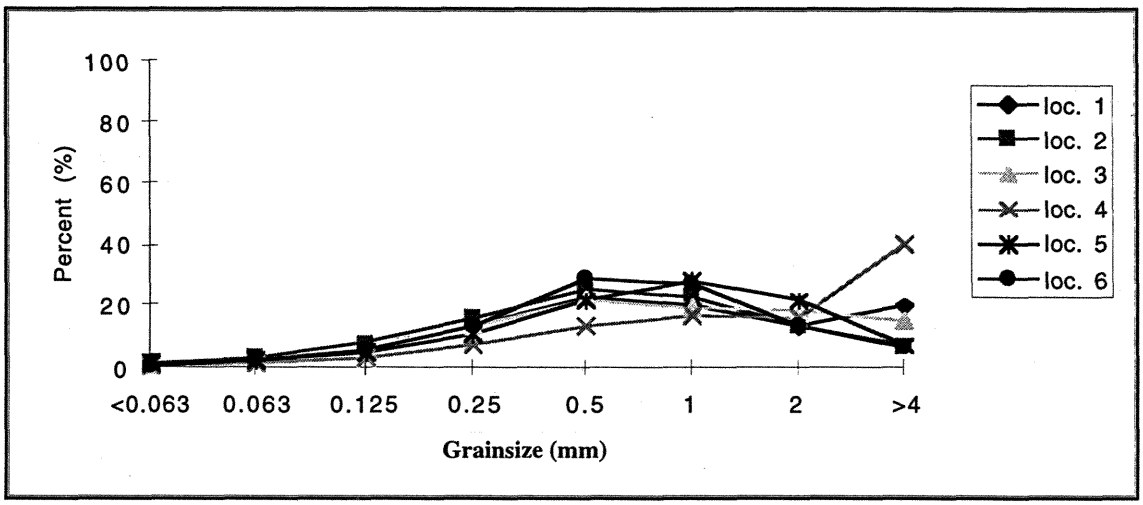

Figure 5.5 Spatial variability of soil grainsizes at the Coombs Hills site, samples taken from a depth of 0.10–0.15 m.

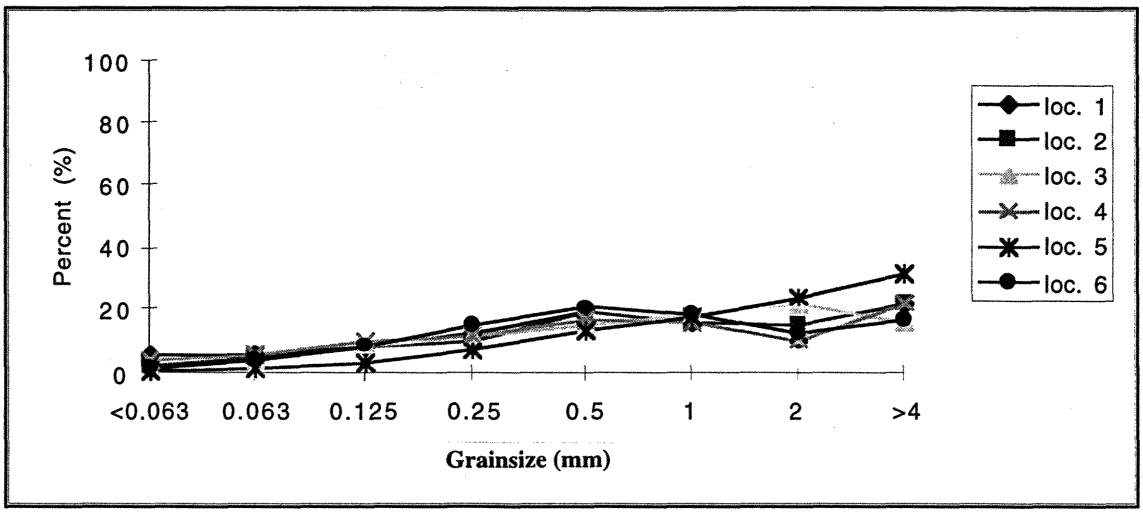

Figure 5.6 Spatial variability of soil grainsizes at the Northwind Valley site, samples taken from a depth of 0.0–0.05 m.

5.1.4.6 Northwind Valley spatial variability

The grain size distribution curves at the Northwind Valley site (Figure 5.6) are generally less steep than those at the other two sites. This means there are similar amounts of each particle size at each location. There is still a general decrease in the number of smaller grainsizes due to the soils origin and slow weathering rate in cold conditions. The grainsize distribution at location five is however slightly different because there are more large particles and less small ones compared to the other locations.

The overall spatial variability of grain sizes at this site is therefore similar to that observed at the Coombs Hills site, but shows significantly less spatial variability than that seen at the Scott Base site.

5.1.5 SOIL SALINITY

Total soluble salt content data (%) are presented in Table 5.8 and Figure 5.7 which shows the Scott Base site has the overall lowest salt content and the Coombs Hills site has the highest, which is probably due to their relative ages (Chapter 4). The least amount of salt was found in the 0.05-010 and 0.15-0.20 m depths at the Scott Base site and the most salt was found in the 0.10-0.15 m depth at the Coombs Hills site.

Table 5.8 Soluble salt content (%) of soil from the temperature probe pit at each field sites on removal of the temperature probes.

Site	0.0-0.05 m	0.05-0.10 m	0.10-0.15 m	0.15-0.20 m	Mean (s.dev.)
Scott Base (31 Dec. 1995)	1.05	0.23	0.57	0.23	0.52 (0.34)
Coombs Hills (17 Jan. 1995)	2.10	11.47	15.29	12.99	10.46 (5.01)
Northwind Valley (22 Jan. 1995)	4.59	10.51	8.60	8.60	8.08 (2.16)

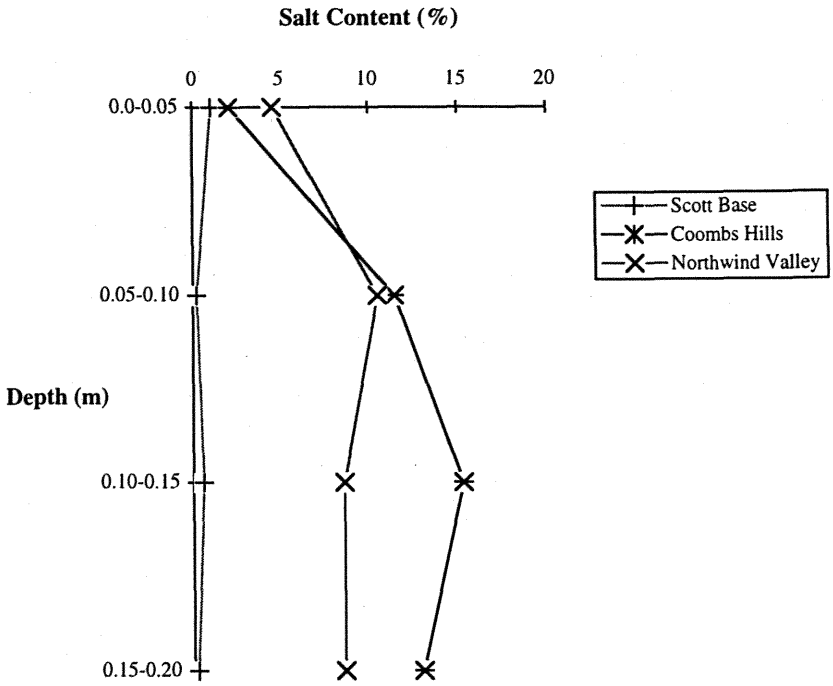

Figure 5.7 Soluble salt content (%) at each field site for the temperature probe pit.

The least amount of variation between depths was found at Scott base and although salt content varied significantly at the Northwind Valley site, the greatest variation was seen at the Coombs Hills site due to the low 0.0–0.05 m depth value.

As shown in Table 5.9, soluble salts do not show a high degree of spatial variability within the Scott Base site, but are noticeably variable at the Coombs Hills and Northwind Valley sites. This is a result of salt redistribution by moisture movement. Dissolved salts move along films of inter-granular moisture until temperatures are high enough for the films to evaporate and the salts precipitate out (Campbell and Claridge, 1987).

Table 5.9 Spatial variability of soluble salts (%) at the Scott Base, Coombs Hills and Northwind Valley sites.

Site	loc. 1	loc. 2	loc. 3	loc. 4	loc. 5	loc. 6	Mean (s.dev.)
Scott Base (0.0 - 0.05 m)	0.31	0.31	1.62	0.29	0.10	0.96	0.60 (0.53)
Coombs Hills (0.10 - 0.15 m)	0.57	2.10	3.25	3.06	5.54	1.15	2.61 (1.62)
Northwind valley (0.0 - 0.05 m)	8.60	3.82	8.03	14.91	8.60	6.31	8.38 (3.36)

5.2 SOIL THERMAL PROPERTIES

Thermal properties which determine the soil thermal regime are specific heat, thermal conductivity, and thermal diffusivity. These properties were measured for the temperature probe pit at each site and at six randomly chosen locations within the field site as was done in Section 5.1.

Measurements are repeated a minimum of five times on all samples and analysis of variance carried out with Microsoft Excel 'ANOVA' to determine the statistical difference between the means of these samples using the 95% confidence interval.

The Anova two-factor with replication test is initially used to make comparisons between the three sites and then each site is investigated separately. The Anova single-factor test is used to identify differences between means from the same site and the least significant difference (LSD) test is then used to identify which value(s) are significantly different within that group. A more detailed description of both Anova analysis techniques can be found in the Microsoft Excel Users guide, version 5, and an outline of the procedures used in the LSD test can be found in Gomez and Gomez (1984).

5.2.1 SOIL HEAT CAPACITY

Soil heat capacity measurements for the temperature probe pit at each field site are presented in Table 5.10. Measurements were made using the specific heat probe in the laboratory on oven dry samples which were then corrected for field moisture content based on Equation 2.8.

According to Oke (1987), dry sandy soils like those found in the Antarctic should have a heat capacity of about 1.28 MJ $m^{-3}K^{-1}$. This is, however, dependent on the mineralogical composition. Pure quartz, for example, has a specific heat of ~2 MJ $m^{-3}K^{-1}$ as Koorevaar *et al.,* (1983). This is similar to some of the values measured using the specific heat probe which suggests these soils consists of materials which have relatively high heat capacities.

These results show that the mean soil heat capacity at the Coombs Hills and Northwind Valley sites are significantly different from the other mean measurements, and the mean heat capacity at the Scott Base site is only statistically different from the Northwind Valley mean.

Table 5.10 Mean soil heat capacity measurements (MJ $m^{-3}K^{-1}$) for the Scott Base, Coombs Hills, and Northwind Valley temperature probe pits corrected for field moisture content (Appendix 1 contains oven dry values). The '*' indicates values which are significantly different at the 95% confidence level within rows, and the '#' indicates significantly different values within columns. These results are based on the LSD test.

Site	0.0–0.05 m	0.05–0.10 m	0.10–0.15 m	0.15–0.20 m	Mean
Scott Base	1.931	2.075*	1.797	1.779	1.896
± std error	±0.053	±0.046	±0.057	±0.050	
Coombs Hills	1.711	1.818	1.763	1.735	1.757
± std error	±0.032	±0.062	±0.048	±0.038	
Northwind Valley	1.575	1.482	1.619	1.522	1.550#
± std error	±0.034	±0.033	±0.051	±0.034	

It therefore takes more energy to raise dry soil temperature by a unit amount at the Scott Base and Coombs Hills sites than it does at the Northwind Valley site. In soil with low heat capacity greater heat flux is experienced due to the larger thermal gradients created at the surface.

Soil heat capacity at the 0.05–0.10 m depth at the Scott Base temperature probe pit is significantly higher than the heat capacity of the other three layers. As a result of this, soil at this depth acts as a buffer which absorbs energy and reduces extreme temperature variations further down the profile.

Heat capacity measurements for the temperature probe pit at the Coombs Hills site range between 1.71 MJ $m^{-3}K^{-1}$ and 1.81 MJ $m^{-3}K^{-1}$ and shows no significant variation with depth. This trend is also seen at the Northwind Valley site where soil heat capacity range between 1.48 MJ $m^{-3}K^{-1}$ and 1.62 MJ $m^{-3}K^{-1}$. Consequently, the rate of temperature change throughout the profile at these sites would be fairly constant.

The spatial variability of soil heat capacity is quantified in Table 5.11 which shows there is no significant difference at any site over short distances (~10 m). The Scott Base site has the highest mean soil heat capacity as in Table 5.10, although none of the values exceeded 2 MJ $m^{-3}K^{-1}$ as it did in temperature probe pit at this depth.

This is probably due to the large spatial variability of soil particle sizes at this depth which effects the number of air gaps within the soil (see section 5.1.4). This is important because air has a heat capacity of ~0.00012 MJ $m^{-3}K^{-1}$.

Table 5.11 Mean (± std error) soil heat capacity measurements (MJ $m^{-3}K^{-1}$) from six randomly chosen locations within the Scott Base, Coombs Hills, and Northwind Valley field sites. Samples were taken from a depth of 0.0–0.05 m at Scott Base and the Northwind Valley, and 0.10–0.15 m at Coombs Hills. The '#' indicates a value which is significantly different from the other mean values according to the LSD test at the 95% level of confidence.

Site	loc. 1	loc. 2	loc. 3	loc. 4	loc. 5	loc. 6	Mean (s.dev)
Scott Base	1.714	1.799	1.913	1.951	1.802	1.947	1.854#
± std error	±0.056	±0.028	±0.104	±0.101	±0.068	±0.063	(0.09)
Coombs Hills	1.549	1.706	1.669	1.707	1.645	1.595	1.645
± std error	±0.053	±0.013	±0.090	±0.073	±0.078	±0.065	(0.06)
Northwind valley	1.662	1.590	1.715	1.617	1.542	1.628	1.626
± std error	±0.042	±0.032	±0.077	±0.050	±0.054	±0.030	(0.05)

The mean soil heat capacity at the Northwind Valley site is once again the lowest, although the mean value at the Coombs Hills is not much greater. These values are also slightly different from those given for the temperature probe pit, which again is probably due to the spatial variability of soil particle sizes which influences the number of air filled pores.

5.2.2 SOIL THERMAL CONDUCTIVITY

Soil thermal conductivity was measured using 2 probes, a powerless and a powered probe which changes temperature proportionately to the soils thermal conductivity once inserted into the soil. To determine which is most useful, the results obtained using each technique at the Scott Base site will be examined. Based on these finding, the most realistic thermal conductivity measurements at each site will be presented and compared.

5.2.2.1 Comparison of measurement techniques

Thermal conductivity measurements for the Scott Base temperature probe pit using the various measurement techniques are presented in Table 5.12. There was usually only one measurement for each sample with the powerless probe and five measurements were made with the powered probe.

Table 5.12 Thermal conductivity measurements ($Wm^{-2}K^{-1}$) for the temperature probe pit at Scott Base using the hot and cold powerless probe and the powered probe

	0.0–0.05 m	**0.05–0.10 m**	**0.10–0.15 m**	**0.15–0.20 m**
field measurements				
Powerless Probe - hot	0.222	0.222	0.188	-
Laboratory measurements				
(Field Moisture)				
Powerless Probe - hot	0.400	0.413	0.295	0.3319
Powerless Probe - cold	0.498	0.460	0.514	0.464
Laboratory measurements				
(Oven Dry)				
Powerless Probe - hot	0.558	0.494	0.264	0.379
Powerless Probe - cold	0.440	0.320	0.175	0.265
Powered Probe ± std error	0.261	0.255	0.254	0.272
(done back in New Zealand)	±0.012	±0.017	±0.016	±0.015

The thermal conductivity of sandy soil like those found in Antarctica should be between 0.25–0.3 $Wm^{-2}K^{-1}$ according to Oke (1987).

Most of the measurements made using the hot and cold powerless probe are well above these ideal values which makes the accuracy of this technique questionable. The only measurements which appear to be consistently realistic are those obtained in the laboratory using the powered probe. The field measurements using the hot powerless probe are similar to these values.

Cold powerless probe measurements are always higher than the hot probe values on field moist samples, and the hot probe measurements are always higher then the cold probe values on oven dry samples.

This first discrepancy is probably due to condensation forming on the cold probe once inserted, which increases the soil moisture content, and subsequently soil thermal conductivity around the probe. The hot probe trend on oven dry samples is not fully understood.

Laboratory measurements made with the powerless probe were all greater than both the measurements using the hot powerless probe in the field and the powered probe in the laboratory. This suggests thermal conductivity measurements are being over estimated using the powerless probe technique and again questions its reliability.

These problems could be associated with difficulties encountered during probe insertion. If the probe was not held still during insertion, an air gap was created around the probe which reduced the probes contact with the soil necessary for an accurate measurement. When stones were struck, this also disturbed the soil around the probe and allowed the probes temperature to change significantly before it was fully inserted.

The powerless probe data shows lower thermal conductivity at the 0.10–0.15 m depth. This is not shown in the powered probe results. This soil layer contains a high percentage of large soil particles (Figure 5.1) which have numerous air spaces between them. Therefore, lower thermal conductivity at this depth would be consistent with the soil composition and structure.

The same measurement techniques were also used to determine the spatial variability of thermal conductivity at Scott Base (Table 5.13). These results show that thermal conductivity measurements made with the powerless probes are often questionably high and the same hot and cold probe trends are apparent as seen previously.

Soil thermal conductivity does not significantly change with a 5% increase in moisture content using the hot powerless probe. This indicates the technique is not sensitive to moisture content variations because thermal conductivity should increase as moisture content increases (Oke, 1987).

All measurement techniques show the same pattern of varying thermal conductivity between locations, and again, the powered probe gave results similar to those found in the literature. Field measurements using the hot powerless probe were similar to the powered probe results which suggests these values are realistic.

Table 5.13 Soil thermal conductivity measurements ($Wm^{-2}K^{-1}$) for 6 randomly chosen locations within the Scott Base field site using the hot and cold powerless probe and the powered probe. All samples taken from a depth of 0.0–0.05 m.

	loc. 1	loc. 2	loc. 3	loc. 4	loc. 5	loc. 6
field measurements						
Powerless Probe - hot	0.259	0.232	0.202	0.234	-	0.227
Laboratory measurements						
(Field Moisture)						
Powerless Probe - hot	0.339	0.419	0.411	0.550	0.279	0.432
Powerless Probe - cold	0.400	0.400	0.468	0.705	0.400	0.507
Laboratory measurements						
(Field moisture + 5%)						
Powerless Probe - hot	-	0.475	0.375	0.557	0.363	0.498
Laboratory measurements						
(Air Dry)						
Powerless Probe - hot	0.448	0.499	0.366	0.438	0.406	0.522
Powerless Probe - cold	0.400	0.496	0.300	0.280	0.294	0.346
Laboratory measurements						
(Oven Dry)						
Powerless Probe - hot	0.337	0.473	0.414	0.518	0.510	0.550
Powerless Probe - cold	0.275	0.400	0.290	0.344	0.338	0.480
Powered Probe ± std error	0.225	0.246	0.195	0.347	0.227	0.210
(done back in New Zealand)	±0.021	±0.012	±0.017	±0.012	±0.016	±0.019

Based on this information, thermal conductivity measurements made with the powered probe in the laboratory seem to be the most realistic and reliable. Measurements made using this technique will consequently be used to characterise soil thermal conductivity at each site.

These samples are however disturbed which could alter their natural thermal conductivity. To avoid this, future field measurements could be easily made with the powered probe because of its small size, ease of insertions and reliability.

5.2.2.2 *Thermal conductivity results for each field site*

Thermal conductivity measurements for the temperature probe pit at each field site are presented in Table 5.14 which shows the mean thermal conductivity at each site is significantly different.

Thermal conductivity measurements at the Scott Base site do not vary significantly with depth unlike those at the Coombs Hills site. Soil at the 0.05–0.10 m, and 0.15–0.20 m depths at this site have significantly lower thermal conductivity which means heat will not pass through these layers as readily. Soil thermal conductivity also varies with depth at the Northwind Valley site. Soil at the 0.05–0.10 m depth has a significantly lower thermal conductivity than the other layers which will increase the time taken for temperature changes to reach the lower part of the profile.

Table 5.14 Mean soil thermal conductivity measurements ($Wm^{-2}K^{-1}$) for the temperature probe pit at the Scott Base, Coombs Hills, and the Northwind Valley field sites. Measurements were made using the powered thermal conductivity probe in the laboratory on oven dry samples. The '*' identifies significant statistical differences within rows at the 95% level of confidence using the LSD test. The '#' indicates significant differences within columns.

Site	0.0–0.05 m	0.05–0.10 m	0.10–0.15 m	0.15–0.20 m	Mean
Scott Base	0.261	0.255	0.254	0.272	0.261#
± std error	±0.012	±0.017	±0.016	±0.015	±0.004
Coombs Hills	0.273	0.187*	0.226	0.182*	0.217#
± std error	±0.009	±0.011	±0.017	±0.014	±0.021
Northwind Valley	0.232	0.179*	0.200	0.209	0.205#
± std error	±0.013	±0.008	±0.009	±0.009	±0.011

Soil thermal conductivity is not spatially variable as shown in Table 5.15 apart from a significantly different value at location 4 of the Scott Base site. The soil at this depth has a lower bulk density and higher particle density than the other layers (see Table 5.7) which could cause this. Soil thermal conductivity at location 2 of the Northwind Valley site also appears to be higher than the other five measurements, but this is not a statistically significant difference.

The mean values for each depth are similar to the results obtained from the temperature probe pit which therefore supports the reliability of this method.

Table 5.15 Mean soil thermal conductivity ($Wm^{-2}K^{-1}$) for 6 randomly chosen locations within the Scott Base, Coombs Hills, and Northwind Valley field sites. Samples were taken from a depth of 0.0–0.05 m at Scott Base and the Northwind Valley, and 0.10–0.15 m at Coombs Hills. The '*' indicates value(s) within rows which are significantly different at the 95% confidence level based on the LSD test.

Site	loc. 1	loc. 2	loc. 3	loc. 4	loc. 5	loc. 6	Mean (s.dev)
Scott Base	0.225	0.246	0.195	0.347*	0.227	0.210	0.242
± std error	± 0.021	± 0.012	± 0.017	± 0.012	± 0.016	± 0.019	±0.022 (0.054)
Coombs Hills	0.227	0.219	0.258	0.235	0.253	0.211	0.234
± std error	± 0.016	±0.013	±0.020	±0.019	±0.020	±0.010	±0.008 (0.019)
Northwind valley	0.226	0.314	0.267	0.260	0.249	0.257	0.262
± std error	±0.028	±0.027	±0.019	±0.016	±0.021	±0.020	±0.012 (0.029)

5.2.2.3 Soil Thermal conductivity with changing moisture content

The influence of changing moisture content on the thermal conductivity of Antarctic soils was determined. Water was incrementally added to samples taken from a depth of 0.0–0.05 m at each site. This depth was chosen because it is the surface layers which receive most moisture and controls the movement of heat into, and out of, the profile. The samples were mixed well and re-packed to a consistent bulk density and the soil thermal conductivity measured (Table 5.16). Soil moisture content was determined by sub-sampling after each conductivity measurement and oven drying as described in Section 3.3.3.

Fine quartz sand was used as a control during this experiment since its thermal response to increasing moisture content has been well documented. The soil moisture content was increased until the sample became saturated and moisture pooled at the bottom of the container.

Oke (1987), Riha *et al.*, (1980), Wierenga *et al.*, (1969), Sepaskhah and Boersma (1979), and numerous other researchers have reported that soil thermal conductivity increases as soil moisture content increases. As shown in Figure 5.8, this classic trend was observed for the sand sample, but was only apparent for the Scott Base, Coombs Hills, and Northwind Valley samples after an initial decline of thermal conductivity. This behaviour has not been reported by any of the previously mentioned authors.

Table 5.16 Soil thermal conductivity with increasing moisture content.

Sand				
Volumetric moisture content	0%	2%	6%	10%
Thermal conductivity ($Wm^{-2}K^{-1}$)	0.319	0.336	1.170	1.540
± std error	±0.049	±0.020	±0.206	±0.202
Scott Base soil				
Volumetric moisture content	0%	5%	8%	12%
Thermal conductivity ($Wm^{-2}K^{-1}$)	0.549	0.428	0.299	0.826
± std error	±0.040	±0.035	±0.024	±0.124
Coombs Hills soil				
Volumetric moisture content	0%	5%	9%	15%
Thermal conductivity ($Wm^{-2}K^{-1}$)	0.545	0.400	0.427	0.794
± std error	±0.076	±0.047	±0.129	±0.117
Northwind Valley soil				
Volumetric moisture content	0%	4%	9%	12%
Thermal conductivity ($Wm^{-2}K^{-1}$)	0.608	0.526	1.636	3.351
± std error	±0.037	±0.023	±0.274	±0.469

Noborio and McInnes (1993) found that the thermal conductivity of salt affected soils decreased as salinity increased. It is therefore possible that the decrease in thermal conductivity observed is due to an initial increase in the moistures salt content as salt crystals coating individual grains dissolve. This is possible with the Northwind Valley soil which has a relatively high salt content at this depth, but is unlikely for the Scott Base or Coombs Hills soils which have low salt contents (Table 5.8).

It is possible that because the Scott Base soil is basaltic and highly vesicular, moisture is initially adsorbed into the particles instead of forming menisci between particles which is what causes increased thermal conductivity. Salt coating the soil particles at the Coombs Hills site may also prevent menisci from forming, hence initially reducing its initial thermal conductivity.

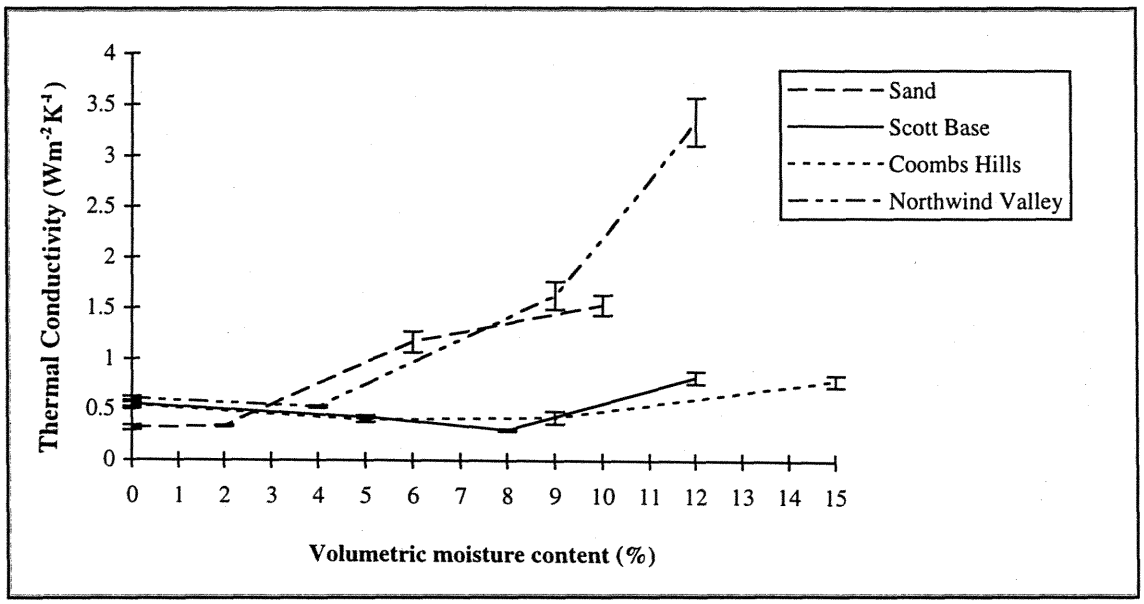

Figure 5.8 Antarctic soil thermal conductivity at various moisture contents. The error bars indicate increasing measurement error with increasing moisture content.

As soil moisture content increases, the standard error increased for all samples which indicates increasing measurement error. The reason for this is not understood.

Measurements for oven dry soil (0% moisture content) were all ~0.3 $Wm^{-2}K^{-1}$ larger than the results obtained when the initial sample soil thermal conductivity was measured (Figure 5.14). The standard error was not significantly greater for either set of measurements which suggests that, although the measurements made consecutively are reliable, they are not reproducible once the equipment has been dismantled and reassembled. An adequate explanation for this is not yet available.

The overall trends however show that the Northwind Valley site's thermal conductivity increase most with increasing moisture content and the Coombs Hills soil increases least. This means under moist conditions, the rate of heat transfer in the Northwind Valley soil will increase more than that in the Coombs Hills and Scott Base soil.

5.2.3 SOIL THERMAL DIFFUSIVITY

From the soil heat capacity and thermal conductivity results, the soil thermal diffusivity for the temperature probe pit (Table 5.17) is calculated using Equation 2.9 to determine the rate temperature changes travel through the soil. The spatial variability of this thermal property is also summarised in Table 5.18.

These values are lower than those given by Oke (1987) for dry sandy soil (0.24×10^{-6} m^2 s^{-1}). This does however show that thermal admittance varies slightly with depth at each site, but on average is similar at all sites.

Table 5.17 Soil thermal diffusivity (m^2 $s^{-1}\times10^{-6}$) calculated from the soil thermal conductivity and heat capacity measurements (Equation 2.9) made in Sections 5.2.1 and 5.2.2.

Site	0.0–0.05 m	0.05–0.10 m	0.10–0.15 m	0.15–0.20 m	Mean (s.dev)
Scott Base	0.135	0.123	0.141	0.153	0.138 (0.011)
Coombs Hills	0.160	0.103	0.128	0.105	0.124 (0.023)
Northwind Valley	0.147	0.121	0.124	0.137	0.132 (0.011)

Table 5.18 Spatial variability of soil thermal diffusivity (m^2 $s^{-1}\times10^{-6}$) calculated from the soil thermal conductivity and heat capacity measurements made (Equation 2.9) in Sections 5.2.1 and 5.2.2.

Site	loc. 1	loc. 2	loc. 3	loc. 4	loc. 5	loc. 6	Mean (s.dev)
Scott Base	0.131	0.137	0.102	0.178	0.126	0.108	0.130 (0.025)
Coombs Hills	0.147	0.128	0.155	0.138	0.154	0.132	0.142 (0.010)
Northwind valley	0.136	0.197	0.156	0.161	0.161	0.158	0.162 (0.018)

Spatially, soil thermal diffusivity does not vary significantly at any site, but on average, is highest at the Northwind Valley site and least at the Scott Base site. Therefore heat will move most rapidly and penetrate deeper in the Northwind Valley soil, and will move most slowly and only reach relatively shallow depths at the Scott Base site.

This trend was not apparent in Table 5.17, but could be a significant determinant of the soil thermal regime over larger distances.

5.3 SURFACE RADIATION BALANCE

Radiation inputs in the Antarctic during December and January are relatively large because the sun is above the horizon for 24 hours a day. Due to the influence solar altitude has on incoming radiation, maximum inputs occur at solar noon and minimum radiation reaches the surface at midnight. At Scott Base during January for example, the solar angle can reach 35° during the day, but only reaches about 8° at midnight (Thompson and Macdonald, 1962).

The surface radiation balance at each field site is described under clear sky and cloudy conditions to quantify the likely range of incoming, reflected and outgoing solar radiation. Surface albedo is described in detail because of its importance in determining the amount of energy entering the soil system.

5.3.1 INSTRUMENT ACCURACY

By comparing $K\downarrow$ data collected at the Scott Base field site with measurements made at the permanent Scott Base climate station by the New Zealand Antarctic Programme (NZAP), the relative accuracy of the equipment used can be assessed (Figure 5.9).

Both data sets are very similar and indicate radiation measurements made at the field site are fairly accurate. The slight difference in magnitude could be due to different instruments being used at each site or the instruments positioning, mounting angle or stability.

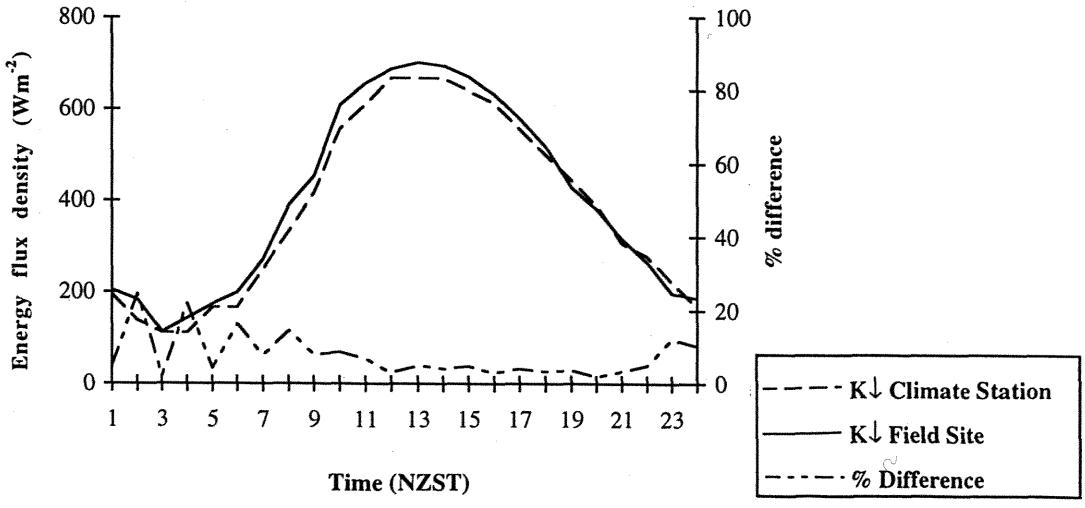

Figure 5.9 Comparison of $K\downarrow$ measurements made at the Scott Base field site and the Scott Base climate station on 23 December, 1994. Climate Station data supplied by the National Institute of Water and Atmospheric Research, Wellington.

5.3.2 SCOTT BASE

During the measurement period at Scott Base (December 18–29), several snowfall events and hoar frosts were experienced which covered the instruments in snow and rime. The results obtained during these times are unreliable and will therefore be ignored when analysing the data.

5.3.2.1 Radiation balance components at Scott Base under clear sky conditions

Several clear sky days were experienced at Scott Base of which only December 23 shows the surface radiation balance for this surface type free from snow (Figure 5.10).

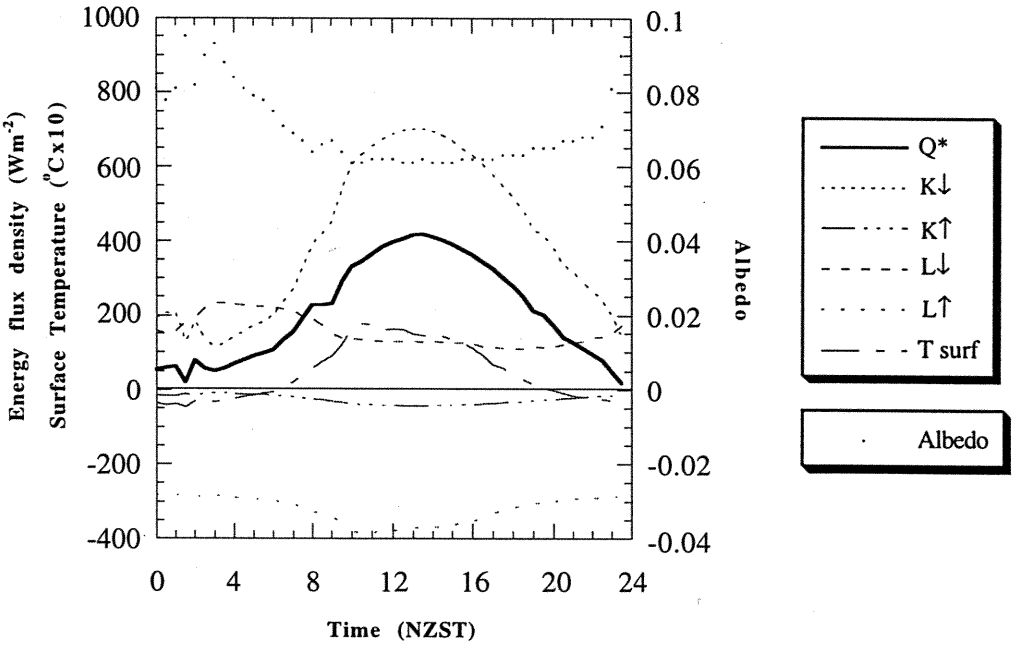

Figure 5.10 Measured and estimated radiation balance components for a clear sky day at the Scott Base Site, 23 December, 1994. Albedo is dimentionless.

Excluding morning measurements (<0930) which were affected by cloud cover, mean daily Q^* was 18.60 MJ $m^{-2}d^{-1}$. This reached a maximum of 701 Wm^{-2} at 1330 and dropped to a minimum of 143 Wm^{-2} at midnight which corresponds to the times of maximum and minimum solar altitude. These values compare well with those obtained by Balks *et al.*,. (1994) who found that $K\downarrow$ at Scott Base peaked at approximately 680 Wm^{-2} at solar noon in early January and was a minimum of approximately 160 Wm^{-2} at night.

Surface albedo showed a distinct diurnal trend whereby it decreased during the morning to reach a minimum of 0.06 at midday, and increased during the afternoon/evening to 0.09 at 2330. This late evening value is less reliable because of increased relative measurement error at low solar altitudes. The 24 hour albedo for this day was 0.065 and the mean midday albedo (between 1100 and 1300 hours) was 0.062.

As a result of the low mean daily albedo, $K\uparrow$ was only -2.27 MJ $m^{-2}d^{-1}$. This means the dark coloured basalt surface reflects less than 7% of incoming shortwave radiation under these conditions. Maximum $K\uparrow$ of -143 Wm^{-2} was measured at 1330 and a minimum of 12.2 Wm^{-2} was reflected at 2330, which again corresponds to the times of maximum and minimum $K\downarrow$.

$L\uparrow$ was estimated using Equation 3.1 and $L\downarrow$ was calculated by solving the radiation balance (Equation 2.1). On average, $L\uparrow$ = -27.79 MJ $m^{-2}d^{-1}$. The absolute magnitude of $L\uparrow$ steadily increased as the surface heated up during the morning, and then decreased as the surface cooled during the afternoon as the amount of incoming shortwave radiation decreased. Both $L\downarrow$ and $L\uparrow$ are relatively constant, and L^* had an average value of -14.29 MJ $m^{-2}d^{-1}$.

5.3.2.2 Radiation balance components at Scott Base under cloudy conditions

Clouds are frequent over Ross Island due to its maritime climate and these are often associated with precipitation events. December 25 was chosen to describe the radiation balance of the site under cloudy conditions (Figure 5.11).

Due to the low transmissivity of clouds, mean daily Q^* was reduced from 18.60 MJ $m^{-2}d^{-1}$ on the clear sky day to 12.44 MJ $m^{-2}d^{-1}$ on the cloudy day, and mean $K\downarrow$ reaching the surface was significantly smaller (22.58 MJ $m^{-2}d^{-1}$ versus 35.16 MJ $m^{-2}d^{-1}$).

Apart from these magnitude differences, the same diurnal pattern was apparent where Q^*, $K\downarrow$, and surface temperature increased throughout the morning, peaked at about midday, and then decreased during the afternoon and evening.

Mean daily albedo was 0.074 under these conditions which is significantly larger than the 0.065 experienced on the clear sky day. The mean midday albedo was 0.064, which is nearly identical to the albedo experienced on the clear sky day.

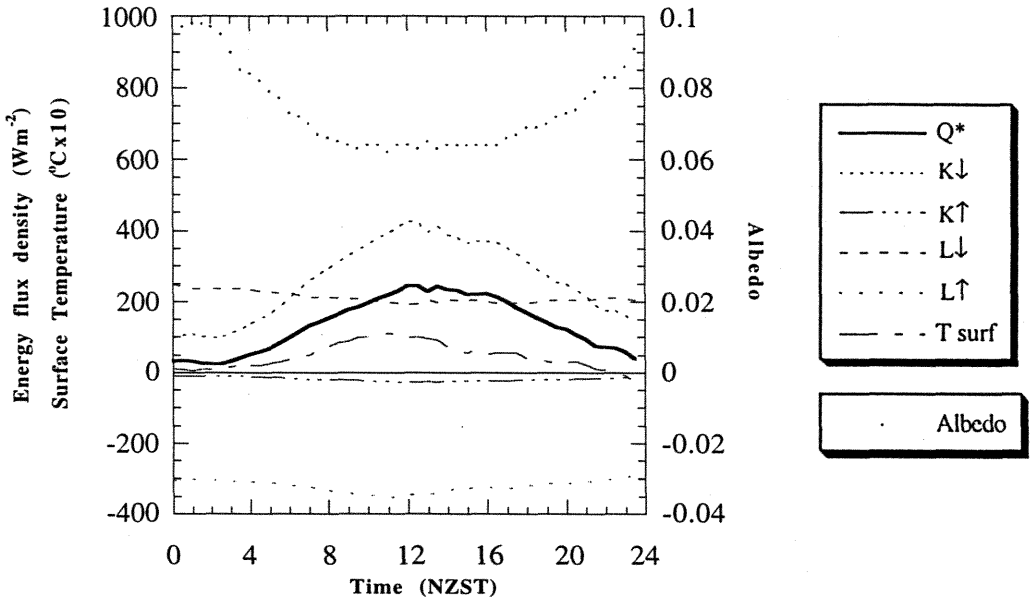

Figure 5.11 Measured and estimated radiation balance components for a cloudy day at the Scott Base site, 25 December, 1994.

On average, $L\uparrow$ = -26.89 MJ $m^{-2}d^{-1}$ for the cloudy day (Table 5.17). This is almost identical to $L\uparrow$ on the clear sky day which was -27.79 MJ $m^{-2}d^{-1}$ due to similar mean surface temperatures on both days. The amount of $L\downarrow$ on the cloudy day (18.33 MJ $m^{-2}d^{-1}$) was greater than that received on the clear sky day (13.50 MJ $m^{-2}d^{-1}$) which is due to the clouds absorbing longwave radiation and re-emitting it back towards the surface.

L^* on the cloudy day was consequently greater than L^* on the clear sky day (Table 5.17) which means Q^* is still significant under cloudy conditions, despite substantially less shortwave radiation entering the system.

5.3.2.3 Surface albedo

The diurnal trend in albedo seen on both clear sky (Figure 5.10) and cloudy (Figure 5.11) days is a regular feature of the Scott Base radiation balance and is a function of changing solar altitude and azimuth as shown in Figure 5.12. Solar altitude was not directly measured, so values were taken from Thompson and Macdonald's (1962) chart showing the sun's altitude and azimuth at Scott Base at any time of the year.

As solar altitude increases during the morning, surface albedo decreases on both clear sky and cloudy days and reaches a minimum value at about solar noon when the maximum solar altitude is reached. This occurs because incoming shortwave radiation is maximised at this time of day and outgoing radiation is minimised (Brown and Fitzharris, 1993).

During the afternoon under both conditions, surface albedo is lower than the morning values and increases as solar altitude decreases. This apparent hysteresis is due to changing solar azimuth throughout the day and anisotropic surface reflectance due to wind polishing (Brown and Fitzharris, 1993). The dominant wind direction at the site for example is from the north-east (Bromley, 1994). This could preferentially polish the north east side of surface stones and effectively increase the surface albedo when solar radiation comes from that direction, as it does in December during the morning (Thompson and Macdonald, 1962). Surface roughness then increases as the solar azimuth changes and as a result surface albedo decreases. It could also be due to the different spectral quality of incoming radiation during the afternoon as recognised by Nkemdirim (1972).

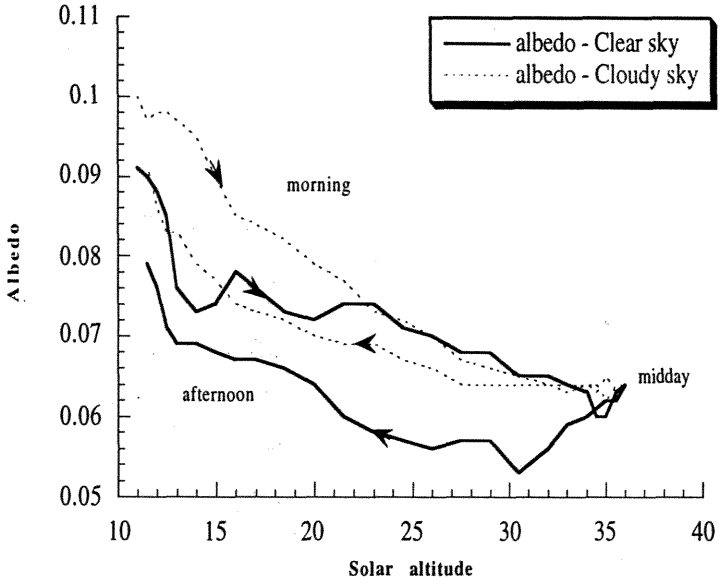

Figure 5.12 Relationship between albedo, solar altitude and azimuth at the Scott Base site under clear sky (26 December, 1994) and cloudy (25 December, 1994) conditions.

Snowfall events, which are common at this site, can also either increase of decrease surface albedo depending on whether a snow pack is formed or it melts and darkens the surface. A maximum albedo of 0.84 for example, was recorded after a heavy snowfall on

December 28 (Figure 5.13). Once this had begun to melt or was blown off the site, surface albedo decreased to about 0.3.

The minimum albedo recorded under sunny, snow free conditions was 0.053. Balks *et al.*, (1995) recorded values as low as 0.046, but found the average albedo during the middle part of the day was about 0.05. These measurements were however made on a slightly sloping site.

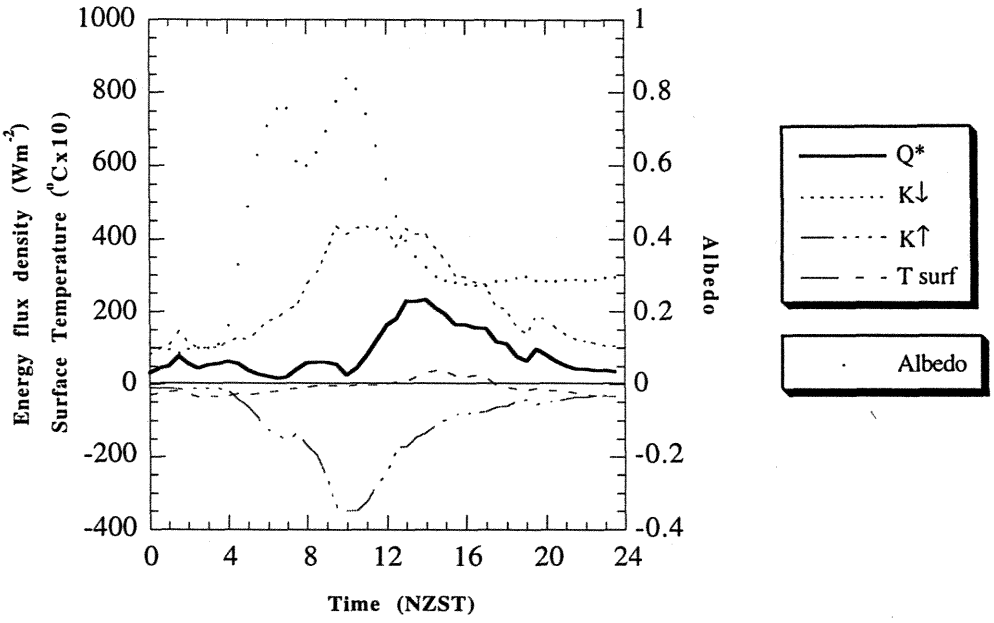

Figure 5.13 Measured radiation balance components for 28 December, 1994 on which it snowed heavily at about 0800 hours causing surface albedo to increase significantly.

The main feature of Figure 5.13, apart from the large rise in albedo, is that maximum $K\uparrow$ (347 Wm^{-2} at 1030 hours) is significantly larger under these conditions than it was on either the clear sky or cloudy day. 81% of $K\downarrow$ is being reflected which means there is minimal energy available to heat the surface and melt the snow. This is due to the high albedo of the snow.

Mean daily $K\downarrow$ (20.00 MJ m^{-2} d^{-1}) was slightly smaller on this day than it was on the cloudy day (22.58 MJ m^{-2} d^{-1}) which is probably due to the dark clouds associated with snowfall events. These measurements are however effected by snow which might have settled on the pyranometer during the snowfall event. Average $K\uparrow$ was -9.10 MJ m^{-2} d^{-1} which is significantly larger than that seen on either the clear sky or cloudy day (Table 5.19).

$L\uparrow$ and $L\downarrow$ could not be calculated under these conditions because soil surface temperature which is used to determined $L\uparrow$ (Equation 3.1) is not representative of the true snow surface temperature. L^* can however be calculated using the radiation balance Equation 2.1.

Table 5.19 Measured and estimated mean daily radiation balance components (MJ m^{-2} day^{-1}) and albedo (dimensionless) for the Scott Base site under clear sky and cloudy conditions.

	Clear Sky (Dec. 23, 1994)	**Cloudy Sky (Dec. 25, 1994)**	**Snow Cover (Dec. 28, 1994)**
K↓	35.16	22.58	20.00
K↑	-2.27	-1.58	-9.10
L↓	13.50	18.33	-
L↑	-27.79	-26.89	-
K*	32.89	21.00	10.9
L*	-14.29	-8.56	-1.46
Q*	18.60	12.44	7.44
Albedo	0.065	0.074	0.46

These values are comparable to those obtained by Balks *et al.*, (1994) at Scott Base from December 1993 to January 1994.

5.3.3 COOMBS HILLS

As a result of the Coombs Hills being situated on the edge of the polar plateau, cloud cover and persistent winds characterise this site. Frequent snowfall events occurred during the measurement period (January 9–17) and snow redistribution by wind was common. These events often changed surface properties at the site such as albedo which must be considered when interpreting these results. The instruments were also covered in rime and snow periodically which also makes some measurements unreliable.

5.3.3.1 Radiation balance components at Coombs Hills under clear sky conditions

Only partly clear sky days were experienced at the Coombs Hills site and out of these, January 11 best describes the diurnal radiation balance at this site under these conditions (Figure 5.14).

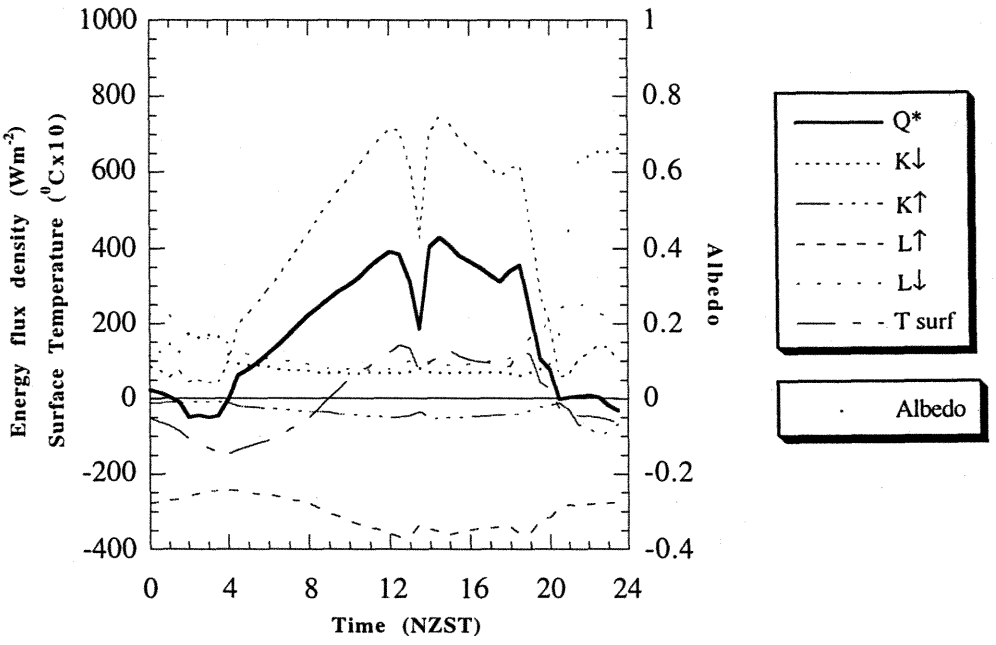

Figure 5.14 Measured and estimated radiation balance components for a predominantly clear sky day (11 January, 1995) at the Coombs Hills site.

As indicated by surface albedo measurements, snow deposited on the site on January 10 had fully melted by 0800 hours as incoming solar radiation increased throughout the morning. At about 1300 hours clouds covered the site which reduced $K\downarrow$, Q^* and surface temperature, and slightly increased $K\uparrow$, $L\uparrow$, $L\downarrow$ and surface albedo.

Once these had cleared, incoming short wave radiation reached a maximum of 745 Wm^{-2} at 1500 hours. This was slightly higher than the maximum recorded at Scott Base (701 Wm^{-2}) which is probably due to altitudinal differences between the two sites. The Coombs Hills for example is ~2000 m above sea level which means the atmosphere is ~1900 m thinner above this site than it is above the Scott Base site. This therefore means there is less opportunity for atmospheric particles to absorb, reflect and dissipate incoming radiation at the Coombs Hills.

On a daily basis (Table 5.18), $K\downarrow$ was greater at the Scott Base site (35.16 MJ $m^{-2}d^{-1}$ versus 33.00 MJ $m^{-2}d^{-1}$). This is probably due to the midday cloud cover which affected the Coombs Hills measurements and possible shading in the evening by the surrounding hills.

A few clouds passed over the site during the afternoon and by about 2000 hours it had fully clouded over and began snowing. Prior to this, minimum surface albedo was 0.063 at 1830 hours which is similar to that recorded at the Scott Base site. On average, surface albedo at the Coombs Hills site between 0800 and 1600 hours was however 0.07 which is slightly higher than that experienced at the Scott Base site over the same time period (0.062). Therefore the surface at the Coombs Hills site is more reflective. This is probably because it has a well developed desert pavement which has been polished by wind abrasion over a long period of time. Surface reflectance is consequently higher at low solar altitudes.

Surface albedo increased dramatically after ~2 hours of snowfall to a maximum of 0.66. There could however be measurement errors involved in this late evening measurement due to low solar altitude and snow settling on the upward facing solarimeter.

Between 0800 and 1600 hours when the site was free of snow, mean $K\uparrow$ was -44 Wm^2 which is slightly higher than that measured at the Scott Base site (-38 Wm^2) under the same conditions. Mean daily absolute $K\uparrow$ was also slightly higher at the Coombs Hills site (-3.14 MJ $m^{-2}d^{-1}$ versus -2.27 MJ $m^{-2}d^{-1}$) which is probably due to the higher surface albedo at this site. After it snowed, $K\uparrow$ became more negative, due to the increased albedo.

The absolute values of $L\uparrow$ increased throughout the morning as snow from the previous day melted and reached a maximum of -368 Wm^2 at 1230 hours. It then decreased once fresh snow covered the site late in the day. $L\downarrow$ increased in response to periodic cloud cover throughout the day, but remained fairly constant the rest of the time. Mean daily L^* was -14.41 MJ $m^{-2}d^{-1}$ which is very similar to that recorded at the Scott Base site (-14.29 MJ $m^{-2}d^{-1}$).

Mean daily Q^* was lower at this site than it was at the Scott Base site (15.45 MJ $m^{-2}d^{-1}$ versus 18.60 MJ $m^{-2}d^{-1}$) due to less $K\downarrow$, and more $K\uparrow$ as a result of the higher surface albedo. There is consequently more energy available at Scott Base to drive surface and sub-surface processes.

5.3.3.2 Radiation balance components at the Coombs Hills site under cloudy conditions

Cloud cover is often accompanied by snowfall events at this site, and as a result there were no fully overcast days with constant surface conditions during the measurement period. January 13 was the most suitable day to examine despite early morning riming of

the solarimeters, a brief period of sunshine at midday and heavy snowfall during the late afternoon (Figure 5.15).

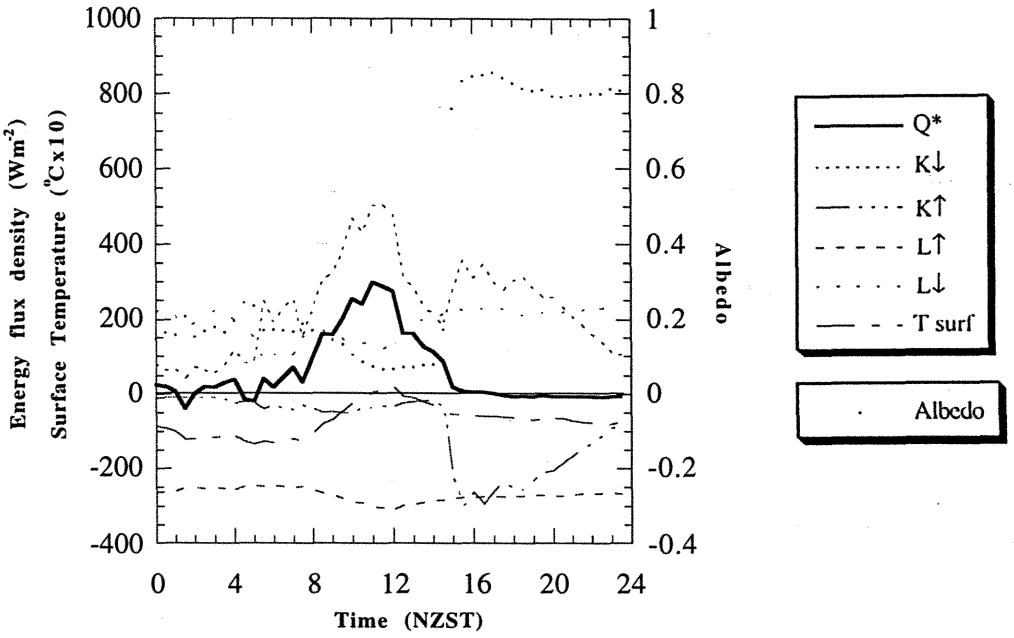

Figure 5.15 Measured and estimated radiation balance components for a cloudy day (13 January, 1995) at the Coombs Hills site.

The maximum amount of incoming short wave radiation recorded on the cloudy day (505 Wm^2) was less than that recorded on the clear sky day (745 Wm^2) which again highlights the effect of cloud cover. Immediately prior to the snowfall event which began at about 1500 hours, $K\downarrow$ decreased noticeably in response to the clouds darkening and then increased for a while during the snowfall event. This shows cloud transmissivity varies throughout the day, during storm events, and with different cloud types.

A diurnal trend in albedo under cloudy conditions is not shown on this day because of the sunny period at ~1200 hours and snow fall which covered the site. A minimum albedo of 0.068 was observed at 1200 hours which corresponds to the sunny period and a maximum albedo of 0.86 was recorded at 1700 hours after it had been snowing for several hours. Measurement error would however be significant due to snow covering the upward facing solarimeter.

Up until about 1400 hours, $K\uparrow$ remained fairly low and only showed a slight response to the late morning rise in $K\downarrow$. However once snow began falling, the amount of $K\uparrow$ significantly increased by ~300 Wm^{-2} and then closely followed trends in $K\downarrow$. Variations

in $K\uparrow$ on the clear sky day at this site were not as pronounced as those described above and were not observed at the Scott Base site at all.

$L\uparrow$ was greatest at times of maximum $K\downarrow$ and fluctuated throughout the day by about -125 Wm^{-2} in response to changing $K\downarrow$ and surface temperature. $L\downarrow$ peaked at times of maximum cloud cover as expected. Mean daily L* was -7.14 MJ $m^{-2}d^{-1}$ which is a lower magnitude than that experienced on the clear sky day. It is also lower than the -8.56 MJ $m^{-2}d^{-1}$ measured at the Scott Base site which means there is less net long wave flux at this site under these conditions. This could be due to darker clouds associated with the snow fall event.

Mean daily Q^* was extremely low compared to that on the clear sky day (5.27 MJ $m^{-2}d^{-1}$) due to the large amount of $K\uparrow$ reflected by the surface which had a mean daily albedo of 0.40 (Table 5.18). Q^* was also a lot lower than it was at the Scott Base site on any day. This, combined with the low air temperatures (Figure 5.24) means that there is little energy available under these conditions to drive microclimatic processes.

5.3.3.3 Radiation balance components at the Coombs Hills site when the surface is covered in snow

Snow periodically covers many areas of the Dry Valleys which significantly change the surface radiation balance and soil thermal regime. On January 13 at the Coombs Hills site, snow covered the site in ~0.1 m snow. Figure 5.16 shows the radiation balance components for the following day. Much of the day remained fine although a few clouds passed overhead and a strong wind sometimes blew which redistributed snow and caused it to accumulate on the leeward side of large surface stones.

$K\downarrow$ exhibits a classic bell shaped curve which increases throughout the morning, peaks at about midday (720 Wm^{-2}) and then decreases throughout the afternoon. Clouds passing over the site do however cause fluctuations in $K\downarrow$ throughout the day. The sudden increase evident at about 2200 hours is probably due to measurement error at low solar altitudes.

The largest albedo recorded was 0.86 at about 0930 hours. As the snow aged and melted, the albedo decreased and reached a minimum of 0.63 at 1200 hours.

As a result of this high surface albedo, $K\uparrow$ was significant throughout the day and reached a maximum of -546 Wm^{-2} at 1330 hours. On average, it was -24.22 MJ $m^{-2}d^{-1}$

which is significantly higher than the -3.14 MJ $m^{-2}d^{-1}$ recorded under the same conditions when the site was predominantly free of snow.

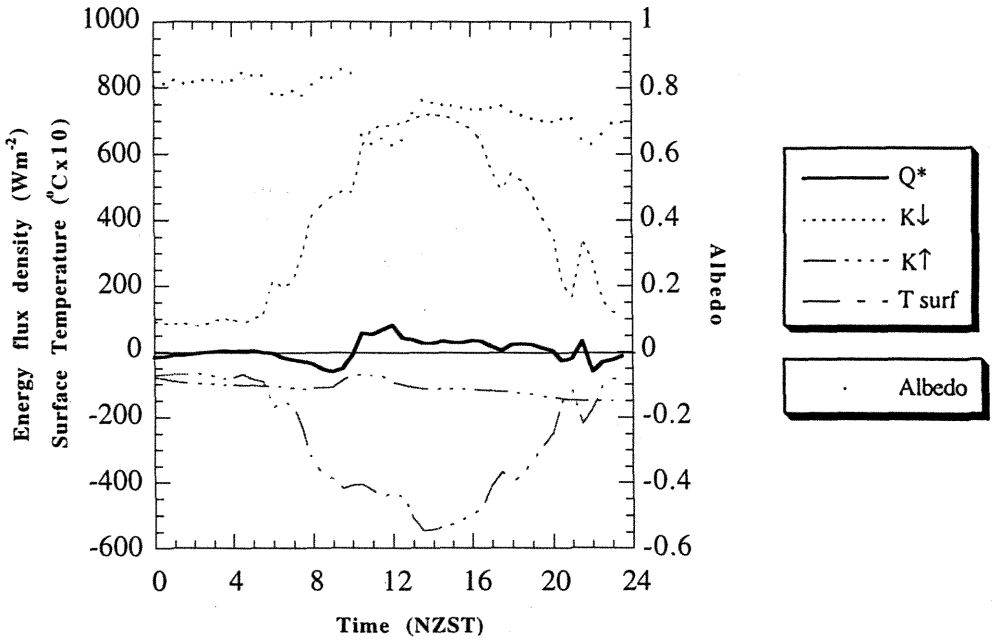

Figure 5.16 Measured radiation balance components for the Coombs Hills site under snow on 14 January, 1995.

Mean daily Q^* was only 0.12 MJ $m^{-2}d^{-1}$ which is extremely low compared to Q^* on the clear sky and cloudy day (Table 2). Q^* remained extremely low for the entire day and reached a maximum of 79 Wm^{-2} at about midday. This is considerably lower than maximum Q^* on the clear sky day (427 Wm^{-2}) and shows how a large amount of energy is being reflected away from the surface and lost from the system.

Table 5.20 - Mean daily radiation balance components (MJ m^{-2} day^{-1}) and surface albedo (dimentionless) for the Coombs Hills site under various conditions.

	Clear Sky (Jan. 11, 1995)	Cloudy sky (Jan. 13, 1995)	Surface Snow (Jan. 14, 1995)
K↓	33.00	20.58	33.07
K↑	-3.14	-8.17	-24.22
L↑	-26.69	-23.81	-
L↓	12.28	16.67	-
Q*	15.45	5.27	0.12
K*	29.86	12.41	8.85
L*	-14.41	-7.14	-8.73
Albedo	0.10	0.40	0.73

5.3.4 NORTHWIND VALLEY

The Northwind Valley site and surrounding sandstone outcrops were covered in ~4 cm of light powder snow on arrival at the Convoy Range which remained there for most of the measurement period (January 17-22). To allow radiation balance and thermal regime comparisons to be made with the other two snow free sites examined, the site was carefully swept with a soft brush which did not disrupt the natural surface. Fine weather was experienced for most of the measurement period although persistent cold winds and snow showers were encountered.

5.3.4.1 Radiation balance components at Northwind Valley under clear sky conditions

Figure 5.17 shows the radiation balance components for the Northwind Valley site free from snow under clear sky conditions.

$K\downarrow$ increased and decreased suddenly at about 0500 and 2100 hours respectively because the sun disappeared behind the surrounding hills for approximately 8 hours each night. $K\downarrow$ increased steadily throughout the morning and reached a maximum of 798 Wm^{-2} at 1420 hours. This is greater than the maximums reached at either of the Scott Base (710 Wm^{-2}) or Coombs Hills sites (745 Wm^{-2}).

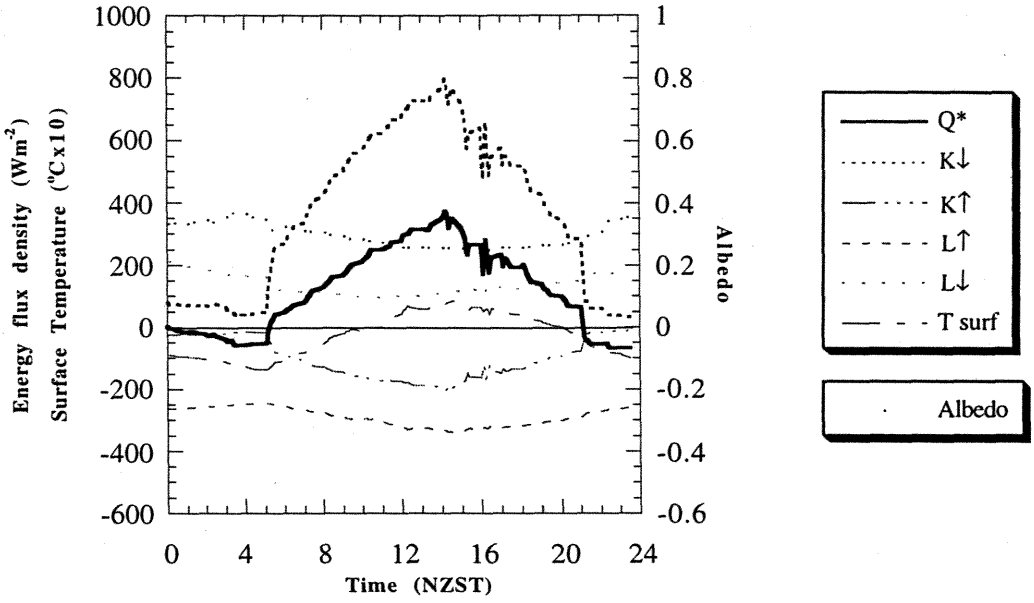

Figure 5.17 - Measured and estimated radiation balance components for a clear sky day (21 January, 1995) at the Northwind Valley site when the surface was clear of snow.

If the altitude hypothesis used to explain the difference between maximum $K\downarrow$ at the Scott Base and Coombs Hills site was valid, maximum $K\downarrow$ at this site should be somewhere in-between these two maximums. Therefore, it is possible that clouds which were sometimes present throughout the day increased the amount of $K\downarrow$ by reflection.

On average, this site received less $K\downarrow$ than the other two sites throughout the day (Table 5.21) which is due to the shading experienced at night and clouds which affected the site in the middle of the afternoon.

Surface albedo fluctuated noticeably throughout the day in response to changing solar altitude. Due to the shiny, highly polished nature of this surface, albedo increases a lot more at low light levels at this site than it did at the other two sites. This means less energy will be absorbed during the early morning and late afternoon. The maximum albedo recorded was 0.38 at 0350 This measurement is however unreliable because it was made when the site was shaded. The minimum albedo recorded was 0.25 at 1610 and 1640 which is larger than the minimum recorded at either of the other two sites which were around 0.06.

This supports Oke (1987) and many other authors who have stated that light coloured surfaces reflect more incoming solar radiation than dark coloured surfaces. Mean daily

albedo of 0.35 was also significantly higher than that experienced at the other two sites (0.065 at Scott Base and 0.10 at the Coombs Hills).

$K\uparrow$ remained relatively constant throughout the day and reached an absolute maximum of -203 Wm^{-2} at 1420 hours which coincides with the time of maximum $K\downarrow$. Mean $K\uparrow$ was -8.54 MJ $m^{-1}d^{-1}$ which is significantly larger than that measured under similar conditions at the other two sites (-2.27 MJ $m^{-2}d^{-1}$ at Scott Base and -3.14 MJ $m^{-2}d^{-1}$ at the Coombs Hills). This is caused by the higher albedo of the polished surface and results in less energy entering the soil system.

$L\uparrow$ and $L\downarrow$ both remained fairly constant throughout the day and had mean values of -24.95 MJ $m^{-2}d^{-1}$ and 11.93 MJ $m^{-2}d^{-1}$ respectively. These are similar to those recorded at the other two sites, except $L\uparrow$ is slightly smaller due to lower surface temperatures. As a result of the lower temperature near the surface, mean daily L^* (-13.02 MJ $m^{-1}d^{-1}$) was also smaller at this site than it was at either of the other two sites (-14.29 MJ $m^{-1}d^{-1}$ at the Scott Base site and -14.41 MJ $m^{-2}d^{-1}$ at the Coombs Hills).

Mean daily Q^* at this site (9.74 MJ $m^{-2}d^{-1}$) was less than Q^* at both the Scott Base site (18.60 MJ $m^{-2}d^{-1}$) and Coombs Hills site (15.45 MJ $m^{-2}d^{-1}$). This is partly because $K\uparrow$ is significantly larger at this site due to the unique surface properties, but is also a result of the site being shaded. At about midday when Q^* peaked and albedo is still relatively large, Q^* was 372 Wm^{-2} which is only slightly lower than Q^* at the other 2 sites at the same time. This occurred because $K\downarrow$ was ~90 Wm^{-2} larger and $L\uparrow$ was ~20 Wm^{-2} smaller at this site.

5.3.4.2 *Radiation balance components at the Northwind Valley site under cloudy conditions*

Overcast conditions were rare at the Northwind Valley site during the measurement period. The best day to examine the surface radiation balance under these conditions was January 20 despite clear skies in the morning and evening (Figure 5.18).

Ignoring the shading influence noted previously, $K\downarrow$ begins to increase early in the morning as it did on the clear sky day but then dropped suddenly by ~400 Wm^{-2} at about 1000 hours as clouds cover the site. Apart from a brief sunny spell at ~1100 hours shown by the sharp spike in $K\downarrow$, the clouds remained over the site until about 1800 hours. During this time, $K\downarrow$ was on average 297 Wm^{-2} which is significantly less than that recorded on the clear sky day during the same period (659 Wm^{-2}).

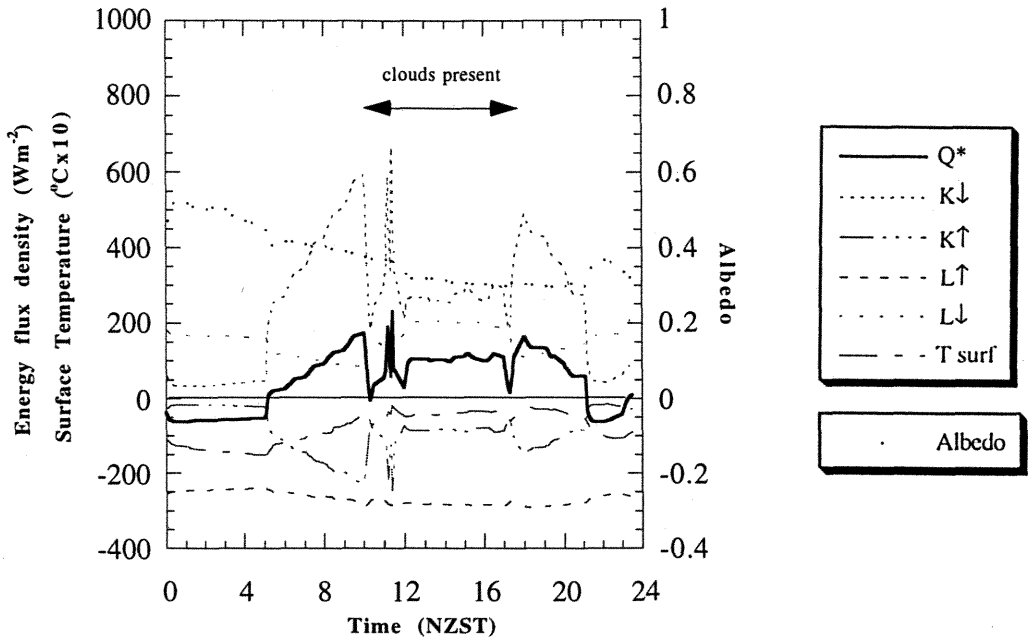

Figure 5.18 Measured and estimated radiation balance components for a cloudy day (20 January, 1995) at the Northwind Valley site.

Surface albedo fell noticeably throughout the day until shading caused it to increase in the late evening. During the cloudy period, mean albedo was 0.33 which is only slightly higher than that measured on the clear sky day during the same period (0.30).

Mean daily K^* was 13.64 MJ $m^{-2}d^{-1}$ which is slightly larger than that seen at the Coombs Hills site and a lot smaller than K^* at Scott Base under similar conditions. This is probably due to the different types of cloud present at each site on the days examined.

The trend noted at the other two sites of increasing mean daily $L\downarrow$ on the cloudy day was also noted here with $L\downarrow$ increasing from 11.93 MJ $m^{-2}d^{-1}$ on the clear sky day to 13.30 MJ $m^{-2}d^{-1}$ on the cloudy day. $L\uparrow$ stayed fairly constant throughout the day with an average of -23.85 MJ $m^{-2}d^{-1}$ which was slightly lower than average $L\uparrow$ on the clear sky day (-24.95 MJ $m^{-2}d^{-1}$) due to higher surface temperatures on that day.

Mean daily Q^* was 3.08 MJ $m^{-2}d^{-1}$ which is similar to that observed at the Coombs Hill site (5.27 MJ $m^{-2}d^{-1}$) but lower than that at the Scott Base site (12.44 MJ $m^{-2}d^{-1}$). This means there is least energy available to drive microclimatic processes at the Northwind Valley site, due to the pale surface colour and its high albedo.

Table 5.21 Mean daily radiation balance components (MJ m^{-2} day^{-1}) and surface albedo (dimensionless) for the Northwind Valley site under clear sky and cloudy conditions.

	Clear Sky (Jan. 21, 1995)	**Cloudy sky (Jan. 20, 1995)**
K↓	31.29	21.03
K↑	-8.53	-7.40
L↑	-24.95	-23.85
L↓	11.93	13.30
Q*	9.74	3.08
K*	22.76	13.64
L*	-13.0 2	-10.55
Albedo	0.27	0.35

5.4 SOIL HEAT FLUX

To determine the thermal response of the soil to surface climatic processes, the proportion of Q^* used to heat the soil needs to be quantified. Soil heat flux (Q_G) measured at each field site on the same clear sky and cloudy days examined in the last section is presented and discussed along with the relevant surface climate data. Corresponding soil temperature measurements are then presented and discussed in Section 5.5.

5.4.1 SCOTT BASE

Figure 5.19 shows Q_G is primarily determined by surface temperature, and surface temperature is determined by Q^* and windspeed. This is apparent because when windspeed increased around 1000–1100 hours, both surface temperature and Q_G decreased, despite increasing Q^*.

As wind speed increases, convective heat loss at the surface increases which cools the surface, decreasing the soil temperature gradient, and decreasing the soil heat flux. If this continues for long periods of time, Q_G becomes negative and the soil profile begins to cool.

The wind direction also influences surface temperature and Q_G. If the wind is from a southerly or easterly direction, it is usually cold because it passes over the ice shelf before it reaches the Hut Point Peninsula. This causes a sizeable temperature gradient near the surface which induces significant convective energy losses from the soil. When it comes from the north or west on the other hand, it passes over the basalt surface of Ross Island which allows it to warm slightly. This reduces the air temperature gradient and consequently reduces the amount of convective energy lost by the surface. According to Bromley, 1994, about 60% of the time, wind is from the north-east. This therefore means that wind induced surface temperature changes are not usually significant.

In general, Q_G shows a diurnal cycle where it increases throughout the morning as surface temperature increases in response to rising Q^*, and then decreases with surface temperature throughout the afternoon as solar altitude and Q^* decreases. Q_G also fluctuates noticeably throughout the day as wind speed and air temperature change in response to the larger synoptic situation.

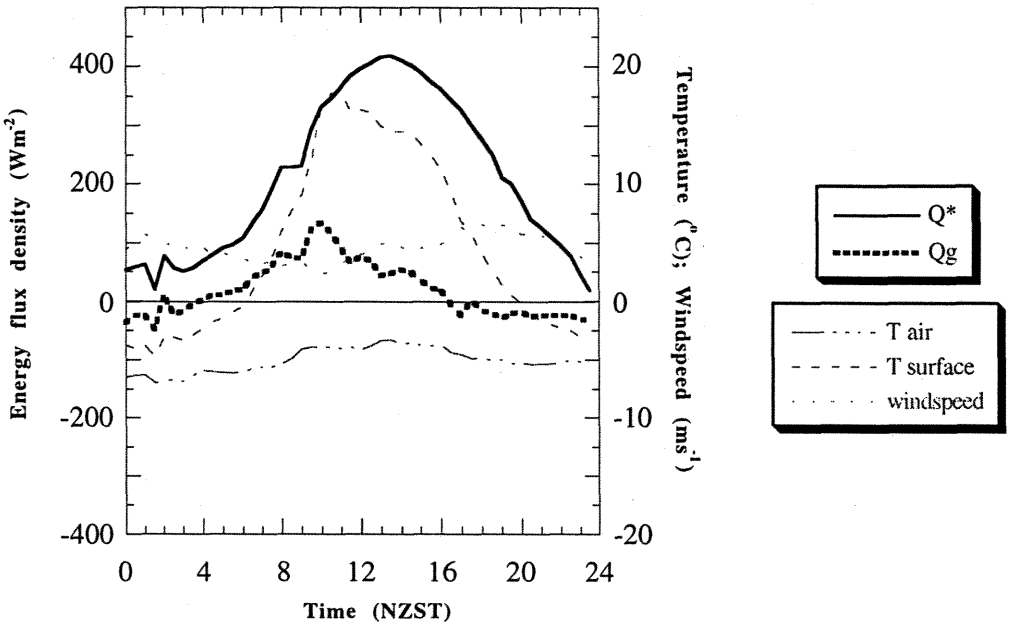

Figure 5.19 - Soil heat flux for a clear sky day (23 December, 1994) at Scott Base with corresponding net radiation, surface temperature, air temperature and wind speed measurements.

In total for the clear sky day, Q_G (1.59 MJ $m^{-2}d^{-1}$) only accounted for 8.5% of Q^* (18.6 MJ $m^{-2}d^{-1}$). This means a large proportion of net radiation on a daily basis is being used to either heat the overlying air in the form of sensible heat, or evaporate water as latent heat. This result is supported by Saunders and Bailey (1994) who found that the majority of energy balance studies find mean daily Q_G to be a small percentage of Q^*, with the mean value of Q_G/Q^* being ~0.09 (9%). Oke (1987) also found that in sandy desert environments , the sensible heat flux consumed about 90% of Q^*, leaving only about 10% to heat the soil.

Daily maximum values of Q_G however often exceeded 30% of Q^* and on this clear sky day reached a maximum of 133.2 Wm^{-2} at 1000 hours which is 40.34% of Q^*. This suggests Q_G becomes an important energy sink at certain times of the day under certain conditions. These maximum values correspond to times of maximum surface temperature and low wind speeds, but do not seem to be related to maximum Q^*. This is due to increasing windspeed at about midday. Q_G reached a minimum of -48 Wm^{-2} at 0200 hours when Q^*, surface temperature and air temperature were also lowest.

The greatest soil temperature gradient was experienced during the morning at about 1100 hours (Figure 5.28) when surface temperature was greatest which resulted in maximum Q_G. After this time, the soil temperature gradient decreases and reverses sometime between 1600–2000 hours causing Q_G to become negative.

Under cloudy conditions, the general trends identified on the clear sky day are also present, although the magnitude of the variables examined are significantly different (Figure 5.20).

Q^* only reached a maximum of 245 Wm^{-2} under cloudy conditions compared to the 417 Wm^{-2} on the clear sky day, and maximum surface temperature was reduced from 17.8°C on the clear sky day to 11°C with clouds present. Maximum Q_G was consequently reduced by at least half from 133 Wm^{-2} on the clear sky day to 60.0 Wm^{-2} on the cloudy day.

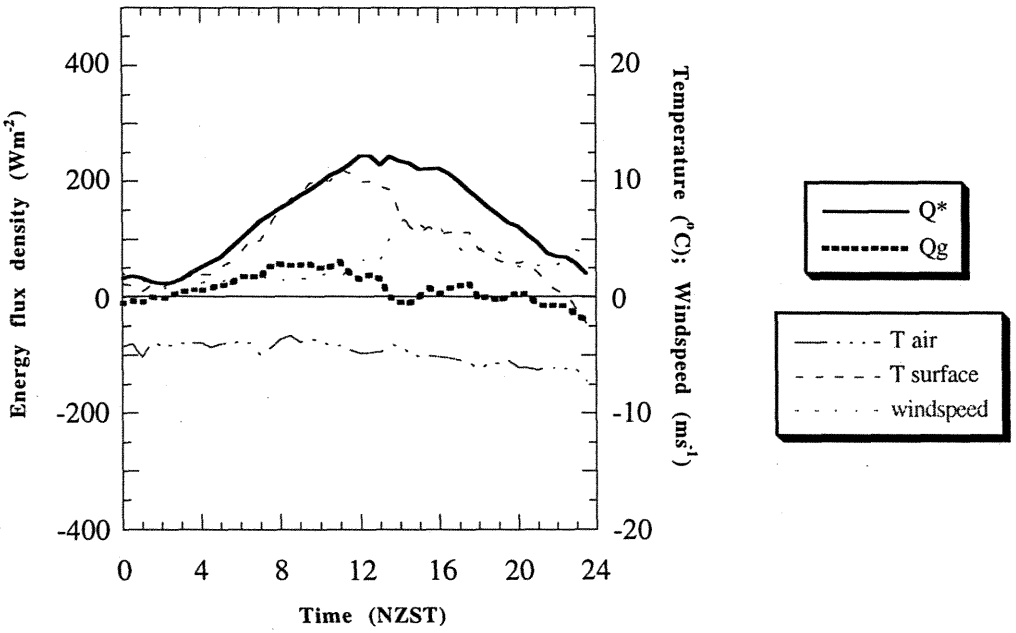

Figure 5.20 Soil heat flux for a cloudy day at Scott Base (25 December, 1994) with corresponding net radiation, surface temperature, air temperature and wind speed measurements.

Between 1300–1400 hours, surface temperature and Q_G decreased noticeably in response to increasing windspeed as seen on the clear sky day, and once again results in Q_G being out of phase with Q^*.

Mean daily Q_G (1.19 MJ $m^{-2}d^{-1}$) was still relatively high compared to 1.59 MJ $m^{-2}d^{-1}$ measured on the clear sky day. Average Q_G/Q^* was 10% which exceeded the 8.5% observed on December 23. This is because Q_G was negative for a shorter period of time on this day and the soil temperature gradient was smaller which resulted in less Q_G being lost.

Mean air temperature was similar for both days (-5.2°C on the clear sky day and -4.9°C on the cloudy day) as was soil surface temperature (4.6°C for clear and 4.7°C for cloudy conditions). The mean wind speed for the clear sky day (4.6 ms^{-1}) was however greater than that experienced on the cloudy day (2.9 ms^{-1}) which would have caused the surface to cool more under clear sky conditions due to convective heat losses. Consequently, minimum Q_G (-39 Wm^{-2}) was slightly higher on the cloudy day than it was on the clear sky day.

On December 28, snow fell on the site between about 0500 and 1000 hours which increased surface albedo from ~0.1 to ~0.8 (Figure 5.21). This caused Q* to be low which resulted in low surface temperatures and negligible Q_G. This continued until the snow began melting at about 1100 hours as shown by the decrease in surface albedo.

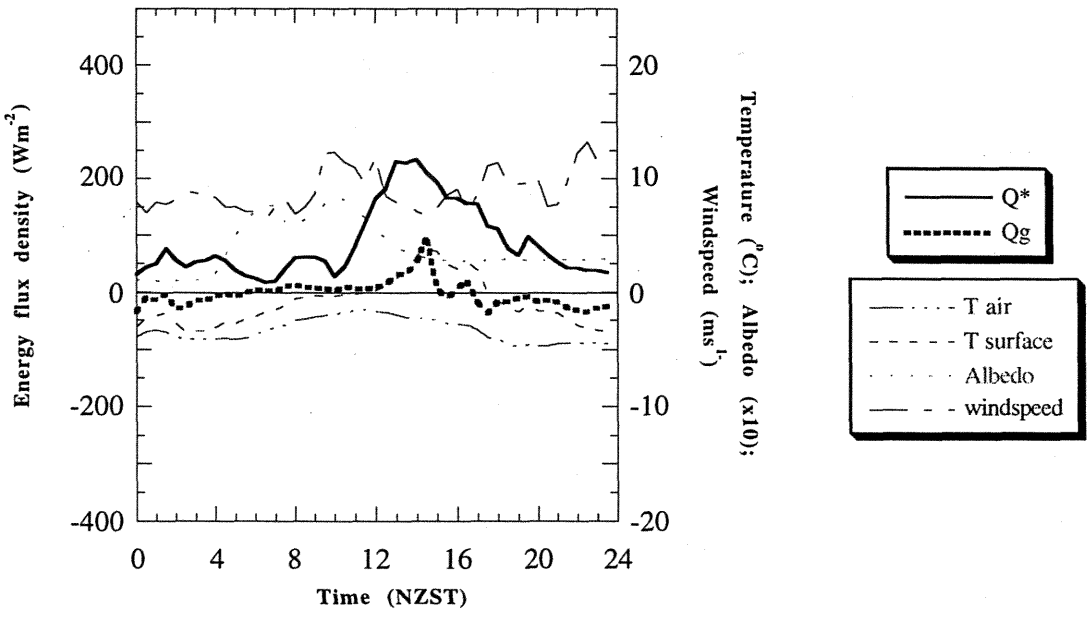

Figure 5.21 Soil heat flux for 28 December 1994 at Scott Base with 60% of the ground covered in snow. The corresponding net radiation, albedo, surface temperature, air temperature and wind speed measurements are also given.

Q_G then reached a maximum of 96 Wm^{-2} at about 1430 hours when surface temperature was highest (3.8°C) and the soil temperature gradient was strongest. This occurred just after a period of high Q^* which was responsible for melting some of the surface snow and increasing surface temperature. Q_G then decreased rapidly as Q^* decreased and windspeed increased. Despite this maximum, mean daily Q_G was -0.30 MJ $m^{-2}d^{-1}$ which means energy was lost from the soil system.

Q_G/Q^* reached 45.7% at 1430 hours which indicates the soil heat flux under these conditions can still be a significant energy sink. This occurs because some of the incoming radiation passes through the opaque snow where it is absorbed by the dark soil. The soil is also insulated by the snow which means windspeed has less influence on soil surface temperature. Therefore, a greater proportion of Q^* will be used to heat the soil under these conditions than if there was no snow pack.

As a result of soil temperature measurement errors at the Coombs Hills and Northwind Valley sites (see Sections 5.52 and 5.53), the actual Q_G at the surface could not be determined at these sites due to the incorrect ΔT_s values (Section 3.2.2). Therefore, to determine the influence of the soil layer between the surface and the Q_G plates, the corrected Q_G for December 23 at the Scott Base site will be compared to the average measurements made by the four Q_G plates (Figure 5.22). This was the method used to determine Q_G at the other two sites.

The main trends shown in Figure 5.22 are that the un-corrected Q_G measurements under-estimate Q_G throughout the morning and over-estimate Q_G during the afternoon and evening.

Maximum Q_G is underestimated by ~40 Wm^{-2} and the noticeable peaks throughout the day in the corrected measurements are not present for the un-corrected measurements. This is because soil at the ~0.03 m depth does not undergo the large temperature variations experienced at the surface.

Minimum Q_G was underestimated by ~20 Wm^{-2}. Total daily Q_G for the corrected data was 1.55 MJ $m^{-2}d^{-1}$ and that for the un-corrected data was 1.58 MJ $m^{-2}d^{-1}$. Therefore, although the magnitude of individual fluctuations of Q_G are out by 20–40 Wm^{-2} at times, the total daily Q_G is very similar.

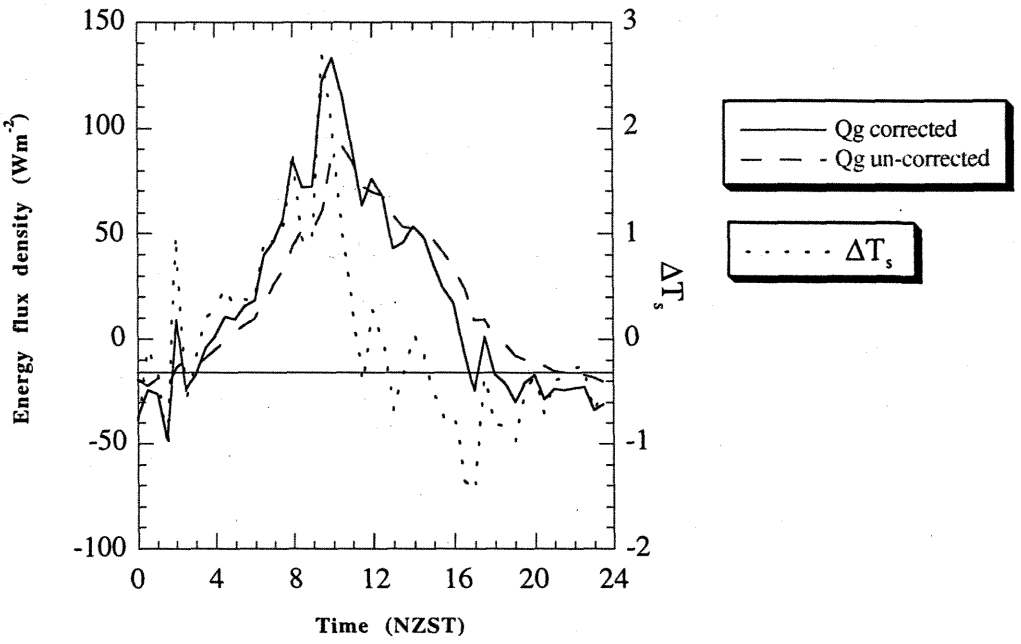

Figure 5.22 Comparison of corrected and un-corrected Q_G at the Scott Base site for 23 December, 1994. ΔT_s which is unreliable at the Coombs Hills and Northwind Valley sites is also plotted to show the change in storage in the ~0.03 m of soil between the heat flux plates and the soil surface.

5.4.2 COOMBS HILLS

When interpreting this data, it must be recognised that surface temperature measurements at both the Coombs Hills and Northwind Valley sites are likely to contain errors of up to 2–3°C due to problems experienced with the instruments (see Section 5.5.2 and 5.5.3).

The soil heat flux on the clear sky day at the Coombs Hills site (Figure 5.23) fluctuated noticeably in response to changing Q^*, surface temperature and wind speed as seen at the Scott Base site. Maximum Q_G was 128 Wm^{-2} at 0900 which despite possible underestimation, is similar to that experienced at Scott Base (133 Wm^{-2}) at 1000 hours on the clear sky day. Surface conditions at both sites were similar, as was mean wind speed and net radiation.

The effect of windspeed on Q_G is clearly seen. From about 0800 to 1300 hours Q_G increases noticeably in response to decreasing windspeed. Q_G then decreases once

windspeed increases. Clouds which covered the site at about midday significantly reduced Q^*, causing air and surface temperature to decrease and Q_G to become negative due to the rapid soil temperature gradient reversal.

Although Q^* rose sharply at about 1400 hours, surface temperature and Q_G remained relatively low due to the persistently cold, and relatively strong wind present. Q_G remained low for the rest of the afternoon until the wind died down and Q^* increased which allowed surface temperature to increase.

Once it had clouded over at about 2000 hours, Q^* became minimal and surface and air temperature decreased. This caused Q_G to reach a minimum of -107 Wm^{-2} when it began snowing at about 2030 hours. Surface temperature fell significantly as snow settled on the site. Q_G increased steadily from about 2130 hours despite minimal net radiation inputs and low air and surface temperatures. This occurred because the snow insulates the soil which decreases the temperature gradient. As a result the temperature profile would become more isothermal.

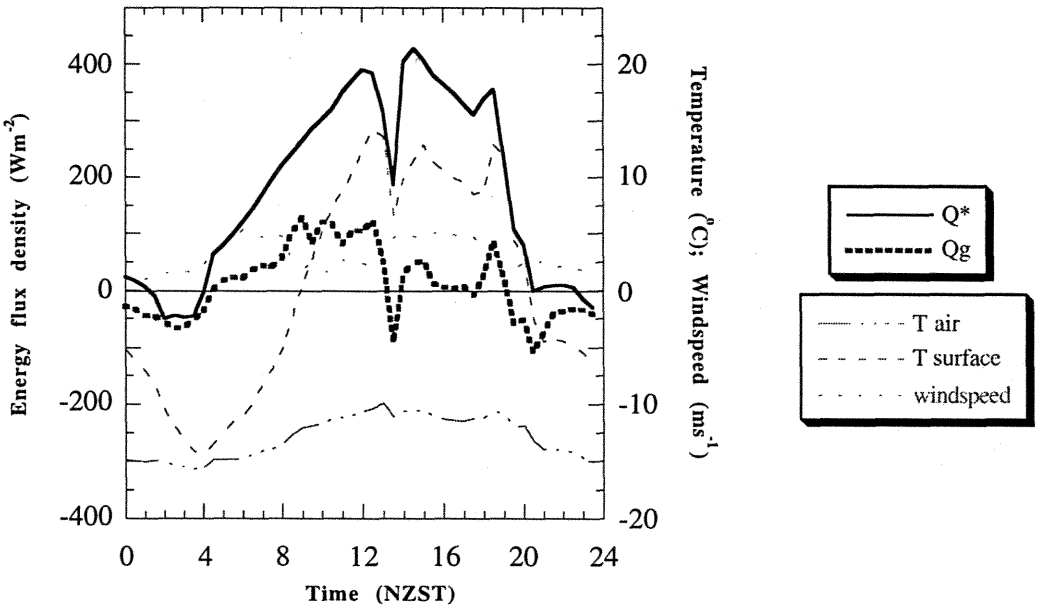

Figure 5.23 Soil heat flux for the Coombs Hills site (11 January, 1995) with corresponding net radiation, surface temperature, air temperature and wind speed measurements.

On average, Q_G (0.98 MJ $m^{-2}d^{-1}$) accounted for 6.3% of Q^* (15.45 MJ $m^{-2}d^{-1}$) throughout the day which is less than that recorded under similar conditions at the Scott

Base site where it was 8.6%. Due to the dry nature of the soil at this site, the sensible heat flux must be considerable (~90% of Q^*). This occurs because the cold air temperatures cause a significant temperature gradient near the surface.

Under cloudy conditions (Figure 5.24), Q_G peaked with Q^* at about 1100 hours but only reached a maximum of 58 Wm^{-2} compared to 128 Wm^{-2} on the clear sky day. This is largely due to reduced radiation inputs under cloudy conditions (60 Wm^{-2} at 1100 hours on the cloudy day versus 179 Wm^{-2} at the same time on the clear sky day). This resulted in significantly lower surface temperatures. Average wind speed on both the cloudy and clear sky day was similar, and air temperature was -16°C on the cloudy day and -13°C on the clear sky day.

Q_G fluctuated just below 0 Wm^{-2} for the rest of the day due to minimal net radiation inputs and snow which covered the site at about 1500 hours. During the afternoon, wind speed had no influence on Q_G because the snow layer prevented significant sensible heat losses from the soil. As a result of this, soil surface temperature was also generally warmer after the snowfall event.

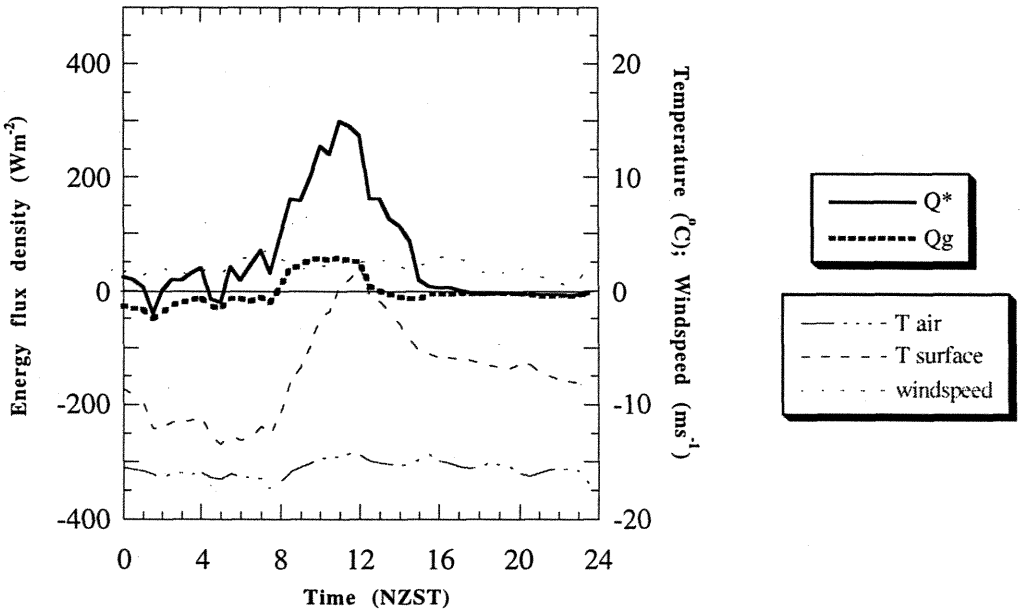

Figure 5.24 Soil heat flux for a cloudy day at the Coombs Hills site (13 January, 1995) with corresponding net radiation, surface temperature, air temperature and wind speed measurements.

Total daily Q_G was significantly lower on the cloudy day (-0.30 MJ $m^{-2}d^{-1}$) than it was on the clear sky day (0.98 MJ $m^{-2}d^{-1}$) due to the smaller soil temperature gradient which was caused by reduced solar inputs, and the snow which fell on the site.

When the ground was completely covered in snow (Figure 5.25), Q_G remained negative and fairly constant throughout the day apart from a slight increase at 0900 hours due to rising surface temperature. The timing and magnitude of this temperature change is however unusual (see Figure 5.39) and is consequently unreliable.

Q_G did not respond to the rise and peak of Q^* at about midday because surface temperature was decreasing due to the snow cover, air temperature was still very low, and there was a strong wind (~10 ms^{-1}) present. There was consequently more energy being lost from the system than there was gained.

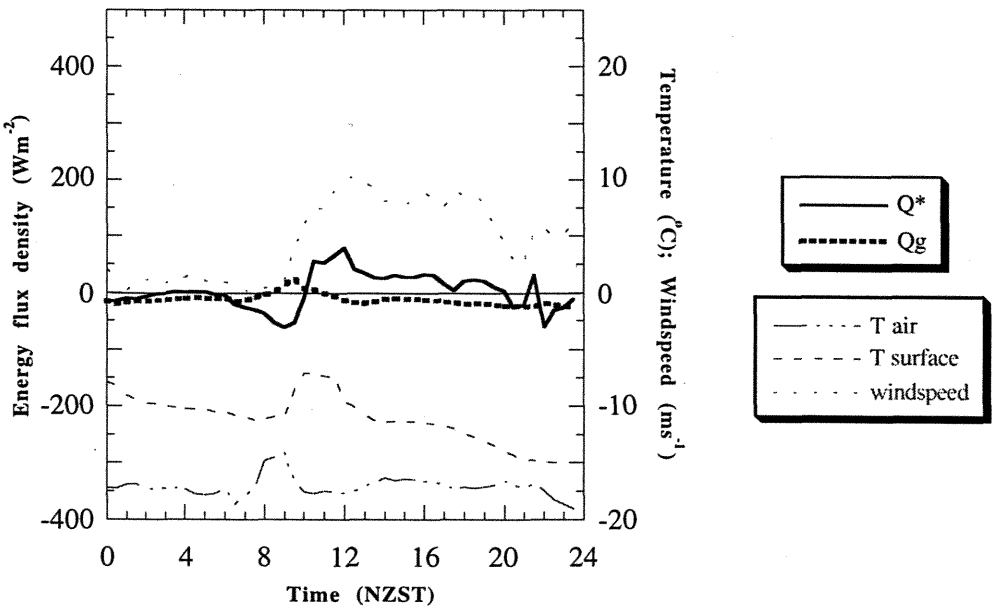

Figure 5.25 Soil heat flux for the Coombs Hills site under full snow cover on 14 January, 1995 with corresponding net radiation, surface temperature, air temperature and wind speed measurements.

Compared to the clear sky and cloudy day, Q_G did not fluctuate greatly due to the snow pack present as seen at the Scott Base site. In total, Q_G was -1.15 MJ $m^{-2}d^{-1}$ which is lower than Q_G on either of the other two days, and slightly lower than that on December 28 at the Scott Base site under similar conditions.

5.4.3 NORTHWIND VALLEY

On the clear sky day at the Northwind Valley site (Figure 5.26) Q_G increased throughout the morning as Q^* and surface temperature rose then decreased throughout the afternoon as they diminished as seen at the other two sites. Q_G peaked ahead of Q^* which is also consistent with the other sites measurements and occurs because Q_G is determined by the surface temperature gradient.

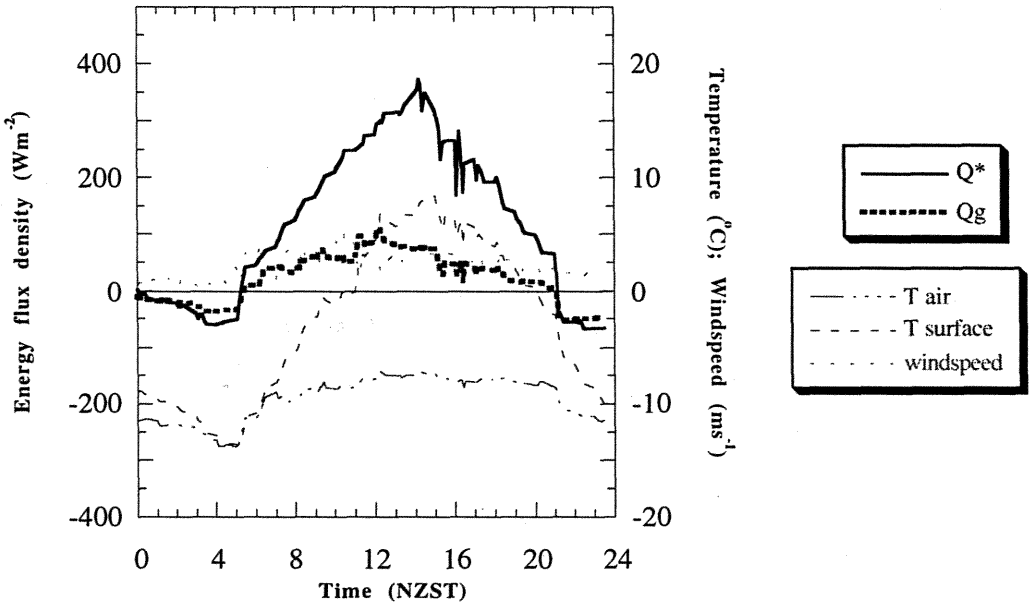

Figure 5.26 Soil heat flux for the Northwind Valley site (21 January, 1995) with corresponding net radiation, surface temperature, air temperature and wind speed measurements.

Mean daily Q_G/Q^* was 17.5% which is significantly larger than that encountered at the other two sites. This is because Q_G is positive throughout the entire time Q^* is positive which was not seen at the other two sites. Q_G peaked before Q* as seen at the other two sites, but surface temperature peaked after it. This trend was not seen at either the Scott Base or Coombs Hills site, and is not fully understood.

Q_G decreased as surface temperature and Q^* peaked at about 1400 hours because Q_G peaked when the temperature gradient was maximised which occurred before the maximum surface temperature (Figure 5.44) This is the same pattern observed at the other two sites.

As soon as the sun went behind the hills at about 2100, surface and air temperature fell dramatically, along with Q_G which reached a minimum of -54 Wm^{-2} at 2130 hours, which is similar to the minimum experienced at both the Scott Base site (-48 Wm^{-2}) and the Coombs Hills site (-49 Wm^{-2}) under similar conditions.

When the site was covered by clouds on January 20 as shown in Figure 5.27, total daily soil heat flux was reduced from 1.70 MJ $m^{-2}d^{-1}$ on the clear sky day to 0.67 MJ $m^{-2}d^{-1}$ due to reduced solar inputs and lower surface temperatures.

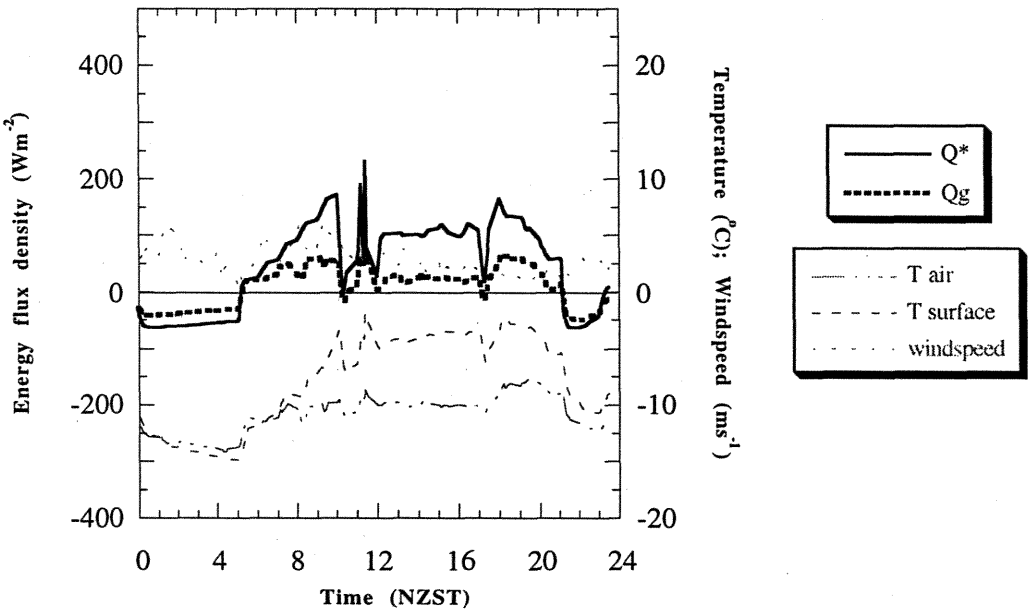

Figure 5.27 Soil heat flux for a cloudy day at the Northwind Valley site (20 January, 1995) with corresponding net radiation, surface temperature, air temperature and wind speed measurements.

There was a gap in the clouds at about 1000 hours when Q^* peaked noticeably. Q_G also rose suddenly at this time in response to rising surface temperature. This shows how surface temperature is dependant on Q^* and Q_G is regulated by surface temperature. Wind speed did not seem to influence Q_G greatly during this event or during the sudden decrease in Q^*, surface temperature and Q_G which occurred at about 1630 hours.

Q_G/Q^* was 17.47% which is very similar to that on the clear sky day and again higher than that experienced at the other two sites. Therefore, despite minimal radiation inputs, a relatively large proportion of available energy is used to heat the soil.

Minimum Q_G (-50 Wm^{-2}),was similar to that at the Scott Base site (-40 Wm^{-2}) but higher than that at the Coombs Hills site (-107 Wm^{-2}) under similar conditions, once again occurred in the evening despite surface and air temperature being lowest at about 0400. This is because energy losses from the system were greatest at this time as shown by Q^*. Therefore, it is apparent that the temperature gradient determines negative Q_G. A greater negative Q_G can consequently occur at low surface temperatures than high temperatures, as long as the temperature gradient is larger.

5.5 SOIL TEMPERATURE

This section presents soil temperature data from each site and relates these to the surface processes driving the thermal regime.

5.5.1 SCOTT BASE

Figures 5.28, 5.29, 5.30 and 5.31 show diurnal temperature variations at the Scott Base site during the same clear sky and cloudy days previously discussed in Sections 5.3 and 5.4. On both days, temperatures in the near surface layers fluctuate widely and peaked at about 1100 hours when solar inputs were greatest. With depth, the amplitude of these variations decrease and the lag in the diurnal temperature wave increases.

Maximum surface temperature on the clear sky day was 17.8°C at 1100 hours (Figure 2.28) which coincided with the period of lowest wind speed. This temperature peak was recorded at a depth of 0.12 m after a time lag of about 6 hours, and there was virtually no diurnal variation detected at 0.24 m.

The highest surface temperature observed during the measurement period was 25°C on December 24 at 1100 hours which was a clear sky morning. Windspeed at this time was 3.04 ms^{-1} and air temperature was -4.1°C.

The minimum surface temperature recorded on the clear sky day was -4.7°C at about 0130 hours when air temperature was -7.1°C which was the coldest that day. Hence the soil surface is consistently warmer than the air temperature.

Figure 5.29 shows that soil temperature fluctuations decrease with depth and at about 0.24 m they remain relatively constant. According to Figure 5.29, the diurnal range in surface temperature was about 20°C. Maximum surface temperature was however recorded at ~1030 hours which is not included on the 4 hourly profile. Therefore, the true diurnal surface temperature range is about 22°C.

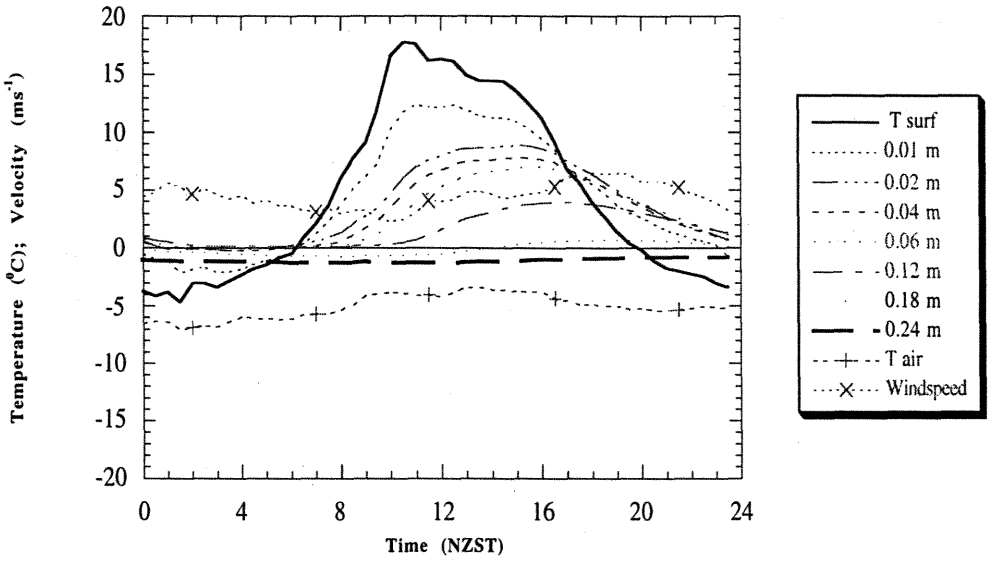

Figure 5.28 Diurnal soil temperature regime for the Scott Base Site under clear sky conditions, 23 December, 1994.

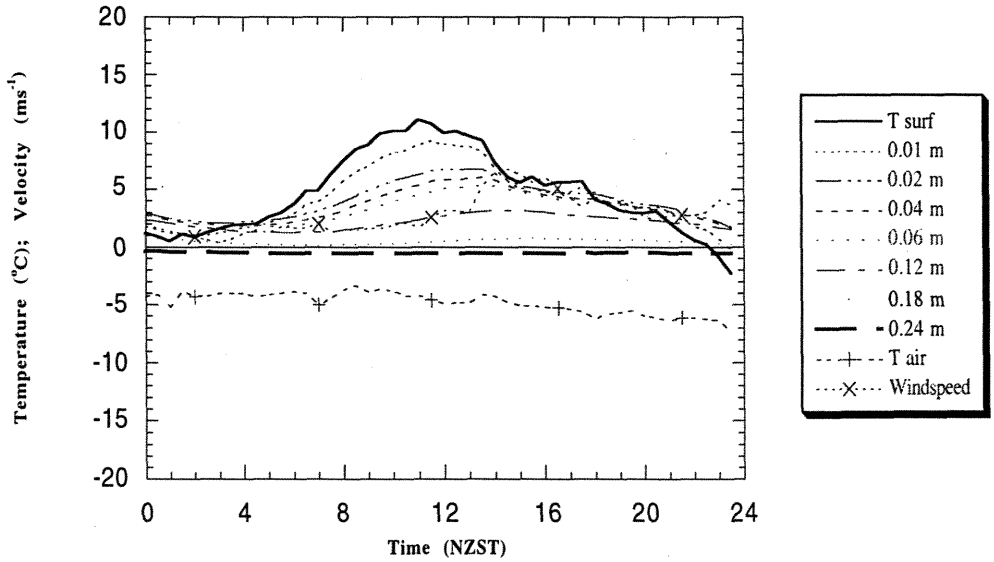

Figure 5.29 Diurnal soil temperature regime for Scott Base site under cloudy conditions, 25 December, 1994.

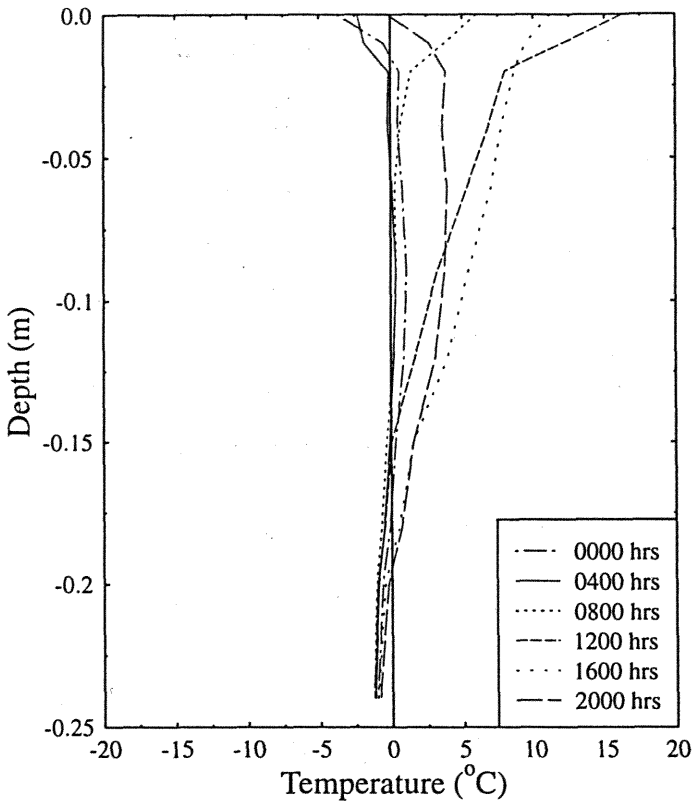

Figure 5.30 4 hourly temperature profiles for the Scott Base site under clear sky conditions, 23 December, 1995.

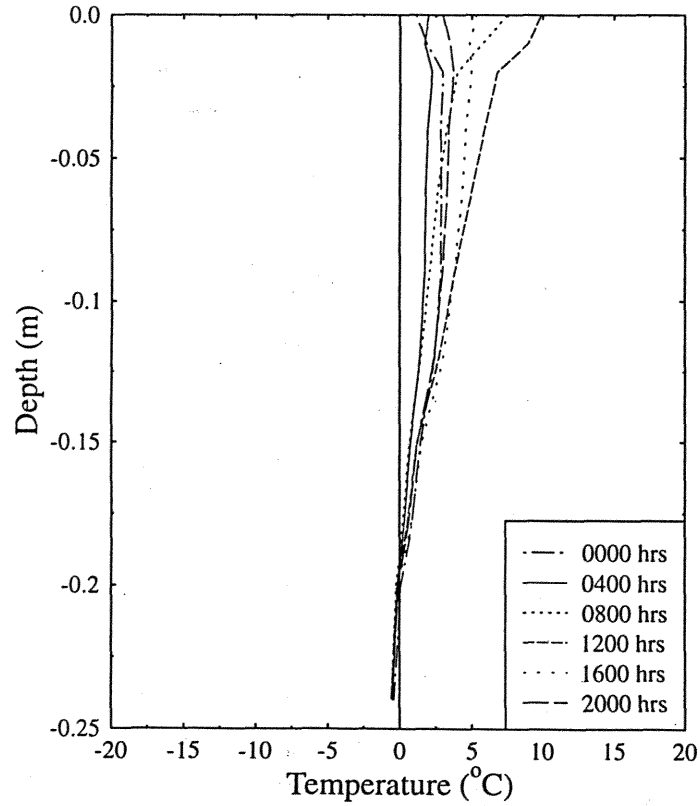

Figure 5.31 4 hourly temperature profiles for the Scott Base site under cloudy conditions, 25 December, 1994.

On the cloudy day (Figures 5.29 and 5.31), maximum surface temperature was lower than the clear sky day reaching 11.0°C at 1100 hours. This coincided with a period of relatively low windspeed. It took about 4 hours for the maximum temperature to reach a depth of 0.12 m which is less than the time taken for the maximum temperature to reach the same depth on the clear sky day.

Minimum surface temperature was -2.3°C at 2330 hours which is almost 2.5°C warmer than that on the clear sky day. Due to this and the lower maximum surface temperature, the diurnal range in surface temperature was significantly smaller than that experienced on the clear sky day (Figure 5.31). This means there are less temperature extremes on the cloudy day which reduce the magnitude of the temperature wave passing into the profile. Consequently, for most of the day, all soil temperatures above 0.24 m remained positive. This was not seen on the clear sky day and implies that cloud cover dampens the extreme temperature changes seen in Figure 5.28. This is consistent with Oke (1987), who states that with overcast skies, absolute temperatures are lower by day but warmer at night, and the wave amplitude is smaller.

Surface temperature dropped quickly at about 1300 hours in response to increasing wind speed, as seen on the clear sky day, and continued to fall throughout the afternoon along with air temperature. Mean daily surface temperature was 4.7°C which is very similar to that experienced on the clear sky day which was 4.6°C.

Diurnal temperature fluctuations were virtually undetectable at 0.24 m on both days which suggests the diurnal damping depth at this site is between 0.25–0.30 m. The temperature at 0.24 m was fairly constant at about -1°C on the clear sky day but was 0.5°C warmer on the cloudy day.

To determine why this occurred, temperature fluctuations at this depth are plotted with surface temperature measurements for the entire measurement period (Figure 5.32). Soil temperature at 0.24 m fluctuated regularly throughout the measurement period by 1–2°C in response to changing surface temperature. These temperature variations at the surface take about 9 hours to reach the 0.24 m depth and consequently temperature variations from the previous day are apparent at this depth.

It is therefore evident that the 0.24 m depth approximately marks the maximum penetration of the 0°C isotherm, hence indicating the approximate level of the permafrost.

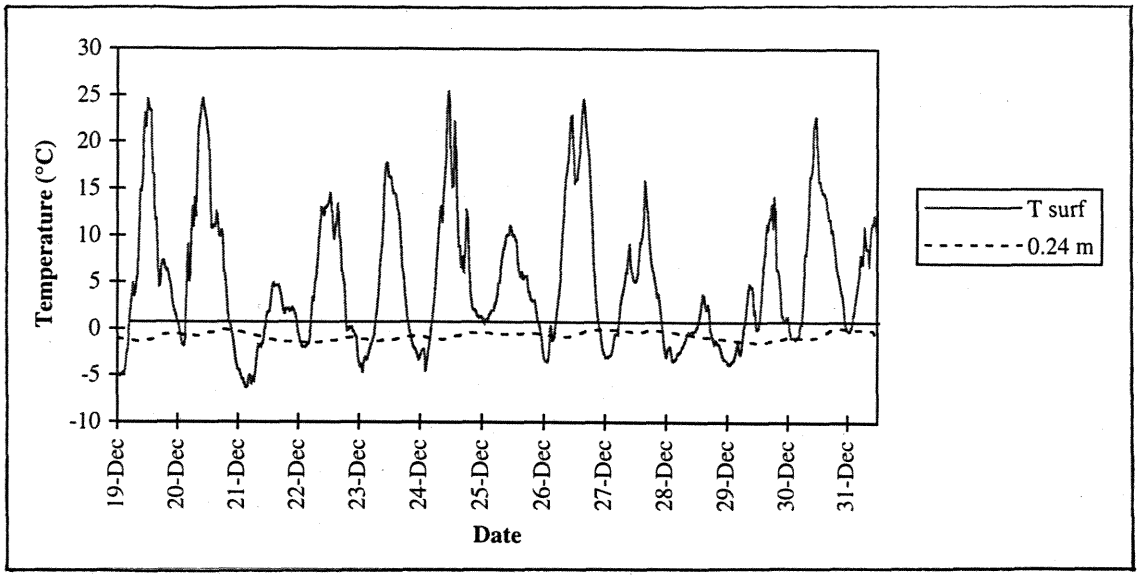

Figure 5.32 Soil temperature measurements at the surface and 0.24 m at the Scott Base site from 19–31 December, 1995.

Near surface temperatures were much lower when the ground was covered by ~0.03 m of snow as shown in Figures 5.33 and 5.34. Soil at depth was also warmer than the surface layers (0–0.01 m) in the early morning and late evening which suggests at these times heat is moving from depth towards the surface.

The maximum surface temperature was only 3.8°C which occurred mid-afternoon when the snow had partially melted, and coincided with a period of relatively low wind speed and falling air temperature. Average wind speed (9.11 ms^{-1}) was much higher than that encountered on either the clear sky or cloudy day and the average air temperature (-3.4°C) was slightly warmer.

When wind speed increased at 1400 hours and then fell again at about 1600 hours, surface temperature responded in a mirror like fashion by dropping and then increasing at similar times. This indicates surface temperature is heavily dependent on wind speed, although surface temperature is still responding to changing Q^* (Figure 5.21).

For 10 hours of the day, surface temperature was below 0°C and the coldest temperature reached was -3.6°C at 0230 hours before the snow pack began melting.

Soil temperature at a depth of 0.24 m decreased throughout the day which suggests a thick snow pack present for a number of days would cause the profile to cool until an equilibrium temperature was reached.

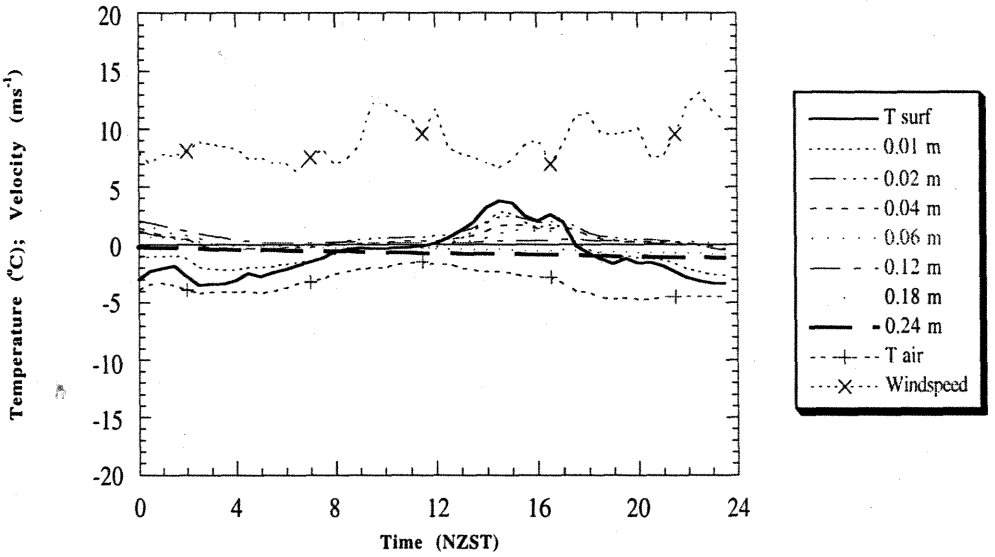

Figure 5.33 Soil temperature measurements at the Scott Base site with 60% of the surface covered in ~0.03 m snow, 28 December, 1994.

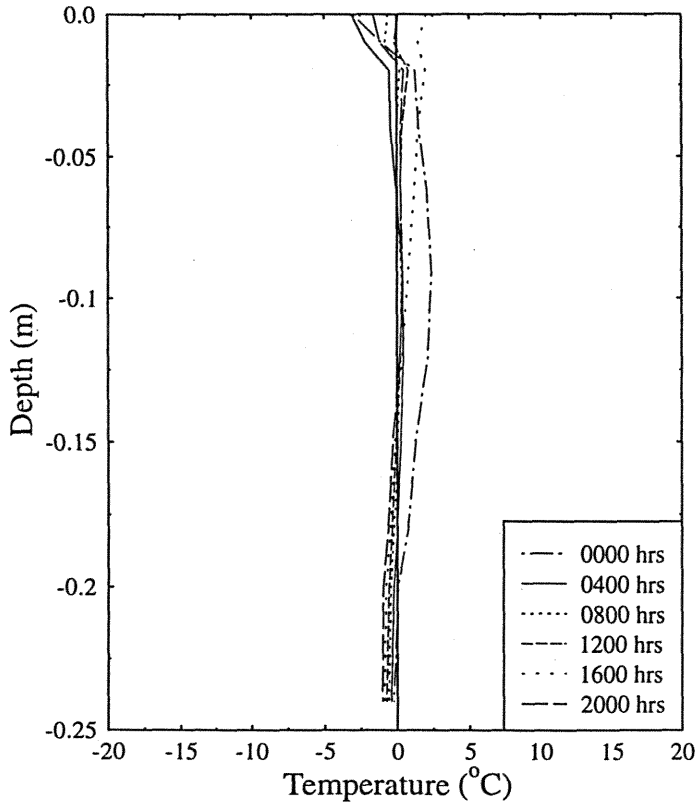

Figure 5.34 4 hourly temperature profiles for the Scott Base site with 60% of the surface covered in ~0.03 m snow, 28 December, 1994.

As shown in Figure 5.34, the diurnal range in surface temperature under these conditions was about 8°C, and was a lot smaller than on either the clear sky or cloudy days.

Overall, these results show that the diurnal surface temperature varies significantly in response to changing surface conditions. Surface temperature is usually greater than air temperature which means the soil is continually loosing heat to the air via the sensible heat flux. Under clear sky and cloudy conditions, the maximum penetration depth of diurnal temperature variations is about 0.20 m. This is reduced to a few centimetres when the site is covered in snow because the profile becomes almost totally isothermal at or just below 0°C.

5.5.2 COOMBS HILLS

During the measurement period at the Coombs Hills, unusual trends were noticed in the soil temperature data. Temperature variations were being recorded throughout the profile down to a depth of 0.23 m with little change in their magnitude (Eg Figure 5.35). This was not seen at the Scott Base site and is unrealistic considering the similar radiation balance and thermal properties at each sites. The source of measurement error in the thermocouple system was not determined either in the field or subsequently.

An alternative set of thermistors temperature probes were consequently delivered from Scott Base so reference measurements could be made at the Northwind Valley site. From these, a clear diurnal error difference is apparent between the thermocouples and the thermistors (Section 5.5.3) which can give a maximum error of 3°C around midday. Therefore, due to the uncertainty associated with the Coombs Hills data, they are of limited value. Examining the main features of the temperature profiles is the only useful interpretations that can be made.

Figures 5.35, 5.36, 5.37 and 5.38 show the diurnal temperature regime and 4 hourly temperature profile for the same clear sky and cloudy days at the Coombs Hills site examined in Sections 5.3 and 5.4.

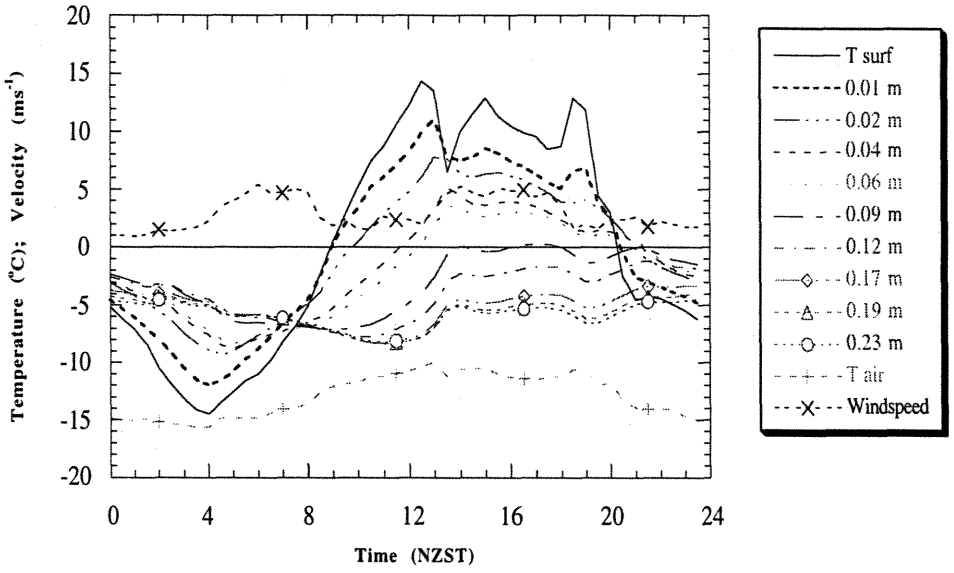

Figure 5.35 Diurnal soil temperature regime for the Coombs Hills Site under clear sky conditions, 11 January, 1995.

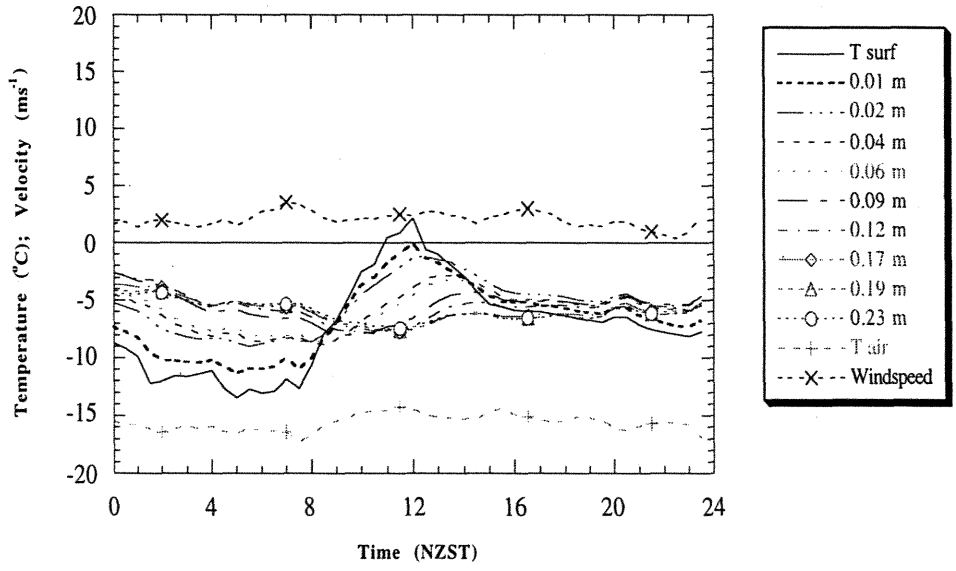

Figure 5.36 Diurnal soil temperature regime for the Coombs Hills site under cloudy conditions, 13 January, 1995.

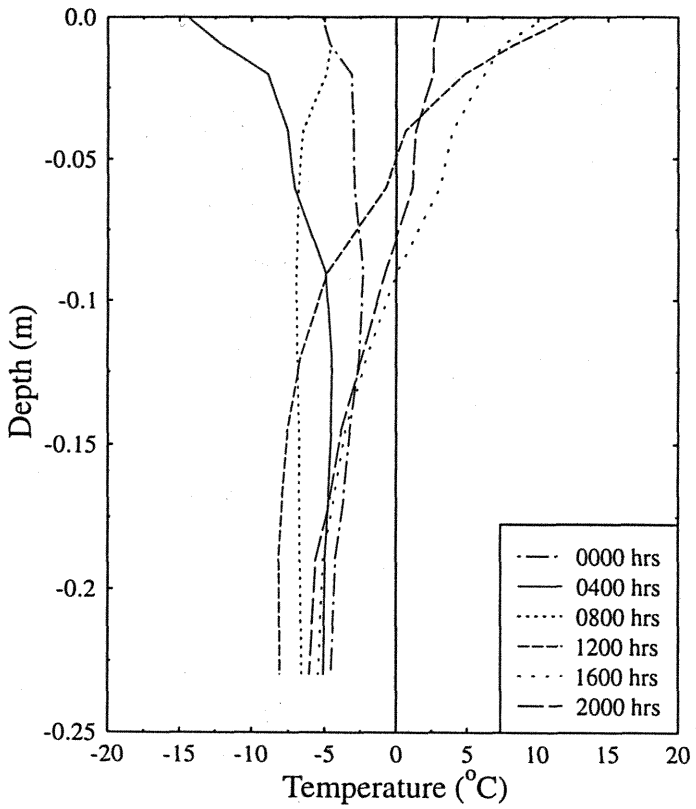

Figure 5.37 4 hourly temperature profiles for the Coombs Hills site under clear sky conditions, 11 January, 1995.

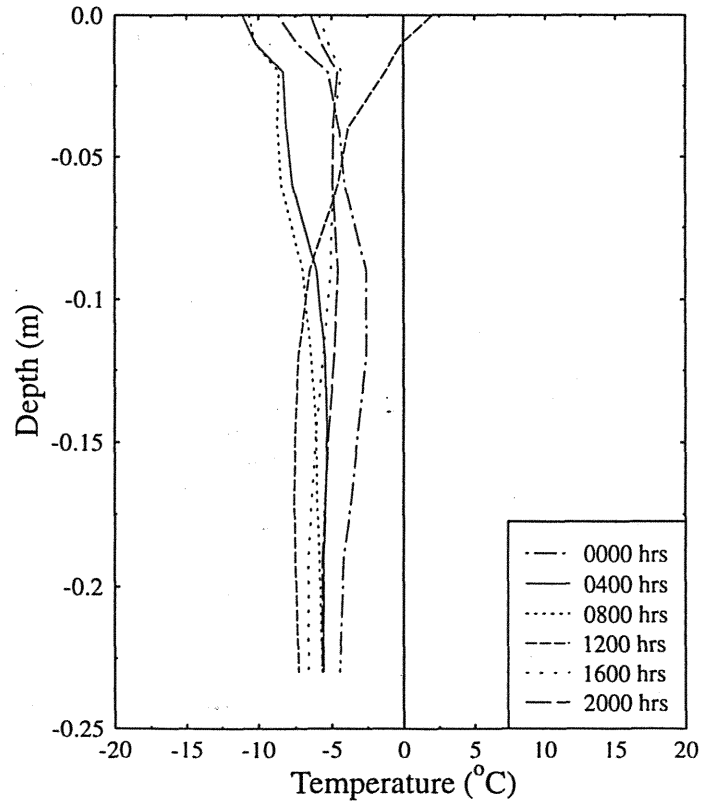

Figure 5.38 4 hourly temperature profiles for the Coombs Hills site under cloudy conditions, 13 January, 1995.

The most noticeable feature of Figure 5.35 is that in the early morning, soil at the 0.23 m depth is warmer than the surface layers. It then cools throughout the morning as the rest of the profile heats up. The layers continue to lose heat until about 1100 hours when heat from the surface layers reaches that depth. Due to the large magnitude of the event, it is probably a real feature of the soil's thermal regime, and was also seen under snow covered conditions at the Scott Base site. The reason for this is the large diurnal surface temperature range experienced at this site which was about 27°C (±3°C) (Figure 5.37). Consequently the diurnal damping depth at this site is greater than that at the Scott Base site.

From about 0400–1200 hours, soil temperature at the 0.23 m depth continued to fall despite surface temperature increasing rapidly. This is because it takes time for the temperature wave to reach the 0.23 m depth, and consequently, soil temperature at this depth did not begin to respond to the surface temperature increase until ~4 hours later. This shows how energy is stored at depth within the profile during the day, and is lost during the evening when surface temperatures are colder. This trend was also seen at the Scott Base site.

It is important to realise that due to the relatively small magnitude of the temperature variations at the deeper layers, the effect of errors is likely to be great. This can be seen by comparing the deep soil temperature data for the Coombs Hills with that at the Scott Base and Northwind Valley site which show no short-duration fluctuations.

Ice cement was encountered at ~0.20 m when installing the temperature probes, but was absent when they were removed. This indicates it was a temporary feature of the profile which is probably temperature dependant.

Soil below ~ 0.09 m did not exceed 0°C for the entire day (Figure 5.35) despite intense surface warming. Therefore the 0°C isotherm at this site under these conditions was shallower than it was at the Scott Base site under similar conditions which was about 0.24 m (Figure 5.28). This is because of the colder surface conditions experienced at the Coombs Hills, and the colder temperature at depth.

As shown in Figure 5.36, soil at the 0.23 m depth was also warmer than surface temperature in the early morning on the cloudy day, as seen on the clear sky day, and continues to cool until surface temperature reaches its maximum at about midday. The magnitude of the temperature changes are less than on the clear sky day which are due to the reduced energy inputs into the system.

Average temperature at a depth of 0.23 m is similar on both days clear sky and cloudy days, despite greater fluctuations on the clear sky day.

The temperature change at about 2030 hours is recorded at all depths within a very short space of time and this is an artefact of the measurement errors. Throughout the afternoon, the range in surface temperature decreases noticeably which was not seen on the clear sky day. This shows that with reduced radiation inputs, the temperature variations within the profile are significantly reduced.

Only the surface layer exceeded 0°C to reach a maximum of about 2°C. This is significantly lower than that reached on the clear sky day which was about 14°C.

When the site was covered with snow on January 14, soil temperatures were all negative and soil at depth was warmer than the surface layers throughout the entire day (Figures 5.39 and 5.40). This was not observed at the Scott Base site under similar conditions where the soil continued to be heated when covered in a thin layer of snow.

Soil at the 0.23 m depth cooled only slightly throughout the day while surface temperature dropped noticeably. This temperature divergence is due to the surface layers cooling faster than the deeper layers, and indicates the profile is loosing energy to the atmosphere. This is consistent with the Scott Base results.

The diurnal range in temperatures experienced at the Coombs Hills site under snow was greater than that experienced at Scott Base. This is due to the measurement errors associated with these measurements.

From these results, it can be concluded that there is a greater diurnal range in surface temperature at this site than at the Scott Base site which causes the damping depth to be greater. Surface temperature is consistently higher than air temperature as seen at the Scott Base site which means heat is continually being lost by the soil surface as sensible heat as seen at the Scott Base site.

The effect of reduced Q^* on the cloudy day was very noticeable at this site. Soil temperatures were strongly negative compared to those on the clear sky day and the profile became more isothermal (Figure 5.37). Under snow cover, the temperature profile was even more isothermal as seen at the Scott Base site.

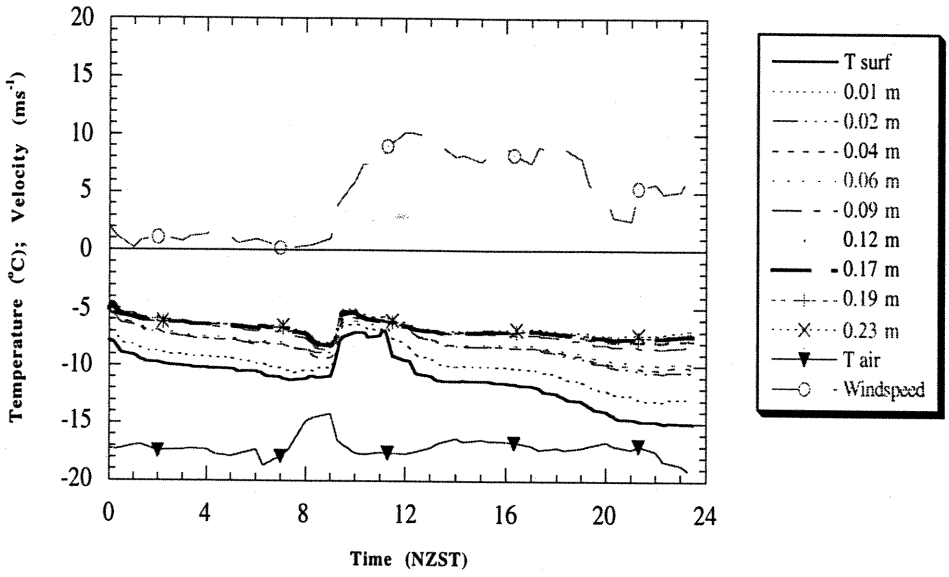

Figure 5.39 Diurnal soil temperature regime for Coombs Hills site covered in snow, 14 January, 1995.

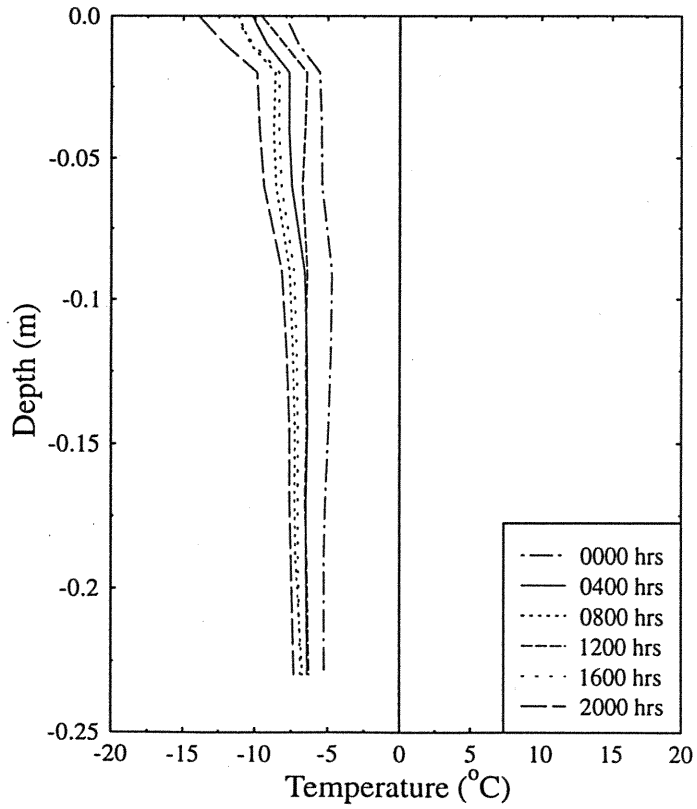

Figure 5.40 4 hourly temperature profiles for the Coombs Hills site covered in snow, 14 January, 1995.

5.5.3 NORTHWIND VALLEY

Due to the unusual trends seen in the data collected at the Coombs Hills site, five Campbell Scientific 107B thermistor probes were installed alongside the thermocouples at the Northwind Valley site to determine the accuracy of the thermocouples. The difference between the two sets of measurements are shown in Figure 5.41.

This clearly shows that the thermocouples were recording different temperatures than the commercially built thermistors. The error shows a diurnal trend increasing throughout the morning to reach a maximum error at about 1300 hours and then decreases throughout the afternoon. The magnitude of the error varies for each sensor, and the reason for these errors is unclear and therefore cannot be corrected. These errors were present throughout the entire measurement period at this site and were probably causing the unusual temperature variations seen at the Coombs Hills site. The Scott Base data is considered reliable because none of the inconsistencies seen at the Coombs Hills site were observed within the Scott Base data.

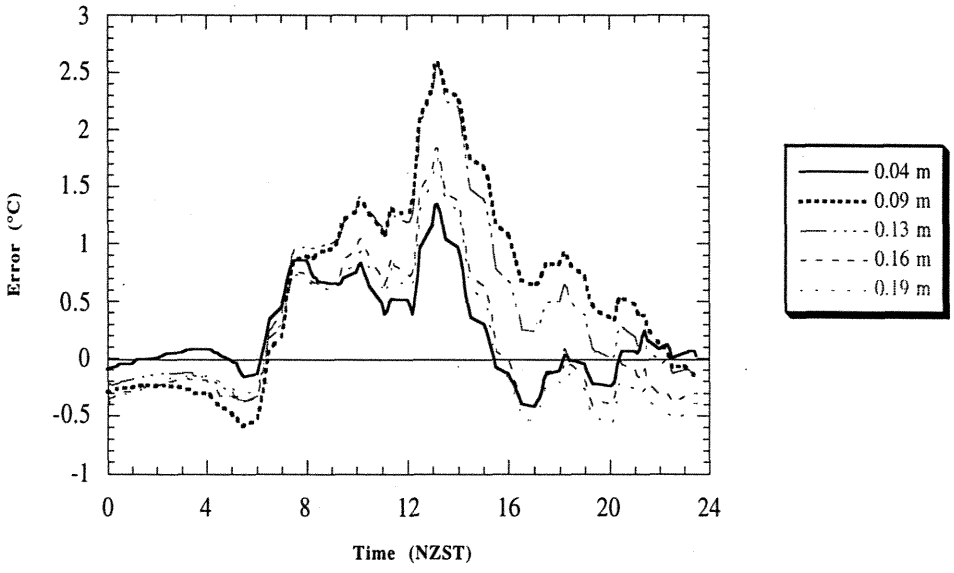

Figure 5.41 Comparison of soil temperature measurements made with thermistors and thermocouples at the Northwind Valley site, 21 January, 1995.

Although the exact cause of the error has not been determined at this stage, it is assumed that either something went wrong with the equipment when it was dismantled, transported and re-assembled at the Coombs Hills site, or the environmental conditions

at the Coombs hills site were too extreme for the thermocouples and data logger to function properly.

Due to the unreliability of the thermocouple system, measurements made with the thermistors at the Northwind Valley site will be used to describe profile temperature changes. Thermocouple measurements made at the surface will still be used due to the lack of thermistors available to make surface and near surface measurements.

Figures 5.42, 5.43, 5.44 and 5.45 show the diurnal temperature trends and four hourly temperature profiles for the Northwind Valley site under the same clear sky and cloudy conditions discussed previously in Sections 5.3 and 5.4.

On the clear sky day (Figure 5.42), soil temperature increased throughout the morning in response to increasing Q^* as seen at the other two sites. Maximum surface temperatures were generally lower than those at the Coombs Hills site because of the higher albedo.

As a result of this, much of the profile remained below 0°C for the entire day and only the top 0.04 m warmed sufficiently to record positive temperatures. Positive temperatures were recorded down to a depth of 0.18 m at Scott Base, and between 0.06–0.12 m at the Coombs Hills site. Soil temperature at the 0.19 m depth at the Northwind Valley site is on average -6.9°C which is less than those at the same depths at the other two sites under similar conditions.

Consequently, the active layer is thinnest at the Northwind Valley site under these conditions, deepest at the Scott Base site, and intermediate at the Coombs Hills site. This is partly because of the warm coastal climate at Scott Base, but is mainly due to the dark surface at Scott Base and the Coombs Hills which have a relatively low surface albedo. Hence more Q^* is available to heat the soil at these two sites than at the Northwind Valley.

The minimum surface temperatures were recorded when the sun was behind the surrounding hills and are significantly lower than the minimum recorded at the Scott Base site under similar climatic conditions, and is slightly warmer than the coldest temperatures at the Coombs Hills site under clear sky conditions. Minimum temperatures at all sites occurred in the early morning when the sites receive minimal radiation and have cooled throughout the 'night'.

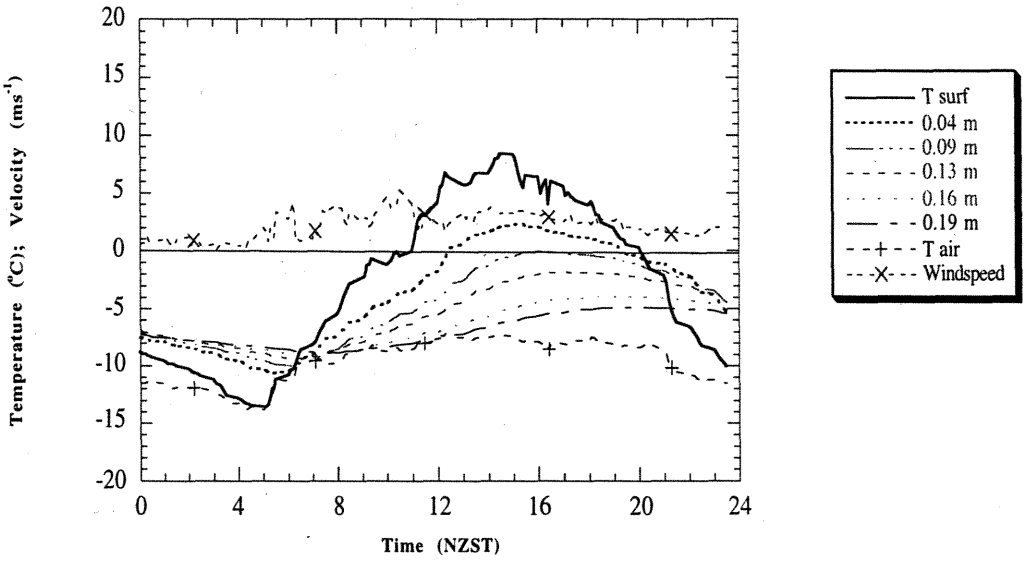

Figure 5.42 Diurnal soil temperature regime for the Northwind Valley site on 21 January, 1994 which was a clear sky day

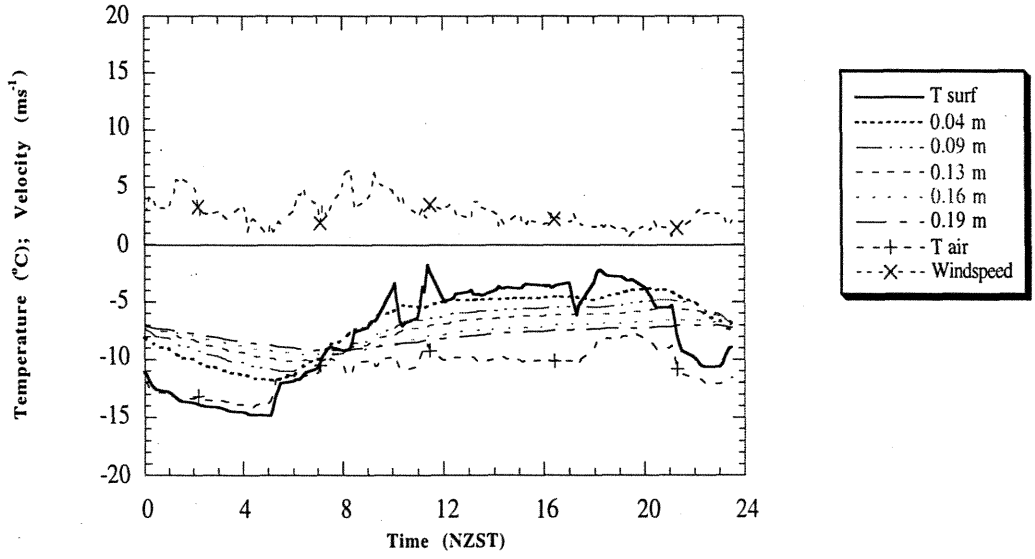

Figure 5.43 Diurnal soil temperature regime for the Northwind Valley site under cloudy conditions, 20 January, 1994.

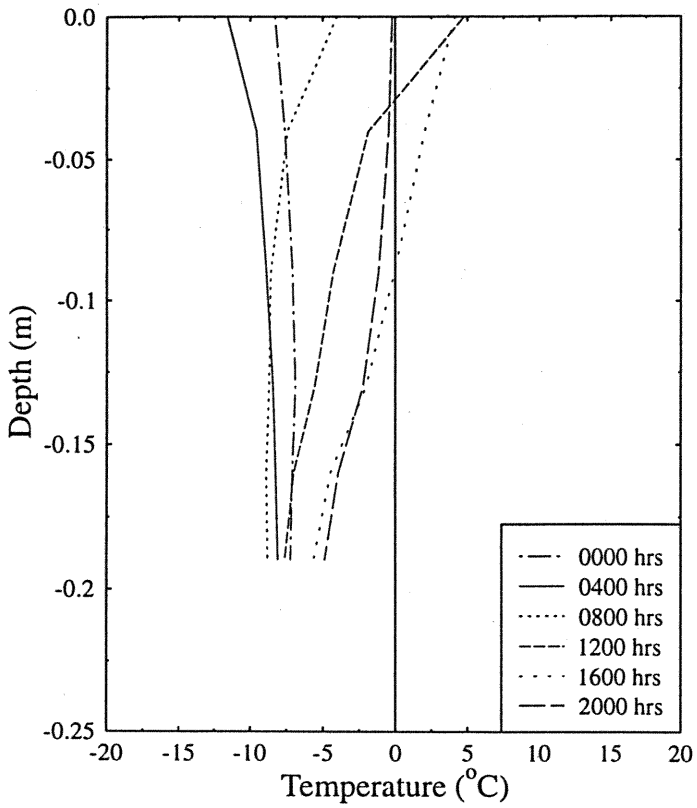

Figure 5.44 4 hourly temperature profiles for the Northwind Valley site under clear sky conditions, 21 January, 1995.

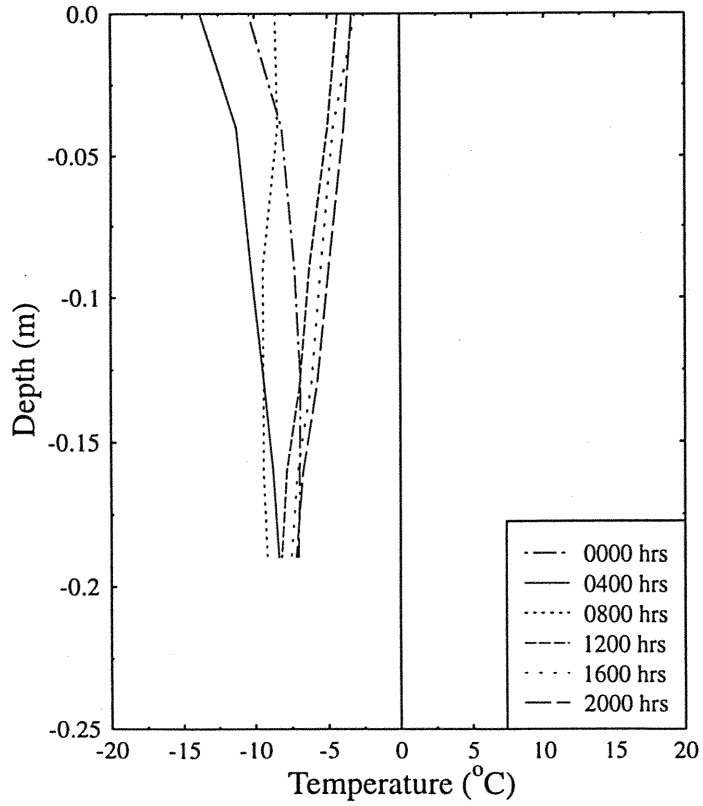

Figure 5.45 4 hourly temperature profiles for the Northwind Valley site under cloudy conditions, 20 January, 1995.

It took approximately 5 hours for the maximum surface temperature to reach a depth of 0.19 m which was slightly less time than it took for larger temperature changes to travel to that depth at the Scott Base site. This is probably due to the relatively low heat capacity of this soil type which allows the soil to heat up quicker with less energy inputs. It is not due to higher thermal conductivity (Section 5.2.2). As a result of this, soil temperatures throughout the profile (Figure 5.44) fluctuate more and to a greater depth at this site than they do at the other two sites.

Soil at depth is generally cooler than the surface layers, as seen at the other two sites, apart from in the early morning as at the Coombs Hills site. Air temperature is colder than the surface temperature which means sensible heat is lost to the air.

Figure 5.45 shows that under cloudy conditions, soil temperature does not exceed 0°C at any depth. This is similar to the Coombs Hills results where only the surface and 0.01 m layers were positive, but is totally different to the Scott Base results where the entire profile was positive down to a depth of 0.24 m. This shows that soil temperature temperatures are colder at depth at the Coombs Hills and Northwind Valley sites. This is a function of the amount of absorbed incoming radiation, the wind speed and air temperature at each site.

Maximum surface temperature was less than it was on the clear sky day due to the reduced radiation inputs, and is also significantly smaller than the maximum temperatures recorded at the Scott Base and Coombs Hills site under similar overcast conditions. This is caused by differences in surface albedo and the proportion of incoming radiation absorbed.

Minimum surface temperatures were experienced during the early hours of the morning as at the other sites, and these appear to be slightly colder than the minimum temperatures recorded on the clear sky day. At the other two sites, surface temperatures were slightly colder on the clear sky day than they were on the cloudy day as expected for desert like environments. The diurnal range of surface temperatures experienced on this day were smaller than those seen on the clear sky day as seen at the other two sites (Figure 5.45).

Overall, these results show that soil temperatures at this site are generally lower than the other two sites which is probably due to the relatively low surface albedo. This results in the Northwind Valley soil having the thinnest active layer of all sites and the narrowest diurnal surface temperature range. Temperature variations are however greater at depth due to the soils relatively low heat capacity.

5.6 SUMMARY

5.6.1 SOIL PHYSICAL PROPERTIES

- Soil at the Scott Base site had the overall highest moisture content (~6%) and the Northwind Valley soil had the lowest (~3%).
- Soil moisture content is highly spatially variable at both the Scott Base and Northwind Valley site, but is fairly uniform at the Coombs Hills site.
- The Scott Base soil has the highest mean soil bulk density (1778 kg/m^3) and the Northwind Valleys has the lowest (1638 kg/m^3) which is similar to that at the Coombs Hills site.
- Soil bulk density is highly spatially variable at all three sites.
- Soil particle density ranges from a mean of 2886 kg/m^3 to 2622 kg/m^3 with the largest being measured at Scott Base and the lowest at the Northwind Valley. The Coombs Hills soil has a particle density midway between the two.
- Soil particle density is only noticeably spatially variable at the Coombs Hills site.
- Soil at the Scott Base and Coombs Hills sites are coarser than the Northwind Valley soil due to its sandstone origin, and the Scott Base soil is the coarsest overall.
- At both the Scott Base and Coombs Hills sites soil becomes noticeably coarser with depth.
- There are more fine particle at both the Coombs Hills site and Northwind Valley site than there is at the Scott Base site due to the ages of the soils and sources of fine materials.
- At all three sites, the greatest abundance of fines is found in the surface layers, and decreases with depth.
- Soil grainsize distribution is not particularly spatially variable for particles <1 mm at any site, but is with the larger particles at all sites
- Soluble salt content varies from a mean of ~10.5% at the Coombs Hills site to ~0.5% at the Scott Base site and the Northwind Valley site has an average salt content of ~8%. Salt content is highly variable with depth at all sites and is also spatially variable.

5.6.2 SOIL THERMAL PROPERTIES

- The Scott Base soil has the highest mean soil heat capacity (1.896 MJ m^{-3} K^{-1}) and the Northwind Valley soil has the lowest (1.550 MJ m^{-3} K^{-1}). It was not significantly spatially variable at any site.
- The Scott Base soil has the highest average soil thermal conductivity (0.261 Wm^{-2} K^{-1}), and the Northwind Valley soil has the lowest (0.205 Wm^{-2} K^{-1}) which is similar to that at the Coombs Hills site. Soil thermal conductivity is not highly spatially variable at any site.
- With increasing moisture content, the thermal conductivity of all three soils initially decreased, but then increased at varying rates. This is possibly due to influence of soil salts and the structure of the soil grains. Soil thermal conductivity of the Northwind Valley soil increased the most as moisture content increased, and the Coombs Hills soil increased the least.
- Soil thermal diffusivity was similar at all sites, although it was slightly lower at the Coombs Hills site. It was not highly spatially variable at any site.

5.6.3 SURFACE RADIATION BALANCE

Table 5.22 summarises the total daily radiation balance components for each site under various conditions.

- The Scott Base and Coombs Hills sites received similar amounts of $K\downarrow$ under both clear sky and cloudy conditions and the Northwind Valley site received slightly less due to site shading during the evening and early morning (Table 5.22).
- Soil surface albedo was highest at the Northwind Valley site (~0.30) and lowest at the Scott Base (~0.07) and Coombs Hills (~0.10), largely due to soil colour.
- Albedo at the Scott Base and Coombs Hills sites was highly variable with time due to changing snow cover, and this has a dominant role in determining energy availability. Variations in albedo at the Northwind Valley site will be less than those at Scott Base and Coombs Hills due to the relatively high albedo of the light coloured bare soil.
- Albedo at all sites has a diurnal trend of minimum values during the middle of the day coinciding with the highest solar angle, and highest values at night caused by increased surface reflection at low solar angles.

Table 5.22 Radiation balance components and resultant soil heat flux for each site under various conditions. All fluxes are daily totals, units are MJ $m^{-2}d^{-1}$.

Location	Altitude	Measurement period	Conditions	$K\downarrow$	$K\uparrow$	$K*$	α	$L\downarrow$	$L\uparrow$	$L*$	$Q*$	Q_G
Scott Base 75°50'S,166°45'E	~100 m	Dec. 18–30, 1994	Clear sky	35.16	-2.27	32.89	0.065	13.50	-27.79	-14.29	18.60	1.59
			Cloudy	22.58	-1.58	21.00	0.074	18.33	-26.89	-8.56	12.44	1.19
			Surface snow	20.00	-9.10	10.90	0.46	-	-	-1.46	7.44	-0.30
Coombs Hills 76°48.3'S,159°54.1'E	~2000 m	Jan. 9–17, 1995	Clear sky	33.00	-3.41	29.86	0.10	12.28	-26.69	-14.41	15.45	0.98
			Clouds + snow	20.58	-8.17	12.41	0.40	16.67	-23.81	-7.14	5.27	-0.30
			Surface snow	33.07	-24.22	8.85	0.73	-	-	-8.73	0.12	-1.15
Northwind Valley 76°46.3'S160°45.1'E	~1400 m	Jan. 18–22, 1995	Clear sky	31.29	-8.53	22.76	0.27	11.93	-24.95	-13.02	9.74	1.70
			Cloudy	21.03	-7.40	13.64	0.35	13.30	-23.85	-10.55	3.08	0.67

- K^* was greatest under clear sky and cloudy conditions at Scott Base, and was least at the Northwind Valley site.
- $L\uparrow$ was greatest at the Scott Base site on both clear sky and cloudy days due to the warmer surface temperature, and lowest at the Northwind Valley site under these conditions due to the cooler surface temperatures.
- $L\downarrow$ increased significantly at all three sites on cloudy days, and was greatest at the Scott Base site. $L\downarrow$ was smallest at the Northwind Valley site. This is due to the differing cloud base temperatures. The temperature of the cloud base at high altitudes is colder than those at low altitudes.
- L^* was similar at all three sites on the clear sky day, but was greatest at the Northwind Valley site on the cloudy day.
- Q^* was greatest at the Scott Base site under clear sky and cloudy conditions, and was smallest at the Northwind Valley site, due to its high albedo.
- When snow covered the Scott Base and Coombs Hills sites, $K\uparrow$ significantly increased due to increased surface albedo, causing Q^* to decrease.

5.6.4 SURFACE ENERGY BALANCE

- The total daily Q_G was greatest at the Northwind Valley site on the clear sky day despite having the lowest Q^*, and was lowest at the Coombs Hill site (Table 5.22 and 5.23). This could be due to energy partitioning favouring the soil heat flux because the air–surface temperature gradient is not so large at this site.
- On the cloudy day, Q_G was greatest at the Scott Base site, and least at the Coombs Hills site. This occurs because the soil surface heats up more at the Scott Base site under these conditions due to its relatively warm climate.
- Under snow cover, Q_G was negative at both the Scott Base and Coombs Hills sites which means energy was lost from the soil system.
- Q_G peaked before maximum surface temperature at all sites under all conditions because maximum Q_G is determined by the maximum near-surface soil temperature gradient, which occurs mid-morning while Q^* is increasing.

5.6.5 SOIL TEMPERATURE

- The Scott Base site had the overall warmest soil temperatures due to its relatively warm maritime climate, and the Northwind Valley had the coldest due to its location on the edge of the Polar plateau (Figure 5.46).

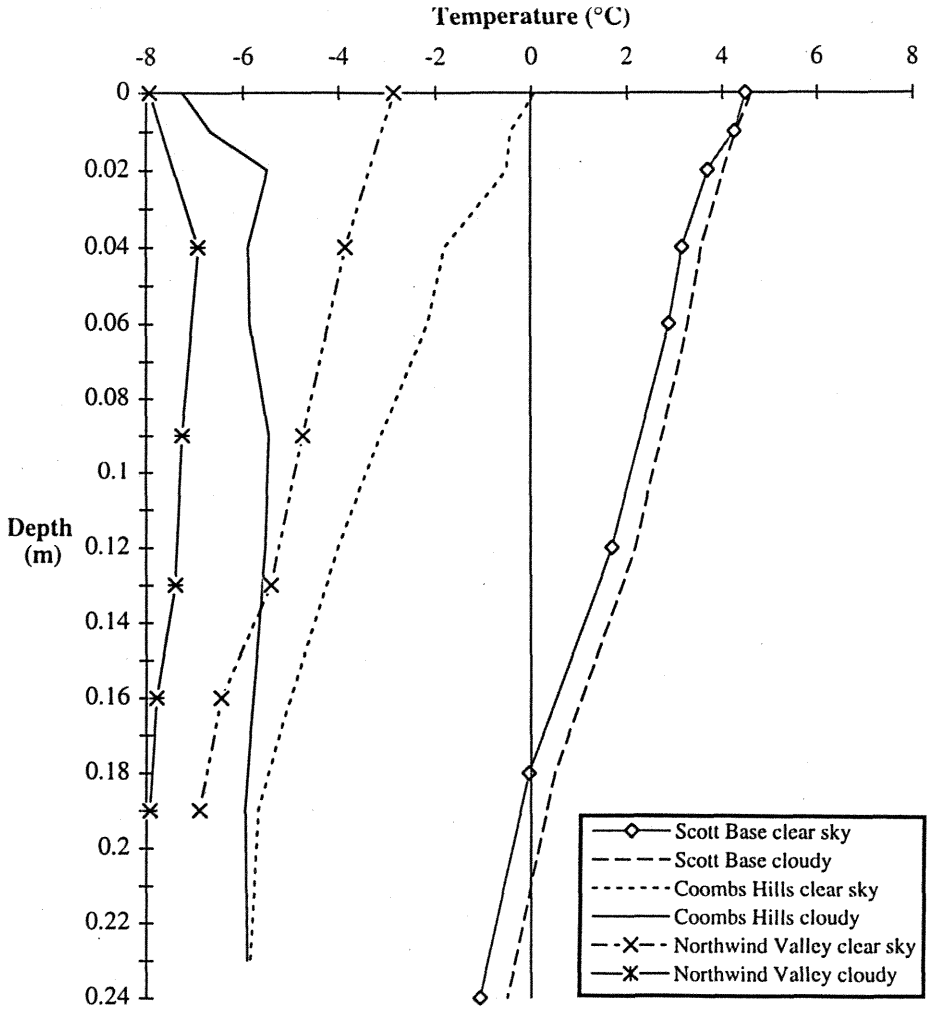

Figure 5.46 Mean daily soil temperature profiles for the clear sky and cloudy days at each field site.

- Soil surface temperature is determined mainly by $K\downarrow$ and windspeed. This was also demonstrated by Balks *et al.*, (1995).
- Soil surface temperature was always higher than air temperature at all sites which resulted in a sizeable sensible heat flux at all sites. It was warmer and showed greater short duration fluctuations on the clear sky day than it was on the cloudy day at all sites.

- The amplitude of the temperature wave moving into the profile decreased with depth at all sites, and the lag in the diurnal temperature wave increased.
- The average daily soil temperature gradient is steepest at the Scott Base site and least steep at the Northwind Valley site (Figure 5.46). This is due to the high surface temperatures experienced at the Scott Base site.
- Soil temperature at a depth of 0.24 m remained relatively constant at the Scott Base site throughout the measurement period, but fluctuated noticeably at this depth at the other two sites.
- The greatest diurnal range in surface temperature was experienced at the Coombs Hills site, and the least at the Northwind Valley. This is a function of surface albedo which determined the amount of $K\downarrow$ reflected or absorbed, and the difference between air and surface temperature at each site (Table 5.23).
- Soil temperature at the Coombs Hills and Northwind Valley sites was warmer at a depth of 0.23 m than surface temperature in the early morning, but then cooled throughout the morning as the rest of the profile heated up. This continued until about 1100 hours when heat from the surface reached that depth. This was not seen at the Scott Base site.
- The 0°C isotherm was deeper on the clear sky days than it was on the cloudy days at all sites, and was deepest at the Scott Base site and shallowest at the Northwind Valley site.
- On the cloudy day, the entire soil profile at the Northwind Valley site remained below 0°C due to the cold surface temperatures and relatively low Q^* (Table 5.23). This was not seen at the other two sites.
- When the Scott Base site was covered in snow, the maximum penetration depth of the diurnal temperature variations was reduced from ~0.20 m under clear sky and cloudy conditions, to only a few centimetres. At the Coombs Hills site under similar conditions, the entire profile remained colder than 0°C, soil at depth was the warmest, and the surface layers cooled noticeably throughout the day.

Table 5.23 Characteristic features of each sites thermal regime and microclimate. Caution must be taken when interpreting the Coombs Hills and Northwind Valley temperature data due to problems associated with the temperature measurement equipment.

Location	Altitude	Measurement period	Conditions	Q^* (MJ $m^{-1}d^{-1}$)	Q_G (MJ $m^{-2}d^{-1}$)	Temperature (°C) Surface max.	Surface min.	Average	Mean Air	Windspeed (ms^{-1})
Scott Base	~100 m	Dec. 18–30, 1994	Clear sky	18.60	1.59	17.8 (1100 hrs)	-4.7 (0130 hrs)	4.49	-5.2	4.6
75°50'S,166°45'E			Cloudy	12.44	1.19	11.0 (1100 hrs)	-2.3 (2330 hrs)	4.61	-4.83	2.9
			Surface snow	7.44	-0.30	3.78 (1430 hrs)	-3.55 (0230 hrs)	-0.93	-3.4	8.9
Coombs Hills	~2000 m	Jan. 9–17, 1995	Clear sky	15.45	0.98	14.3 (1230 hrs)	-14.4 (0400 hrs)	0.06	-12.9	2.96
76°48.3'S,159°54.1'E			Clouds + snow	5.27	-0.30	2.2 (1200 hrs)	-13.5 (0500 hrs)	-7.26	-15.61	2.07
			Surface snow	0.12	-1.15	-7.0 (1100 hrs)	-15.1 (2330 hrs)	-11.17	-17.12	4.69
Northwind Valley	~1400 m	Jan. 18–22, 1995	Clear sky	9.74	1.70	8.5 (1430 hrs)	-13.5 (0500 hrs)	-2.87	-9.6	2.16
76°46.3'S160°45.1'E			Cloudy	3.08	0.67	-1.8 (1130 hrs)	-14.9 (0500 hrs)	-7.94	-10.83	2.65

5.6.6 ANTARCTIC SOIL THERMAL REGIMES

These results have identified several features which appear to characterise the microclimates of polar desert soils. In summer, high radiant fluxes, strong surface heating, soil profile warming and extreme near surface vertical air temperature gradients are common in the Antarctic Dry Valleys when atmospheric conditions allow.

Albedo, which is spatially and temporally variable, is the most important soil surface property because it determines the amount of energy available to drive soil thermal processes.

The partitioning of the available energy between the sensible and soil heat fluxes, and the latent heat flux when soil moisture is present, is largely determined by the soil surface temperature, air temperature and windspeed.

The warmest soil profile was found at the Scott Base site due to its relatively warm maritime climate, and the greatest temperature range was recorded at the Coombs Hill site which has similar surface properties to that at Scott Base, but has a much colder climate due to its position on the edge of the polar plateau. Surface temperatures consequently rose significantly during the day in response to increasing $K\downarrow$ at this site when the wind was relatively weak, but then fell dramatically during the evening and early morning when $K\downarrow$ was lowest.

The warmer soil temperatures at Scott Base allowed the active layer to extend down to a maximum depth of about 0.20 m on a diurnal basis, but only 0.10 m at the cooler Coombs Hills site. At the Northwind Valley site, the active layer only reached a maximum depth of 0.08 m because the light coloured surface did not heat up as much.

Ice cement was found at the Scott Base site which probably delineates the approximate position of the permafrost, being the maximum 0°C isotherm on a diurnal basis during summer. This is supported by Campbell *et al.*, (in prep.), who also found ice cement at this depth in the vicinity of Scott Base. At the other two sites there was no permanent ice cement found due to their dry nature, but the permafrost is much nearer the surface.

Under snow cover, Q_G at both the Scott Base and Coombs Hills sites became negative which means energy was being lost from the profile, and the penetration depth of diurnal temperature variations was reduced. Therefore, during the winter months when there is

no incoming solar radiation and snow cover is common in the Dry Valleys, the soil would cool significantly and become isothermal with minimal temperature variations.

CHAPTER SIX

CONCLUSIONS

The hypothesis being tested states that "the microclimatology and thermal regime of Antarctic soils is a function of their geographic location, external climatic influences, and the physical properties of the soil" (Chapter 1). The results presented in this thesis prove this hypothesis to be true and have identified the most important variables influencing Antarctic soil microclimate.

Although the soil physical and thermal properties, air temperature, wind speed and direction, and precipitation, which are determined by a sites geographic location, are important factors controlling soil microclimate, $K\downarrow$ is the most important climatic variable because it determines the amount of energy available to drive microclimatic processes. Despite incoming radiation being similar at all three sites, the amount of energy available to drive surface and sub-surface climatic processes varied significantly due to the different surface albedo at each site. Soil properties including moisture content, thermal conductivity and heat capacity are less important in determining the variations observed.

Surface heating was significant at the Scott Base and Coombs Hills sites due to the dark coloured soil, but the soil heat flux was relatively small (~6–8% of Q^*) due to the extreme vertical air temperature gradient which caused a large sensible heat flux. In contrast, at the Northwind Valley site, the pale surface reflected a larger proportion of incoming radiation which resulted in colder surface temperatures, but the soil heat flux was still relatively large (~17% of Q^*). This is probably because the near-surface air temperature gradient at this site is a lot smaller than that at the other sites which means less energy is lost as sensible heat, so partitioning of the available energy favours the soil heat flux.

Soil surface temperature at all three sites was warmer than air temperature which resulted in significant sensible heat losses to the air. When there was no wind present, soil surface temperature was able to rise significantly which increased the soil heat flux.

As a result of the different surface climates and soil surface properties, the depth of the active layer varies significantly between sites, as does the depth to permafrost.

6.1 FURTHER RESEARCH

Soil microclimate is important for soil biological processes. Therefore, to better understand Antarctic soil biology, the implications of the soil microclimatic processes examined in this research should be considered. Human disturbance of Antarctic soil systems impact on soil microclimates and therefore affect soil biological processes.

A long term measurement programme needs to be established to identify the seasonal and annual microclimate processes of Antarctic soils. This would allow a more comprehensive understanding of seasonal active layer depth variations and determine the depth to permafrost more accurately.

The development of a model Antarctic soil thermal regimes could also be important to give a better understanding of some of the processes examined in this research. The parameters which need to be included in such a model are: incoming solar radiation, surface albedo, air temperature, windspeed, soil moisture content, soil thermal conductivity and heat capacity.

Appendix 1

Oven dry heat capacity measurements made with the specific heat probe and calculated field moist soil heat capacity using Equation 2.8. All units are in MJ m^{-3} K^{-1}.

	Oven dry C_s	% mineral	C_s water	% water	Field C_s
Scott Base					
0.0–0.05 m	1.764	93.08	4.18	6.92	1.931
0.05–0.10 m	1.923	93.26	4.18	6.74	2.075
0.10–0.15 m	1.729	97.24	4.18	2.76	1.797
0.15–0.20 m	1.794	93.36	4.18	6.64	1.952
Coombs Hills					
0.0–0.05 m	1.633	96.92	4.18	3.08	1.711
0.05–0.10 m	1.643	93.11	4.18	6.89	1.818
0.10–0.15 m	1.676	96.51	4.18	3.49	1.763
0.15–0.20 m	1.651	96.68	4.18	3.32	1.735
Northwind Valley					
0.0–0.05	1.530	98.32	4.18	1.68	1.575
0.05–0.10	1.392	96.74	4.18	3.26	1.483
0.10–0.15	1.527	96.52	4.18	3.48	1.619
0.15–0.20	1.433	96.78	4.18	3.22	1.521

REFERENCES

Addison, P.D., and Bliss, L.C., 1980. Summer climate, microclimate, and energy budget of a polar semi-desert on King Christian Island, N.W.T., Canada. *Antarctic and Alpine Research*, **12**: 161–170.

Anderson, D.M. and Tice, A.R., 1989a. Unfrozen water contents of six Antarctic soil materials. in *Cold regions engineering - Proceeding of the Fifth International Conference, American Society of Civil Engineers*, New York.

Anderson, D.M., Tice, R.T., and McKim, H.L., 1989b. The unfrozen water and the apparent specific heat capacity of frozen soil. *US Army Cold Regions Research and Engineering Laboratory*, Hanover, New Hampshire.

Arnfield, A.J., 1975. A note on the diurnal, latitudinal and seasonal variation of the surface reflection coefficient. *Journal of Applied Meteorology*, **14**: 1603–1608.

Barry, R.G., and Chorley, R.J., 1990. *Atmosphere, weather and climate.* fifth edition, Routledge, Chapman and Hall Inc., New York.

Balks, M.R., Campbell, D.I., Campbell, I.B., and Claridge, G.G.C., 1995. *Interim results of 1993/94 soil climate, active layer and permafrost investigations at Scott Base, Vanda and Beacon Heights, Antarctica.* University of Waikato Antarctic Research Unit, Special report No. 1, University of Waikato, New Zealand.

Barkovskaya, Y.N., Yershov, E.D., Komarov, I.A., Cheveriov, V.G., 1983. Mechanism and regularities of change in heat conductivity of soils during the freezing-thawing process. In: *Permafrost Fourth International Conference Proceedings, July 17–22*, National Academy Press, Washington DC.

BAS, 1995. *British Antarctic Survey World Wide Web home page* "http.//www.nbs.ac.uk/public/dotacs.html".

Berg, T.E., and Black, R.F., 1966. Preliminary measurements of growth of non-sorted polygons, Victoria Land, Antarctica. In: *Antarctic Soils and Soil Forming Processes*, Tedrow J.C.F. (ed), Antarctic Research Series, American Geophysical Union, **8**: 61–108.

Blackmore, L.C., Searle, P.L., and Daly, B.K., 1987. *Methods for Chemical Analysis of Soils.* New Zealand Soil Bureau Scientific Report 80, New Zealand Soil Bureau, Department of Scientific and Industrial Research, Lower Hutt, New Zealand.

Blake, G.R., and Hartage, K.H., 1986a. Bulk Density. In: Klute A., (ed) *Methods of Soil Analysis*, Part 1, second edition, Agronomy, Madison, Wisconsin, USA.

Blake, G.R., and Hartage, K.H., 1986b. Particle Density. In: Klute A., (ed) *Methods of Soil Analysis*, Part 1, second edition, Agronomy, Madison, Wisconsin, USA.

Bristow, K.L., White, R.D., and Kluitenberg, G.G., 1994. Comparison of single and dual probes for measuring soil thermal properties with transient heating, *Australian Journal of Soil Research*, **32**: 447–464.

Bromley, A.M., 1994. *The climate of Scott Base*, National Institute of Water and Atmospheric Research (NIWA/Clim/R/94–002), New Zealand.

Brown, R.D., and Fitzharris, B.B., 1993. The surface reflectance of snow tussock. *Weather and Climate*, **13**: 3–9.

Buchan, G.D., 1991. Soil temperature regime. In: Smith K.A., and Mullins C.E. (ed), *Soil Analysis - Physical Methods*, Marcel Dekker Inc, USA.

Bull, C., 1966. Climatological observations in ice-free areas of Southern Victoria Land, Antarctica. In: *Studies in Antarctic meteorology*, Rubin M.J. (ed), Antarctic Research Series, 9: 177–195.

Burk, W., Gabriels D., and Bouma J., (Editors) 1986. *Soil Structure Assessment.* Balkema, Rotterdam, Netherlands.

Campbell, I.B., Claridge, G.G.C., 1992. Soils of Cold regions. In: *Developments in Earth Surface Processes 2 - Weathering, soils and paleosols*, Martini I.P., and Chesworth W. (ed), Department of Land Resource Science, University of Guelph, Canada.

Campbell, I.B., Claridge, G.G.C., 1987. *Antarctica. Soils, Weathering Processes and Environment.* Developments in Soil Science 16, Elsevier Science Publishing Company Inc., New York.

Campbell, G.S., Calissendorff, C., and Williams, J.H., 1991. Probe for measuring soil specific heat using a heat-pulse method. In: *Soil Science Society of America Journal*, **55**: 291–293.

Campbell, G.S, 1985. *Soil physics with basic transport models for soil-plant systems.* Developments in Soil Science 14, Elsevier Science Publishing Company Inc., New York.

Chinn, T.J., Pocknall, D.T., Skinner, D.N.B., Sykes, R., 1994. *Geology of the Convoy Range Area, Southern Victoria Land, Antarctica*, Institute of Geological and Nuclear Sciences Ltd, Lower Hutt, New Zealand.

Clark, M.J., 1988. *Advances in Periglacial Geomorphology*, John Wiley and Sons, New York.

Cole, J.W., Kyle, P.R., Neall, V.E., 1971. Contributions to Quaternary Geology of Cape Crozier, White Island and Hut Point Peninsula, McMurdo Sound Region, Antarctica. *New Zealand Journal of Geology and Geophysics*, **14**: 528–546.

Coulsen, K.L., and Reynolds, D.W., 1971. Spectral reflectance of natural surfaces. *Journal of Applied Meteorology*, **10**: 1285–1295.

Everett, K.R., 1971. Soils of the Meserve Glacier area, Wright Valley, Southern Victoria Land, Antarctica. *Soil Science Society of America*, **112**: 425–438.

Fritschen, L.J., and Gay, L.W., 1979. *Environmental Instrumentation.* Springer-Verlag, New York.

Fuchs, M., 1986. Heat flux, in Klute (ed) *Methods of soil analysis, Part 1.* second edition, Agronomy, Madison, Wisconsin, USA.

Garvril'ev, R.I., 1989. Thermal conductivity of permafrost soils in relation to natural moisture content. *Journal of Engineering Physics*, **56**:701–706.

Gomez, K.A., and Gomez, A.A., 1984. *Statistical Procedures for Agricultural Research.* second edition, John Wiley and Sond Ltd., New York.

Graham, W.G., and King, K.M., 1961. Shortwave reflection coefficient for a field of maize. *Journal of Applied Meteorology*, **2**: 425–428.

Grapes, R.H., Reid, D.L., McPherson, J.G., 1972. Shallow Dolerite Intrusion and Phreatic Eruption in the Allan Hills Region, Antarctica. in *New Zealand Journal of Geology and Geophysics*, **17**: 564–577.

Hill, J, 1983. *New Zealand and Antarctica*, Commission for the Environment, Wellington, New Zealand.

Hillel, D., 1980. *Applications of soil Physics*. Academic Press Inc., New York.

Hanks, R.J., and Ashcroft, G.L., 1980. *Applied Soil Physics - Soil Water and Temperature Applications*. Advanced series in Agricultural Sciences **8**, R.R Donnelley & Sons, Harrisonburg, USA

Jackson, R.D., and Taylor, S.A., 1986. Thermal conductivity and diffusivity, in Klute (ed) *Methods of Soil Analysis, Part 1*, second edition. Agronomy, Madison, Wisconsin, USA.

Jumikis, A.R., 1977. *Thermal Geotechnics*. Rutgers University Press, New Brunswick, New Jersey.

Kluitenberg, J.G., Ham, J.M., and Bristow, K.L., 1993. Error analysis of the heat pulse method for measuring soil volumetric heat capacity. In: *Soil Science Society of America Journal*, **57**: 1444–1451.

Koorevaar, P., Menelik G., and Dirksen C., 1983. *Elements of Soil Physics. Developments in Soil Science*, Elsevier Science Publishing Company Inc., New York.

Kyle, P.R., 1981. Geologic History of Hut Point Peninsula as Inferred from DVDP1,2 and 3 Drillcores and Surface Mapping. *Dry Valley Drilling Project Antarctic Research Series*, **33**.

Lewis, D.W., and McConchie, D.M., 1993. *Analytical sedimentology*. Chapman and Hall, New York.

Linkletter, G., Bockheim, J., and Ugolini, F.C., 1973. Soils and glacial deposits in the Beacon Valley, Southern Victoria Land, Antarctica, *New Zealand Journal of Geology and Geophysics*, **16**: 90–108.

McCraw, J.D., 1967. Soils of Taylor Valley, Victoria Land, Antarctica, with notes on soils from other localities in Victoria Land. In: *New Zealand Journal of Geology and Geophysics*, 4th special Antarctic issue, **10**: 498–539.

McLaren, R.G., and Cameron, K.C., 1990. *Soil Science, an introduction to the properties and management of New Zealand soils*. Oxford University Press, Auckland, New Zealand.

Monteith, J.L., Unsworth, M.H., 1990. *Principles of Environmental Physics*. Second Edition, Edward Arnold, London.

Noborio, K., and McInnes, K.J., 1993. Thermal conductivity of salt-affected soils, In *Soil Science Society of America Journal*, **57**: 329–334.

Nkemdirim, L.C., 1972. A note on the albedo of surfaces. *Journal of Applied Meteorology*, **11**: 867–874.

Oke, T.R., 1987. *Boundary Layer Climates*. University Press, Cambridge, Great Britain.

Pickard, J., 1986. *Antarctic oasis - terrestrial environments and history of the Vestifold Hills*. Academic Press, USA

Richter, J., 1987. *The soil as a reactor, modelling processes in the soil*. Catena Verlag, West Germany.

Riha, S.J., McInnes, K.J., Child, S.W., and Campbell, G.S., 1980. A finite element calculation for determining thermal conductivity. In: *Soil Science Society of America Journal*, **44**: 1323–1325.

Rosenberg, N.J., 1974. *Microclimate, the biological environment*. John Wiley and Sons Inc, United States of America.

Rusin, N.P, 1964. *Meteorological and Radiational Regime of Antarctica*. Israel Program for Scientific Translations, Jerusalem.

Saunders, I.R., and Bailey, W.G., 1994. Radiation and energy budgets of alpine tundra environments of North America. In: *Progress in Physical Geography*, **18**: 517–538.

Schwerdtfeger, W., 1984. *Weather and Climate of the Antarctic.* Developments in Atmospheric Science 15, Elsevier, University of Wisconsin, USA.

Selby, M.J., 1970. Salt weathering of landforms, and an Antarctic example. *Proceedings of the sixth New Zealand Geography Conference, New Zealand Geographical Society*, **1**: 30–35.

Sepaskhah, A.R., Boersma, L., 1979. Thermal conductivity of soil as a function of Temperature and water content. *Soil Science Society of America Journal*, **43**: 439–444.

Soiltronics Ltd 1995. *The thermal conductivity probe.* Soiltronics, 1111 Myrtle Drive, Burlington, WA 98233, USA.

Solopov, A.V, 1969. *Oases in Antarctica.* Israel Program for Scientific Translations, Jerusalem.

Stanhill, G.G., Hofstead, G.J., and Kalma, J.D., 1966. Radiation balance of natural and agricultural vegetation. *Quarterly Journal of the Royal Meteorological Society*, **92**:128–140.

Taylor, S.A., and Jackson, R.D., 1986a. Temperature, in Klute A., (ed) *Methods of soil analysis, Part 1.* second edition, Agronomy, Madison, Wisconsin, USA.

Taylor, S.A., and Jackson, R.D., 1986b. Heat capacity and specific heat, in Klute A., (ed) *Methods of soil analysis, Part 1,* second edition, Agronomy, Madison, Wisconsin, USA.

Tedrow, J.C.F., and Ugolini, F.C., 1966. Antarctic soils. *Antarctic Research Series*, American Geophysical Union, **8**: 161–177.

Tedrow, C.F., 1977. *Soils of the Polar landscapes.* Rutgers University Press, New Brunswick, New Jersey, USA.

Thompson, D.C., and Mcdonald, W.J.P., 1962. Radiation measurements at Scott Base, *New Zealand Journal of Geology and Geophysics, fourth special Antarctic issue*, **5**: 874–909.

Thompson, D.C., Bromley, A.M., and Craig, M.F., 1971a. Ground and surface heat balance in an Antarctic Dry Valley. *New Zealand Journal of Science*, **14**: 245–251.

Thompson, D.C., Bromley, A.M., and Craig, M.F., 1971b. Ground temperatures in an Antarctic Dry Valley. *New Zealand Journal of Geology and Geophysics*, **3**: 477–483.

Weaver, H.L., and Campbell, G.S., 1985. Use of peltier coolers as soil heat flux transducers. *Soil Science Society of America Journal*, **49**: 1065–1067.

Wierenga, P.J., Nielsen, D.R., and Hagan, R.M., 1969. Thermal properties of a soil based upon field and laboratory measurements. *Soil Science Society of America*, **33**: 354–360.